EUROMECH
European Mechanics Society

INSTITUTE OF THERMOMECHANICS
Academy of Sciences of the Czech Republic, v.v.i.

Advanced Modelling of Wave Propagation in Solids

Edited by
Radek Kolman
Arkadi Berezovski
Miloslav Okrouhlík
Jiří Plešek

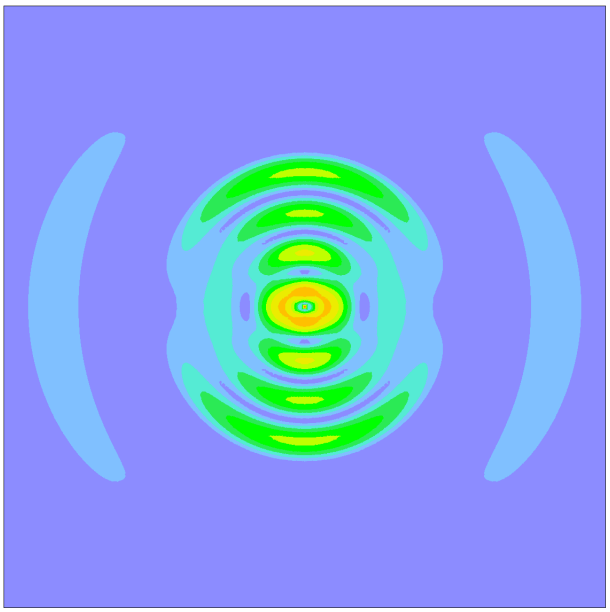

Book of abstracts

EUROMECH Colloquium 540

Prague, Czech Republic

October 1–3, 2012

http://ec540.it.cas.cz

EUROMECH
European Mechanics Society

INSTITUTE OF THERMOMECHANICS
Academy of Sciences of the Czech Republic, v.v.i.

Advanced Modelling of Wave Propagation in Solids

Edited by
Radek Kolman
Arkadi Berezovski
Miloslav Okrouhlík
Jiří Plešek

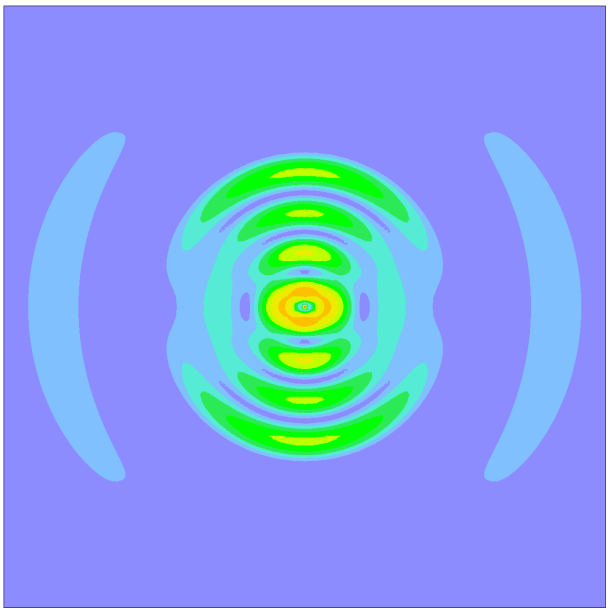

Book of abstracts

EUROMECH Colloquium 540

Prague, Czech Republic

October 1–3, 2012

http://ec540.it.cas.cz

EUROMECH Colloquium 540 - Advanced Modelling of Wave Propagation in Solids, Prague, Czech Republic, October 1–3, 2012

organized by the Institute of Thermomechanics, Academy of Sciences of the Czech Republic, v.v.i.

under the auspices of the European Mechanics Society

in partnership with the Centre for Nonlinear Studies, Institute of Cybernetics at Tallinn University of Technology

the Czech Society for Mechanics

and the Mayor of Prague Prof. Bohuslav Svoboda

Edited by Radek Kolman, Arkadi Berezovski, Miloslav Okrouhlík, Jiří Plešek

The abstracts are reproduced directly from author manuscripts. The authors are solely responsible for the contents and opinions expressed therein.

Note: The book of abstracts has been edoted to the date February 29, 2012, including all electronically registered participants.

Printed in PowerPrint s.r.o., Zikova 19, Prague, Czech Republic

ISBN: 978-80-87012-41-3

Number of pages: 146

Not for sale.

Chairmen

R. Kolman	Institute of Thermomechanics ASCR, v.v.i., Prague
A. Berezovski	Institute of Cybernetics at Tallinn University of Technology, Tallinn

Scientific Committee

J.D. Achenbach	Northwestern University, Evanston
H. Askes	University of Sheffield, Sheffield
J. Engelbrecht	Institute of Cybernetics at Tallinn University of Technology, Tallinn
D. Givoli	Technion - Israel Institute of Technology, Haifa
B. Lundberg	Uppsala University, Uppsala
G.A. Maugin	Universit Pierre et Marie Curie, Paris
M. Okrouhlík	Institute of Thermomechanics ASCR, v.v.i., Prague
J. Plešek	Institute of Thermomechanics ASCR, v.v.i., Prague
S. Sorokin	Aalborg University, Aalborg
E. Zuazua	Basque Center for Applied Mathematics, Bilbao

Local Organizing Committee

R. Kolman
J. Plešek
M. Okrouhlík
D. Gabriel
P. Formánek
P. Pařík
Z. Hrubý
J. Kopačka
R. Marek
V. Sháněl
S. Parma
M. Brejšková
V. Stibralová

Conference webpage

`http://ec540.it.cas.cz`

Preface

The Euromech Colloquium 540 – *Advanced Modelling of Wave Propagation in Solids* took place at the Institute of Thermomechanics in Prague from 1rd to 3th October 2012. It aimed at bringing together engineers and scientists interested in modelling of wave propagation in solids. Wave phenomena play important role in various scientific fields such as continuum mechanics, material science, and physics. The reliable modelling of wave propagation in solids is of utmost importance in industry, material science, security and defence.

The Colloquium focused on topics related to effects in linear and non-linear wave propagation in solids, such as solitary waves, strongly dispersive waves in inhomogeneous solids and waves in materials with microstructure. Attention was also paid to up-to-date formulations of non-linear constitutive equations in case of thermomechanical coupling, finite strains, strain rate effects, viscoplasticity, damage and phase transformation.

Recent advances in numerical approaches and strategies were discussed. To guarantee the accuracy and stability of numerical approaches, proper understanding of methods and ways leading to suppressing artefacts and parasitic effects are essential. Among these are size effects, dispersion, attenuation and appearance of spurious modes and evanescent waves. The main purpose of the Colloquium was to discuss novel methods of wave propagation modelling and to assess the credibility of results especially in cases when experiment validation had not been available.

The selected papers will appear in special issues of the journals of Wave Motion, Proceedings of the Estonian Academy of Sciences, Engineering Mechanics and Applied and Computational Mechanics.

The editors would like to thank all the contributors who made the Colloquium and this book possible. Deep gratitude is also extended to all the members of the scientific committee, the members of the local organizing committee and our colleagues, namely, Dušan Gabriel, Pavel Formánek, Petr Pařík, Zbyněk Hrubý, Ján Kopačka, René Marek, Vítek Sháněl and Slavomír Parma. A substantial help of Marcela Brejšková and Věra Stibralová is greatly appreciated.

October 2012
Prague

R. Kolman, A. Berezovski,
M. Okrouhlík, J. Plešek

CONTENTS

ABSTRACTS

SURFACE WAVES ON A HALF SPACE WITH DEPTH-DEPENDENT PROPERTIES

Jan D. Achenbach, Oluwaseyi Balogun

Department of Mechanical Engineering, McCormick School of Engineering and Applied Science,
Northwestern University, Evanston, IL 60208-3020 USA; e-mail: {achenbach;o-balogun}@northwestern.edu

Keywords: surface waves, depth inhomogeneity, dispersion

Surface waves have probably been studied more thoroughly than any other kind of wave motion in solid materials. In a two-dimensional configuration, surface waves on an elastic body can be distinguished into in-plane and anti-plane surface waves. In this talk we consider in-plane surface waves, which are generally known as Rayleigh Waves. These waves have displacements in the plane spanned by the direction of propagation and the depth direction. They occur at the surface of the earth, induced by earthquakes, and they are frequently generated for applications in science and technology, such as for testing procedures in non-destructive evaluation of materials and structures. It is well known that along the free surface of a homogeneous isotropic elastic body, a classical in-plane surface wave propagates with a velocity that is independent of the wavelength, while the amplitudes of the displacement components decay exponentially with depth.

Many materials are, however, not homogenous. For an important class of materials the elastic moduli may vary with distance from a free surface. Rayleigh surface waves on such an elastic body with depth-dependent properties are of interest in seismology, but also for engineered functionally graded materials. In this presentation we consider in-plane surface waves, but in an axially symmetric configuration, on a half-space of an isotropic material whose elastic moduli λ and μ and mass density, ρ, depend on the depth coordinate z.

For many practical applications the inhomogeneity with depth has been dealt with numerically by replacing the continuous inhomogeneity by a representative layering, see Thompson[1]. The layering may, however, produce effects of the interfaces. An alternative numerical approach is by a formulation amenable to the Runge-Kutta technique, see Aki and Richards[2]. One approximation which leads to analytical solutions is for the case that the elastic moduli and the density decay in the same exponential manner with depth, see Pal & Acharya[3], Destrade[4], and Kulkarni & Achenbach[5]. The present talk is concerned with an analytical technique to investigate surface waves for monotonic depth dependence of the elastic moduli and the mass density. An earlier, and more formal application of a high frequency approach was presented by Alenitsyn[6], see also Baron et. al.[7]. Other high-frequency approaches were presented by Shuvalov[8] and Shuvalov and Every[9].

We consider quite general monotonic dependencies on depth of the elastic moduli and the mass density. The analytical technique is based on a W.K.B. solution for high frequencies, which was worked out for anti-plane surface waves elsewhere (Achenbach & Balogun[10]). The approach by Achenbach & Balogun[10] is not directly applicable to in-plane surface waves. Some simplifications of the governing equations, valid for a gradual change of the properties, are required to obtain a set of equations that produce expressions for the displacements in a simple manner.

Next the expressions for the displacements are used to obtain the stresses. The tractions must vanish at the free surface, which yields an equation that provides a dispersion curve which relates the surface wave velocity to the wave number. For a number of cases of depth dependence of the elastic moduli, the analytically obtained dispersion curves are compared with numerically obtained curves. The numerical results were obtained for an equivalent layering of the half-space. For the cases considered excellent agreement was obtained over a large range of wave numbers.

As an issue of particular interest, it is shown that a computation which yields a reasonable dispersion curve is not necessarily commensurate with displacements that decay exponentially with depth, as is the case for Rayleigh waves on a homogenous elastic solid. For certain classes of materials, whose elastic moduli either increase or decrease with depth, conditions for exponential decay of the displacement amplitudes have been derived.

As a final comment it is noted that the expressions for axially symmetric propagation of in-plane surface waves, provide the basic information to obtain the surface-wave radiation from a time-harmonic normal point load on the surface of a body with z-dependent material properties. The radiating surface waves can be obtained by the use of the reciprocity theorem, as shown in Ref. [12, chapter 8] for a point load on a homogenous body. Since the reciprocity theorem is also valid for inhomogeneous linearly elastic solids the same procedure can be followed as presented in Ref.[12].

References

[1] W.T. Thompson. Transmission of elastic waves through a stratified solid medium. *J. Appl. Phys*. **21:** 89–93, 1950.
[2] K Aki, P.G. Richards. *Quantitative Seismology*, Vol. I, p. 267, W.H. Freeman and Company, San Francisco, 1980.
[3] P.K. Pal, D. Acharya. Effects of inhomogenity on surface waves in anisotropic media. *Sadhana,* **23**: 247–258, 1998.
[4] M. Destrade. Seismic Rayleigh waves on an exponentially graded, orthotropic elastic half-space. *Proc. Roy. Soc. A,* **463:** 495–502, 2001.
[5] S.S. Kulkarni, J.D. Achenbach. Application of reciprocity theorem to determine line-loaded generated surface waves on an inhomogeneous transversely isotropic half-space. *Wave Motion*, **45**: 350–360, 2008.
[6] A.G. Alenitsyn. Raleigh waves in a nonhomogeneous elastic half-space. *J. Appl. Math. Mech*., **27**: 816–822, 1963.
[7] C. Baron, A.L. Shuvalov, O. Poncelet. Impact of localized inhomogeneity on the surface wave velocity and bulk wave reflection in solids. *Ultrasonics*, **46**: 1–12, 2007.
[8] A.L. Shuvalov. The high-frequency dispersion coefficient for the Raleigh velocity in a vertically inhomogeneous anisotropic half-space. *J. Acoust. Soc. Am.*, **13**: 2484–2487, 2008.
[9] A.L. Shuvalov, A.G. Every. On the long wave onset of dispersion of the surface-wave velocity in coated solids. *Wave Motion*, **45**: 857–863, 2008.
[10] J.D. Achenbach, O. Balogun. Anti-plane surface waves on a halfspace with depth-dependent properties. *Wave Motion*, **47**: 59–65, 2009.
[11] J. Heading. An *Introduction to Phase-Integral Methods, Methuen's monographs on physical subjects,* Methuen & Co. LTD., London, 1962.
[12] J.D. Achenbach. *Reciprocity in Elastodynamics*, *Cambridge Monographs on Mechanics*. Cambridge University Press, Cambridge, U.K., 2003.

WAVES IN COMPOSITE MATERIALS: AN INTERPLAY BETWEEN NONLINEARITY AND DISPERSION

Igor Andrianov[1], Vladyslav Danishevs'kyy[2], Dieter Weichert[1]

[1]Institute of General Mechanics, RWTH Aachen University, Aachen, Germany;
e-mail: andrianov@iam.rwth-aachen.de; weichert@iam.rwth-aachen.de
[2]Department of Structural Mechanics and Strength of Materials,
Prydniprovs'ka State Academy of Civil Engineering and Architecture,
Dnipropetrovs'k, Ukraine; e-mail: vdanish@ukr.net

Keywords: composite material, nonlinear wave, homogenization, dispersion

We study influence of geometrical, physical and structural nonlinearity on propagation of elastic waves in periodic composite materials. 1D dilational waves in a layered composite and 2D anti-plane shear waves in a fibrous composite are considered. Geometrical nonlinearity is described by the Cauchy-Green strain tensor. Physical nonlinearity is predicted representing the energy of deformation as a series expansion in powers of the strains. Structural nonlinearity is introduced assuming imperfect bonding conditions between the constitutive components of the composite. The presence of nonlinearity invokes generation of higher-order modes and localization of energy [6, 7].

Successive reflections and refractions of the travelling signal at the interfaces between the components lead to the dispersion of the macroscopic wave field. Dispersion provides scattering of energy and compensates the influence of nonlinearity. In order to predict the effect of dispersion, we use the higher-order asymptotic homogenization method (AHM) [1, 2]. The basic idea of this approach is to search solutions as series expansions in powers of the small parameter $\varepsilon = l/L$, where l is the typical size of the microstructure and L is the wavelength. Application of the AHM reduce the original dynamic problem formulated in multi-connected domain to a recurrent sequence of local problems. Due to the spatial periodicity of the composite structure, local problems are considered within only one distinguished unit cell.

Homogenization of nonlinear dynamical equations has some peculiarities. Since the magnitudes of strains in solids are considerably small, it is sufficient to take into account nonlinear terms only in the first approximation (of the order ε^0). Asymptotic solutions of the nonlinear local problems are developed using series expansions in powers of the gradients of displacements. The higher-order approximations by ε (that describe the effect of dispersion) are evaluated in the framework of the linear model. Eventually, we derive homogenized double dispersion equations and obtain explicit analytical formulas for the effective elastic moduli [3, 4, 8].

The balance state between nonlinearity and dispersion results in formation of stationary nonlinear modes that can be described explicitly in terms of elliptic functions. If the properties of the components are variable, exact solutions are generally not possible. In this case, we develop approximate asymptotic solutions using the Linstedt-Poincaré technique. Convergence of the asymptotic series is improved by the application of Padé approximants. This enables us to construct asymptotic expansions valid even for considerably large rates of nonlinearity.

Analysis of the solutions obtained for stationary waves reveals a number of specific nonlinear phenomena that can be observed in composite solids within a practically admissible range of the strain amplitudes (up to 10^{-4}): (i) dependence of the main wave characteristics (such as shape, velocity, attenuation) upon the amplitude and (ii) localization of energy. It should be noted that different types of nonlinearity lead to different scenarios of localization. Thus, geometrical and physical nonlinearity results in formation of solitary strain waves. The same effect is observed for structurally-nonlinear composites with a hard interface between the components. Meanwhile, heterogeneous materials with a soft nonlinear interface allow propagation of kink strain waves.

Presented numerical results show that the effects of nonlinearity and dispersion in heterogeneous solids can be explored separately. Nonlinear phenomena are detectable at low frequencies, when dispersion is small and, consequently, long-wave methods of analysis (e.g., the AHM) can be applied. In the high-frequency domain the influence of dispersion increase significantly, while nonlinearity is depressed. Then the solution can be developed using linear approaches (e.g., Floquet-Bloch theory [5]). This analysis provides an estimation of the areas of applicability of linear and nonlinear constitutive models.

It should be emphasized that nonlinear properties of composite materials in many cases appear to be more structural sensitive than linear ones [9]. Consequently, monitoring propagation of nonlinear waves gives a possibility to predict very small variations of the microstructure, which are not visible for the linear methods of analysis. This may help to develop new, more precise technologies of non-destructive testing and acoustic diagnostic in engineering, geophysics, biomechanics and other areas dealing with heterogeneous media and structures.

Open problems in the field concern extension of the developed approach to non-stationary dynamic processes (e.g., study of evolution and interaction of nonlinear waves); examination of nonlinear vibrations of heterogeneous structures of finite sizes (composite/reinforced beams, membranes and plates) that can exhibit the effect of internal resonances; prediction of spatial localization of nonlinear waves on local defects in composite solids; development of new dynamic criteria of local failure.

Acknowledgement

This work was supported by the Alexander von Humboldt Foundation (Institutional academic co-operation program, grant no. 3.4-Fokoop-UKR/1070297) and by the German Research Foundation (Deutsche Forschungsgemeinschaft, grant no. WE 736/30-1).

References

[1] I.V. Andrianov, J. Awrejcewicz, V.V. Danishevs'kyy, D. Weichert. Wave propagation in periodic composites: higher-order asymptotic analysis versus plane-wave expansions method. *Journal of Computational and Nonlinear Dynamics*, **6**: 011015-1–011015-8, 2011.

[2] I.V. Andrianov, V.I. Bolshakov, V.V. Danishevs'kyy, D. Weichert. Higher-order asymptotic homogenization and wave propagation in periodic composite materials. *Proceedings of the Royal Society A*, **464**: 1181–1201, 2008.

[3] I.V. Andrianov, V.V. Danishevs'kyy, O. Ryzhkov, D. Weichert. Dynamic homogenization and wave propagation in a nonlinear 1D composite material. *Wave Motion*, submitted, 2012.

[4] I.V. Andrianov, V.V. Danishevs'kyy, H. Topol, D. Weichert. Homogenization of a 1D nonlinear dynamical problem for periodic composites. *Zeitschrift für Angewandte Mathematik und Mechanik*, **91**: 523–534, 2011.

[5] L. Brillouin. *Wave Propagation in Periodic Structures: Electric Filters and Crystal Lattices*, 2nd edn. Dover, Mineola, New York, 2003.

[6] V.I. Erofeev. *Wave Processes in Solids with Microstructure*. World Scientific, Singapore, 2003.

[7] A.V. Porubov. *Amplification of Nonlinear Strain Waves in Solids*. World Scientific, Singapore, 2003.

[8] D. Weichert, I. Andrianov, V. Danishevs'kyy. Asymptotic homogenization and nonlinear elastic waves in periodic composite materials. In *Dynamical Systems. Analytical/Numerical Methods, Stability, Bifurcation and Chaos*, J. Awrejcewicz, M. Kazmierczak et al. (eds). Politechnika Łódzka, Poland, 31–36, 2011.

[9] V.Yu. Zaitsev, V.E. Nazarov, V.I. Talanov. "Nonclassical" manifestations of microstructure-induced nonlinearities: new prospects for acoustic diagnostics. *Physics-Uspekhi*, **49**: 89–94, 2006.

HERMITE METHODS FOR ELASTIC WAVES

Daniel Appelö[1], Thomas Hagstrom[2], Chang Young Jang[3]

[1]Department of Mathematics, The University of New Mexico, Albuquerque, NM USA; e-mail: appelo@unm.edu
[2]Department of Mathematics, Southern Methodist University, Dallas, TX USA; e-mail: thagstrom@smu.edu
[3]Department of Mathematics, Southern Methodist University, Dallas, TX USA; e-mail: cjang@smu.edu

Keywords: Spectral element methods, elastic waves

In recent years there have been impressive developments of spectral element methods to simulate elastic waves, e.g. [1, 2]. In comparison with finite difference methods such as those presented in [3], spectral element methods on unstructured grids can directly provide guaranteed stability and high resolution in complex domains. However, such methods are also expensive. For degree-m polynomials on an unstructured grid in three space dimensions the cost to apply differentiation matrices scales like m^6 (or m^3 per degree-of-freedom) and the time step stability constraint is of the form $\Delta t \leq C\Delta x/m^2$. Thus the total work to solve a problem scales with $m^8/\Delta x^4$ limiting the gains in efficiency arising from increases in the method order.

Hermite methods are spectral element methods defined on staggered computational cells of cuboids. The degrees-of-freedom are tensor-product Taylor polynomials of degree $3m$ (degree m in each coordinate) defined at each vertex. They are evolved as follows:

- Approximate the solution on each cell by a degree $3 \cdot (2m + 1)$ tensor product polynomial, the Hermite interpolant of degree $3m$ tensor product polynomials defined at the vertices.
- Approximately solve an ordinary differential equation in time to advance the solution on the cell center, providing the local, updated polynomial data on the vertices of the dual grid.
- Repeat the process on the dual grid.

A complete analysis of Hermite methods for linear hyperbolic systems, encompassing the elastic wave equation, is presented in [4]. Using Runge-Kutta-Taylor methods of the same order of accuracy, $2m+1$, as the spatial approximations, it is proven that the time step is only limited by the necessary CFL condition. For cell widths Δx, the method is stable if a wave cannot travel from the cell boundary to the cell center in a half time step, $\Delta t < \Delta x/c_{\max}$ **independent of the method order**. Moreover, the time evolution within a cell requires no information from its neighbors once the Hermite interpolation is completed. Lastly, for piecewise constant media (or media which can be locally described by polynomials of degree significantly smaller than m), the cost per step scales like m^4 on each cell. This leads to total work scaling like $m^4/\Delta x^4$, a full factor of m^4 better than standard discontinuous Galerkin schemes. As a result, there is a much higher payoff to increasing the order.

In this talk we will present our first experiments with Hermite methods applied to elastic waves. Precisely we will demonstrate their accuracy on benchmark problems in $2 + 1$ dimensions involving a variety of wave types. In addition we will study their efficiency as a function of propagation distance, error tolerance, and method order.

We note that Hermite methods have a number of other desirable properties. As a large number of degrees-of-freedom are updated independently in each cell over a relatively large time step, and no stage storage is required, memory usage and data communication is minimized. Order-adaptive implementations are relatively straightforward [5], and the method does an excellent job of advecting nonsmooth solutions without oscillations or smearing [6]. However, like finite difference methods, they cannot be applied on unstructured grids and they require additional numerical boundary conditions which can be difficult to derive on complex boundaries. To circumvent these drawbacks we have developed hybrid implementations which use more expensive but more flexible discontinuous Galerkin discretizations on unstructured grids near cell boundaries (with local time-stepping), with the Hermite

scheme applied on regular cells everywhere else. (See Figure 1 for an example of a hybrid grid used to sole the TM Maxwell system in [7].) We will employ this technique to simulate elastic waves in more complex media, coupling the Hermite discretizations with a DG method [2].

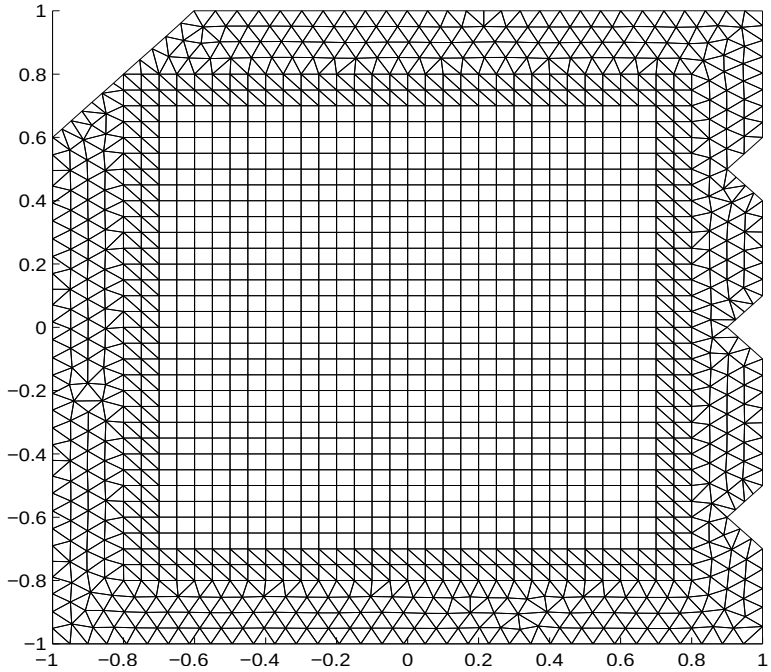

Figure 1: Example of a hybrid grid: the system is solved using a DG method on the unstructured cells near the boundaries and by a Hermite method on the structured cells in the interior.

Acknowledgement

The authors acknowledge the support of NSF Grants OCI-0904773 and OCI-0905045. Work of the second author was also supported by ARO Grant W911NF-09-1-0344 and BSF Grant 890020. Any opinions, findings, and conclusions or recommendations expressed in this material are those of the authors and do not necessarily reflect the views of NSF, ARO or BSF.

References

[1] J. Tromp, D. Komatitsch, Q. Liu. Spectral-element and adjoint methods in seismology. *Commun. Compt. Phys.*, **3**: 1-32, 2008.

[2] L. Wilcox, G. Stadler, C. Burstedde, O. Ghattas. A high-order discontinuous Galerkin method for wave propagation through coupled elastic-acoustic media. *J. Comput. Phys.*, **229**: 9373-9396 2010.

[3] D. Appelö, N.A. Petersson. A stable finite difference method for the elastic wave equation on complex geometries with free surfaces. *Commun. Comput. Phys.*, **5**: 84-107, 2009.

[4] J. Goodrich, T. Hagstrom, J. Lorenz. Hermite methods for hyperbolic initial-boundary value problems. *Math. Comp.*, **75**: 595-630, 2006.

[5] R. Chen, T. Hagstrom. P-adaptive Hermite methods for initial value problems. *ESAIM: Mathematical Modeling and Numerical Analysis*, **46**: 545-557, 2012.

[6] D. Appelö, T. Hagstrom. On advection by Hermite methods. *Pacific J. Appl. Math.*, **4**, 2012.

[7] D. Appelö, R. Chen, T. Hagstrom. A hybrid Hermite-Discontinuous Galerkin method for hyperbolic systems with application to Maxwell's equations. Submitted.

HIGH-ORDER LONG-TIME STABLE ABSORBING BOUNDARY CONDITIONS FOR ELASTODYNAMICS

D. Baffet[1], J. Bielak[2], D. Givoli[3], T. Hagstrom[4], D. Rabinovich[5]

[1]Inter-Departmental Program of Applied Mathematics, Technion, Haifa, Israel; e-mail: bdaniel@technion.ac.il
[2]Dept. of Civil and Env. Eng., Carnegie Mellon University, Pittsburgh, PA 15213, U.S.A.; e-mail: jbielak@cmu.edu
[3]Dept. of Aerospace Engineering, Technion, Haifa, Israel; e-mail: givolid@aerodyne.technion.ac.il
[4]Dept. of Mathematics, Southern Methodist University, Dallas, TX, U.S.A.; e-mail: thagstrom@smu.edu
[5]Dept. of Aerospace Engineering, Technion, Haifa, Israel; e-mail: daniel@aerodyne.technion.ac.il

Keywords: absorbing boundary condition, elastic waves, elastodynamics, Lysmer-Kuhlemeyer, high-order, Higdon, solid-earth geophysics

The need for artificial computational boundaries in the solution of exterior wave problems, called "absorbing boundaries" among other names, arises quite often in various fields of application. In solid-earth geophysics, and in particular earthquake engineering and oil exploration, they are needed for practically every simulation. Since the mid 90's two classes of methods have emerged as especially powerful: the Perfectly Matched Layer (PML) method, devised by Bérenger in 1994 and since then further developed, analyzed and used by many authors, and the method of using high-order Absorbing Boundary Conditions (ABCs), which are local and involve no high derivatives, which was originally devised by Collino [1] in 1993, followed by a few other formulations. Although usually derived by very distinct analyses, recent work has shown that, on the discrete level, the two methods are in fact quite closely related.

The use of ABCs has been very popular since the early 70's, but the term "high-order ABCs" relates to the ability to implement ABCs of an *arbitrarily high order*. In theory, some of the classical ABCs can be defined up to any desired order; however, the appearance of increasingly high order derivatives in these ABCs renders them impractical beyond a certain order, typically 2 or 3. For example, the P-order Higdon ABC [2] involves P-order derivatives in space and time, and is thus very inconvenient for implementation when P is large. In contrast, the high-order ABCs devised by Collino [1] and others involve no high derivatives owing to the use of special auxiliary variables ϕ_j $(j = 1, \ldots, P)$ on the artificial boundary. The schemes are implemented for any order P, which is simply an input parameter provided by the user. Moreover, the computational cost increases only linearly with P. See the review [3].

Most of the high-order ABCs proposed thus far are devised for the acoustic (scalar) wave equation. The only exception that we are aware of is the ABC proposed by Tsogka and Joly for elastic waves [4, 5], and the ABC proposed by Rabinovich *et al.* [6]. *Both turned out to be unstable for long times.*

In the present work, a new high-order local ABC is devised on an artificial boundary for time-dependent elastic waves in unbounded domains, in two dimensions. The elastic medium in the exterior domain is assumed to be homogeneous and isotropic. The order of the ABC determines its accuracy and can be chosen to be arbitrarily high. The ABC involves a product of first-order differential operators, all of them are of the Higdon type, except one which is of the Lysmer-Kuhlemeyer type. The stability of this ABC is shown both theoretically and numerically, thus establishing the fact that *this is the first known local high-order ABC for elastodynamics which is long-time stable.* The initial boundary value problem including this ABC is written as a first-order system, using stresses and velocities as variables. A finite difference scheme in space and time is employed to discretize this system. Numerical experiments demonstrate the performance of the scheme.

Acknowledgement

This work work was supported by the US-Israel Binational Science Foundation (BSF), grant number 890020 (Technion number 2011303).

References

[1] F. Collino. High Order Absorbing Boundary Conditions for Wave Propagation Models. Straight Line Boundary and Corner Cases. In *Proc. 2nd Int. Conf. on Mathematical & Numerical Aspects of Wave Propagation*, R. Kleinman et al. (eds). SIAM, Delaware, 161–171, 1993.

[2] R. L. Higdon. Numerical Absorbing Boundary Conditions for the Wave Equation. *Math. Comput.*, **49**: 65–90, 1987.

[3] D. Givoli. High-Order Local Non-Reflecting Boundary Conditions: A Review. *Wave Motion*, **39**: 319–326, 2004.

[4] C. Tsogka. Modélisation mathématique et numérique de la propagation des ondes élastiques tridimensionnelles dans des milieux fissurés. PhD thesis, Paris IX, 1999.

[5] C. Tsogka, P. Joly, Numerical Methods for Treating Unbounded Media. *In Effective Computational Methods in Wave Propagation*, edited by N.A. Campanis, V.A. Dougalis, J.A. Ekaterinaris, Chapman & Hall/CRC, 2008.

[6] D. Rabinovich, D. Givoli, J. Bielak, T. Hagstrom. A Finite Element Scheme with a High Order Absorbing Boundary Condition for Elastodynamics. *Comp. Meth. Appl. Mech. & Engng.*, **200**: 2048–2066, 2011.

INFLUENCE OF INTERNAL STRUCTURES ON WAVE DISPERSION IN SOLIDS

Arkadi Berezovski[1], Jüri Engelbrecht[1], Mihhail Berezovski[2]

[1]Institute of Cybernetics at Tallinn University of Technology, Tallinn, Estonia; e-mail: Arkadi.Berezovski@cs.ioc.ee
[2]Worcester Polytechnic Institute, Worcester, MA, USA; e-mail: mberezovski@wpi.edu

Keywords: wave propagation, dispersion, internal structure

Theory

Heterogeneous materials can be characterized by their internal structure. The internal structure may be purely stochastic or "natural" like in rocks or alloys, purely regular or "artificial" like in periodic laminates or meta-materials, or a mixture between the former two like in functionally graded materials. It is clear that wave propagation can be directly calculated (asymptotically or numerically) in the case of a regular internal structure on the basis of classical wave equations with prescribed material parameters of heterogeneities. A more complicated model is needed for wave propagation in the case of irregular internal structure. Even if the material parameters for constituents are known, the simple averaging is not sufficient: it predicts unchanged wave profile in the "effective" medium without experimentally observed wave dispersion.

The dispersive wave equations are based on the material modeling, even if this is not supposed explicitly. The two main approaches in the modeling of the wave dispersion may be called as "discrete" and "continuous". The oldest discrete model is the "mass-spring" chain model by Born and von Karman [1]. Though it was shown already by Schrödinger [2] (as it is reminded by Seeger [3]) that the Born-von Karman model is not appropriate one due to the infinite speed of information spreading along the chain, this model still remains as a source for the derivation of dispersive wave equations [4, 5]. Continuous models are based on the balance laws of continuum mechanics. As in the case of discrete models, different dispersive wave equations are proposed following this approach [6].

The natural question is raised: which model is the most appropriate for the description of the wave dispersion in solids? The answer may depend on particular problem in question, but certain features should be taken into account by any model. First, it is desired to have a model which is supported both from discrete and continuous points of view. It appears, that this criterion is satisfied by micromorphic theories [7]. Secondly, due to the presence of higher-order derivatives, the corresponding initial and boundary conditions should be formulated consistently. The boundary conditions could be reformulated appropriately in the framework of the dual internal variables approach developed recently [8]. Third, the additional material parameters should be established. This problem means solving inverse problems [9] combined with both experimental investigations and/or atomistic calculations.

Numerical simulation

In order to understand better the accuracy of models derived from discrete and continuous points of view, a series of numerical simulations is carried on. The computations are performed by means of the finite-volume numerical scheme, which belongs to the class of wave-propagation algorithms. We demonstrate the dispersion effects of 1D waves in materials with different internal structures: microstructure described by micromorphic theory, regular laminates, laminates with substructures, etc.

One of the important problems is to compare the results obtained by means of various models. As an example, the comparison of a direct numerical simulation of a Gaussian stress pulse propagation along the elastic bar containing an inhomogeneous part constructed by periodically alternating layers and a computation based on the Mindlin-type microstructure model [6] is shown in Fig.1.

As one can see, the effect of microstructure in the model manifests itself only locally, whereas the dispersion in the periodic laminate is non-local due to consecutive reflections. In principle, the localization of the microstructure influence is expected, since the presence of the microstructure is invisible in the absence of loading.

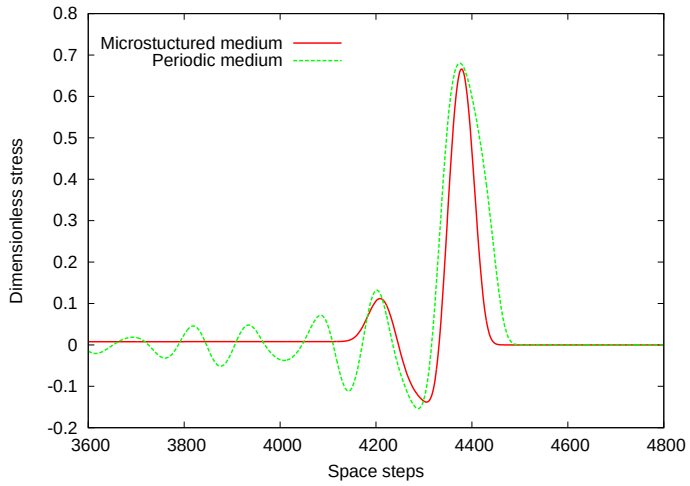

Figure 1: Deformed shape of an initially Gaussian stress pulse in periodic and microstructured solids.

In order to get matching results, one should critically revise the free energy function in the micromorphic theory for adequate modeling of interaction forces between macro– and microstructures. In the considered case, the pulse length is 5 times longer than the inhomogeneity size. This particular case was chosen because it clearly shows the synergy of the two microstructure models unified in [6]. The matching results are obtained by modifying the coupling between macro- and microstructures including also the dependence on gradients of the internal variables. The correlation between models is analyzed in detail for a large range of material parameters and wavelengths.

To sum up, based on concise modeling, dispersion analysis, and numerical simulation, we are able to choose adequate governing equations for wave motion in various microstructured solids. The concept of dual internal variables permits to include thermodynamic considerations into modeling and the dispersion analysis allows to predict the changes in group and phase velocities of waves. This is extremely important for cases when wavelengths are comparable with internal scales.

Acknowledgement

The research was supported by the EU through the European Regional Development Fund and by the Estonian Science Foundation (grant No. 8702).

References

[1] M. Born, T. von Kármán. Über Schwingungen in Raumgittern. Phys. Zeitschrift, 13, 297–309, 1912.
[2] E. Schrödinger. Zur Dynamik elastisch gekoppelter Punktsysteme. Annalen der Physik, 44, 916–934, 1914.
[3] A. Seeger. Historical note: On the simulation of dispersive wave propagation by elasticity models. Phil. Mag., 90, 1101–1104, 2010.
[4] A.V. Metrikine, H. Askes. One-dimensional dynamically consistent gradient elasticity models derived from a discrete microstructure. Part 1: Generic formulation. Eur. J. Mech. A/Solids 21, 555–572, 2002.
[5] H. Askes, A.V. Metrikine, A.V. Pichugin, T. Bennett. Four simplified gradient elasticity models for the simulation of dispersive wave propagation. Phil. Mag., 88, 3415–3443, 2008.
[6] A. Berezovski, J. Engelbrecht, M. Berezovski. Waves in microstructured solids: a unified viewpoint of modeling. Acta Mech. 220, 349–363, 2011.
[7] Y. Chen, J.D. Lee. Connecting molecular dynamics to micromorphic theory. (II). Balance laws. Physica A 322, 377–392, 2003.
[8] P. Ván, A. Berezovski, J. Engelbrecht. Internal variables and dynamic degrees of freedom. J. Non-Equilib. Thermodyn., 33, 235–254, 2008.
[9] J. Janno, J. Engelbrecht. *Microstructured Solids: Inverse Problems*. Springer, Heidelberg, 2011.

A DISCONTINUOUS PETROV-GALERKIN METHOD FOR SEISMIC TOMOGRAPHY PROBLEMS

Jamie Bramwell, Leszek Demkowicz

ICES, University of Texas at Austin, Austin, Texas, USA; e-mail: {jbramwell;leszek}@ices.utexas.edu

Keywords: DPG method, linear elasticity, wave propagation, pollution error, large-scale inverse problems

The imaging of the interior of the Earth using ground motion data, or seismic tomography, has been a subject of great interest for over a century. However, the full elastic wave equations are not typically used in standard tomography codes. Instead, the elastic waves are idealized as rays and only phase velocity and travel times are considered as input data. This results in the inability to resolve features which are on the order of one wavelength in scale. To overcome this problem, models which use the full elastic wave equation and consider total seismograms as input data have recently been developed. Unfortunately, those methods are much more computationally expensive and are only in their infancy.

While the finite element method is very popular in many applications in solid mechanics, it is still not the method of choice in many seismic applications due to high pollution error. The pollution effect creates an increasing ratio of discretization to best approximation error for problems with increasing wave numbers. It has been shown that standard finite element methods cannot overcome this issue. To compensate, the meshes for solving high wave number problems in seismology must be increasingly refined, and are computationally infeasible due to the large scale requirements.

However, a new discontinuous Petrov-Galerkin method with optimal test functions was recently introduced [2]. The main idea is to select test spaces such that the discrete problem inherits the stability of the continuous problem. In this presentation, a discontinuous Petrov-Galerkin method with optimal test functions for 2D time-harmonic model seismic tomography problems will be introduced. Both the general DPG framework and the specific time-harmonic elasticity model will be discussed.

While it has been shown that standard test space norm provides hp-optimal convergence rates for static linear elastic problems [1], numerical evidence indicates that a separate quasi-optimal norm derived from the dual space norm must be used to achieve negligible pollution error for time-harmonic problems [3]. This implies that the method is well-suited to resolve a large number of wavelengths, which is often the case in computational seismology. Supporting evidence from various model elastic wave propagation problems will be presented.

As the method produces hermitian and positive definite stiffness matrices, it is also a natural choice for adjoint-based Lagrangian constrained optimization algorithms. Both Hessian and gradient based numerical optimization schemes for solving the non-linear inverse tomography problem will be presented. As this code is designed for large-scale seismic applications, the implementation will be run on parallel machines where the scalability of the method will be evaluated. To conclude, results obtained from both DPG and standard CG discretization schemes will be compared and the potential effectiveness of DPG as a practical seismic inversion tool will be discussed.

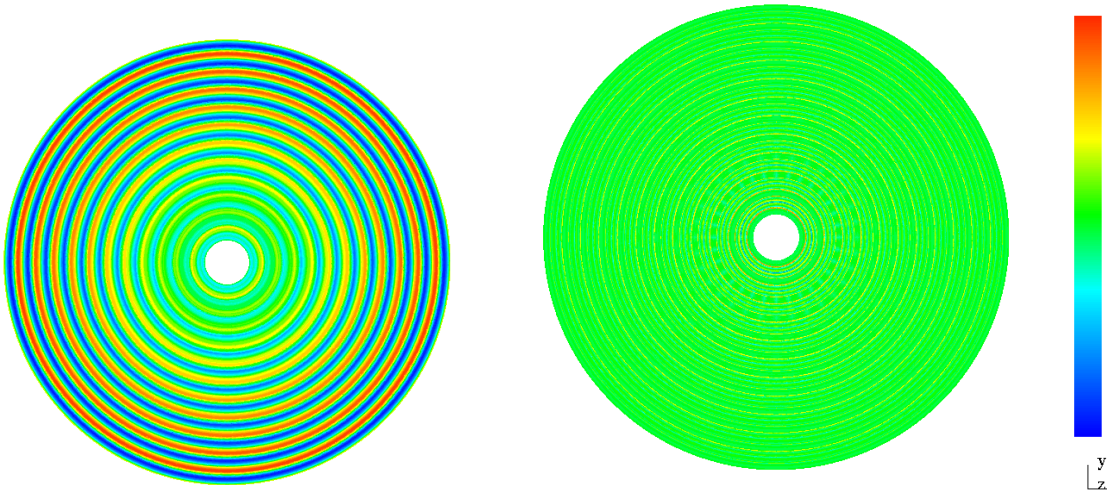

(a) Continuous Galerkin method u_r error. (b) DPG method u_r error.

Figure 1: Radiating cylinder problem, scale indicates ±5% relative error.

References

[1] J. Bramwell, L. Demkowicz, J. Gopalakrishnan, W. Qiu. A locking-free hp DPG method for linear elasticity with symmetric stresses. Technical Report 11-18, The Institute for Computational Engineering and Sciences, The University of Texas at Austin, June 2011. Submitted.

[2] L. Demkowicz, J. Gopalakrishnan. A class of discontinuous Petrov-Galerkin methods. II. Optimal test functions. *Numerical Methods for Partial Differential Equations*, **27**(1): 70–105, 2011.

[3] J. Zitelli, I. Muga, L. Demkowicz, J. Gopalakrishnan, D. Pardo, V. Calo. A class of discontinuous Petrov-Galerkin methods. Part IV: The optimal test norm and time-harmonic wave propagation in 1D. *Journal of Computational Physics*, **230**(7): 2406–2432, 2011.

MODE LOCALIZATION IN MODULAR TRUSSED STRUCTURES SUBJECT TO SLIGHTLY DISORDERED LOADING

Reyolando M. L. R. F. Brasil

Federal University of ABC, UFABC, Sto. Andre, Brazil; e-mail: reyolando.brasil@ufabc.edu.br

Keywords: mode Localization, structural dynamics, geometric stiffness

We present, in this paper, a study of vibration modes localization in structures composed of several nominally identical lightly coupled modular substructures. In an ideal perfect model, the vibration modes are global in nature, spreading to the whole set of modular substructures. In real structures, in the other hand, there are no two completely identical segments. Constructive or loading imperfections generate slight variation of the dynamic characteristics of each module. As the level of disorder grows and coupling between modules becomes lighter, there is a possibility that the resulting vibration modes change considerably in relation to the ideal perfect model. Vibration energy may become confined to a few segments, even to only one of them, as opposed to the ordered case in which it is spread over the whole structure. This is the so-called Mode Localization Phenomenon.

In this paper, we present mathematical models of long modular planar trussed structures. Light coupling is considered between the initially identical modules. We introduce a certain degree of imperfection in the system by adopting a slight variation in the nodal loading of the modules. This loading will generate a certain small variation in the global stiffness of the system as the axial loads in the bars affect their so-called Geometric Stiffness Matrices or Initial Stress Matrices. Although the eigenvalue and eigenvector extraction process is a linear one, the consideration of the loading state of the structure on its stiffness is a result of a nonlinear effect, namely, that of the geometric stiffness. This is a new contribution to the state of art as compared to previous research by the author and collaborators [1,2,3,4].

Next, we present results for a long structure, displayed in Fig. 1, composed of 5 equal equilateral triangles conected by very slender members. Upper nodes masses and loads are inicially equal.

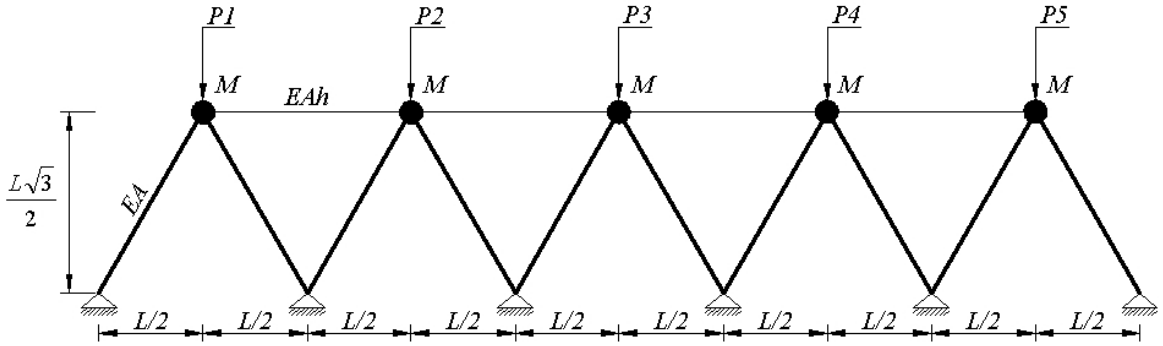

Fig. 1: the 5-degree-of-freedom model

In order to detect the influence of lightly disordered loading on the vibration modes, we initially present the first mode of the perfect model, in Fig. 2, normalized in such way as to make de horizontal displacement of the fist mass equal to one. Then, a very slight variation is introduced in the upper nodes loads so that they are no long exactly equal, keeping the masses identical. The effect in the geometric stiffness radically change the mode as displayed in Fig. 3. Vibraton energy is localized in a few of the substructures while the others experience small motions. This phenomenon suggests possible use as a vibration control device.

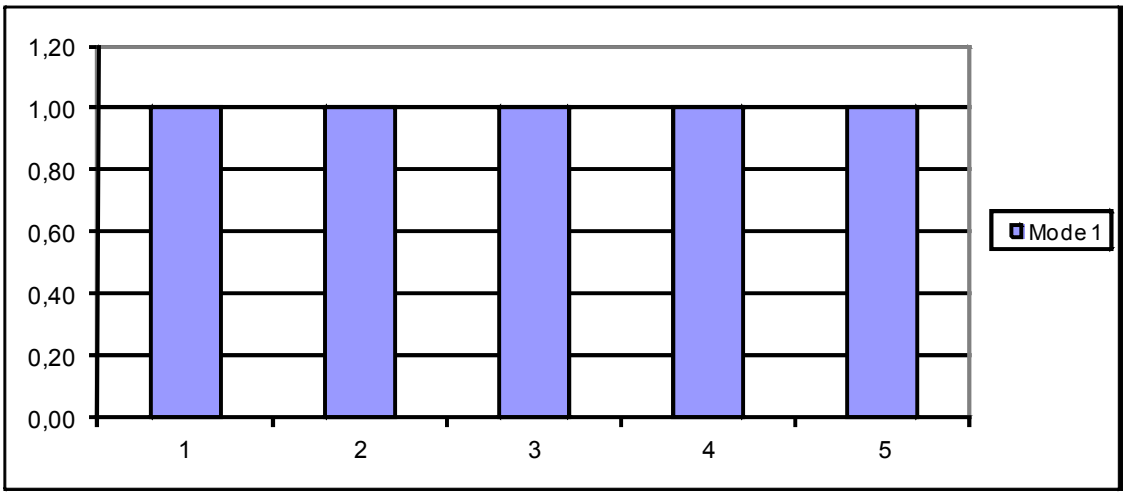

Fig. 2: First mode, perfect model

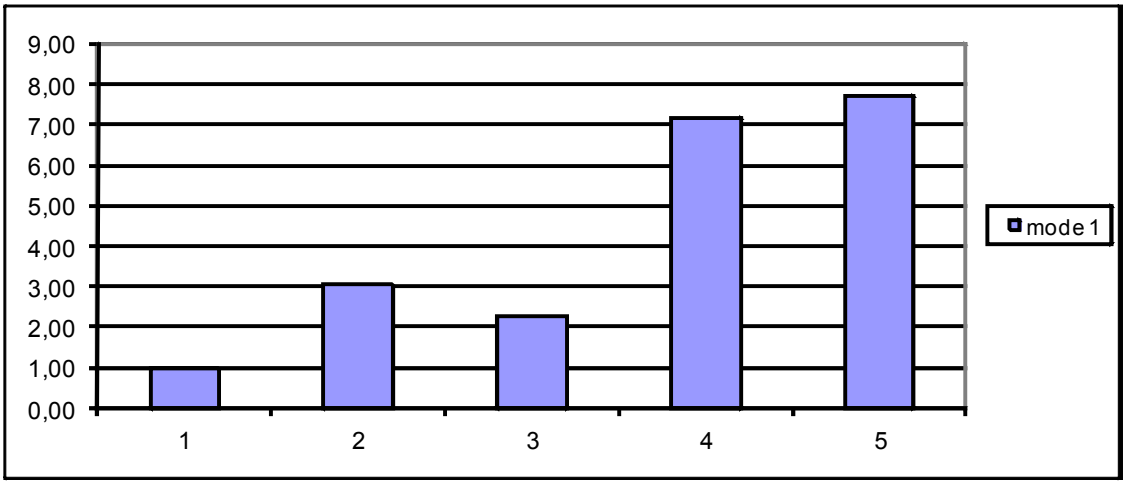

Fig. 3: First mode, imperfect model

Acknowledgement

We acknowledge support by CNPq and CAPES, all Brazilian research funding agencies.

References

[1] R. Brasil, M. Hawwa. The Localization of Buckling Modes in Nearly Periodic Trusses. *Computers and Structures*, **56**: 927–932, 1995.
[2] M. Hawwa, R. Brasil. Vibration Confinement in Trusses. *Journal of Engineering Mechanics - ASCE*, **122**: 286–290, 1996.
[3] R. Brasil, C. Mazzilli. Influence of Loading on Mode Localization in Periodic Structures. *Applied Mechanics Reviews*, **48**: 132–137, 1995.
[4] J. Balthazar, R. Brasil. On Nonlinear Normal Modes of a 2-Dof Model of a Structure with Quadratic Nonlinearities. *Journal of Sound and Vibration*, **182**: 659–664, 1995.

S-WAVE COUPLING IN HETEROGENEOUS ANISOTROPIC MEDIA

Petr Bulant and Luděk Klimeš

Department of Geophysics, Faculty of Mathematics and Physics,
Charles University in Prague, Czech Republic; http://sw3d.cz

Keywords: S-wave coupling, anisotropy, heterogeneous media, coupling ray theory

Traditionally, there are two different high–frequency asymptotic ray theories: the *isotropic ray theory* assuming equal velocities of both S waves, and the *anisotropic ray theory* assuming both S waves strictly decoupled. In the isotropic ray theory, the S–wave polarization vectors do not rotate about the ray, whereas in the anisotropic ray theory they may rotate rapidly about the ray.

In weakly anisotropic models, at moderate frequencies, the S–wave polarization vector tends to remain unrotated about the ray, but is partly attracted by the rotation of the eigenvectors of the Christoffel matrix. The intensity of the attraction increases with frequency. This behaviour of the S–wave polarization vector is described by the *coupling ray theory* proposed by Coates & Chapman in [1]. The coupling ray theory is applicable at all degrees of anisotropy, from isotropic models to considerably anisotropic ones. The frequency–dependent coupling ray theory is the generalization of both the zero–order isotropic and anisotropic ray theories and provides continuous transition between them. The coupling ray theory is particularly important for calculating S waves at degrees of anisotropy and frequencies typical in seismic exploration and structural seismology on all scales, because the isotropic ray theory does not describe the two S waves from the principle, and the anisotropic ray theory often fails to determine correct S–wave polarization.

Both S waves can be calculated along a single reference ray. The numerical algorithm for calculating the frequency–dependent complex–valued S–wave polarization vectors of the coupling ray theory is described in [2] and [3]. For a concise overview of the coupling ray theory refer to [4].

S–wave coupling decreases and S–wave splitting increases with increasing anisotropy and frequency. This behaviour is illustrated in Figure 1 in similar elastic media QIH, QI, QI2 and QI4 of different degrees of anisotropy. The vertically heterogeneous 1–D anisotropic model QI (model WA rotated by 45°) was used by Pšenčík & Dellinger [5] for comparing the coupling–ray–theory synthetic seismograms with the reflectivity method. For a description of models QI, QI2 and QI4 and measurement configuration, refer to [6]. For weak anisotropy, the change of polarization with increasing anisotropy is indicated by a clear increment of the transverse amplitudes in the two upper models. The clear development of S–wave splitting, if anisotropy is increased further, can be observed in the two bottom models.

Acknowledgements

The research has been supported by the Grant Agency of the Czech Republic under contract P210/10/0736, by the Ministry of Education of the Czech Republic within research project MSM0021620860, by the European Commission under contract FP7-PEOPLE-IAPP-2009-230669 (project AIM), and by the members of the consortium "Seismic Waves in Complex 3–D Structures" (see "http://sw3d.cz").

References

[1] R.T. Coates, C.H. Chapman. Quasi–shear wave coupling in weakly anisotropic 3-D media. *Geophys. J. int.*, **103**, 301–320, 1990.

[2] P. Bulant, L. Klimeš. Numerical algorithm of the coupling ray theory in weakly anisotropic media. *Pure appl. Geophys.*, **159**, 1419–1435, 2002.

[3] L. Klimeš. Common–ray tracing and dynamic ray tracing for S waves in a smooth elastic anisotropic medium. *Stud. geophys. geod.*, **50**, 449–461, 2006.

[4] V. Červený, L. Klimeš, I. Pšenčík. Seismic ray method: Recent developments. *Advances in Geophysics*, **48**, 1–126, 2007.

[5] I. Pšenčík, J. Dellinger. Quasi–shear waves in inhomogeneous weakly anisotropic media by the quasi–isotropic approach: A model study. *Geophysics*, **66**, 308–319, 2001.

[6] P. Bulant, L. Klimeš. Numerical comparison of the isotropic–common–ray and anisotropic–common–ray approximations of the coupling ray theory. *Geophys. J. int.*, **175**, 357–374, 2008.

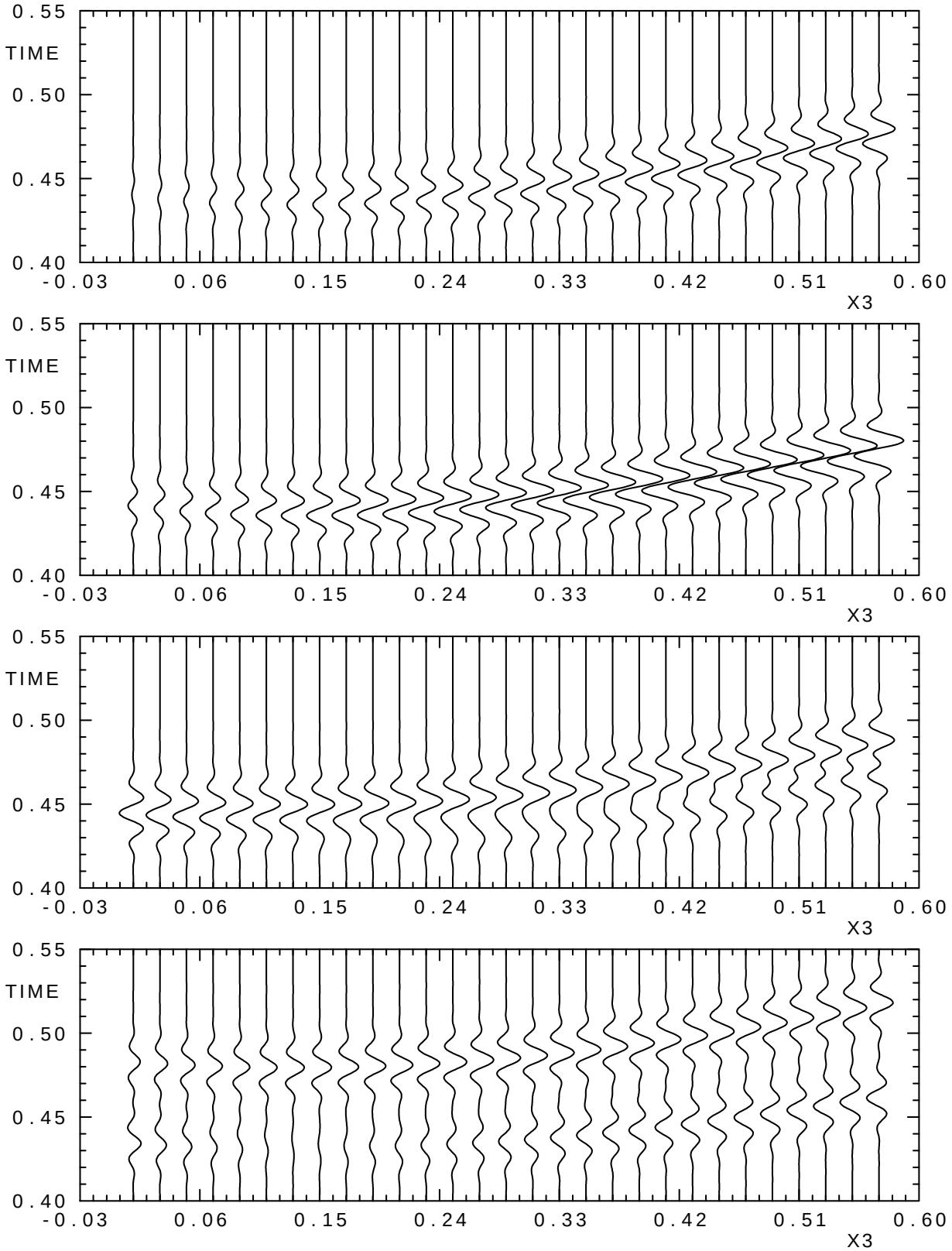

Figure 1: Coupling–ray–theory seismograms in similar elastic media of different degrees of anisotropy. Anisotropy increases from the top to the bottom in the ratio 1:2:4:8. Only the second (transverse) component is shown. This component vanishes in the analogous isotropic medium. See the change of polarization indicated by clear increment of transverse amplitudes in the two upper media, and the clear development of S–wave splitting in the two bottom media.

INFLUENCE OF PRINCIPAL MATERIAL DIRECTIONS OF A THIN COMPOSITE STRUCTURE ON RAYLEIGH-EDGE WAVE VELOCITY

Jan Červ[1], Jiří Plešek[1]

[1]Institute of Thermomechanics AS CR, v.v.i., Prague, Czech Republic; e-mail: cerv@it.cas.cz

Keywords: Rayleigh waves, thin composite structure, linear elastodynamics, plane state of stress

Introduction

The paper is concerned with Rayleigh wave propagation along an edge of a thin composite structure. The first author of the paper has studied the considered problem by finite element and experimental approaches [1]. The aim of the paper is to study the above problem by analytic approach. The analytic solution is based on two approaches: the first, the classic one, very often used in isotropic media [2] and the second, based on the Stroh formalism [3].

Problem formulation

We consider a thin semi-infinite composite structure. The kind of the composite material in mind is one in which a matrix material (e.g.epoxy resin) is reinforced by strong stiff fibres (e.g. carbon fibres) which are systematically arranged in the matrix. The fibres are considered to be long compared to their diameters and the fibre spacing, and to be densely distributed, so the fibres form a substantial proportion of the composite. Since the fibres are systematically orientated, a composite of this kind has strong directional properties, thus macroscopically for sufficiently long wavelength it can be regarded as a homogeneous orthotropic material. It is also assumed that composite thickness is small compared to the shortest wavelength taken into account. Under these conditions one can consider the composite structure as an orthotropic solid in the state of plane stress. The principal directions of orthotropy often do not coincide with coordinate directions that are geometrically natural to the solution of the problem. Therefore it is assumed that body axes x_1, x_2 form a nonzero angle ϑ with principal material axes X_1, X_2 as shown in Fig.1. Third axis x_3 is identical with material axes X_3 and constitutes axis of rotation of principal material axes X_1 , X_2 from body axes x_1 , x_2.

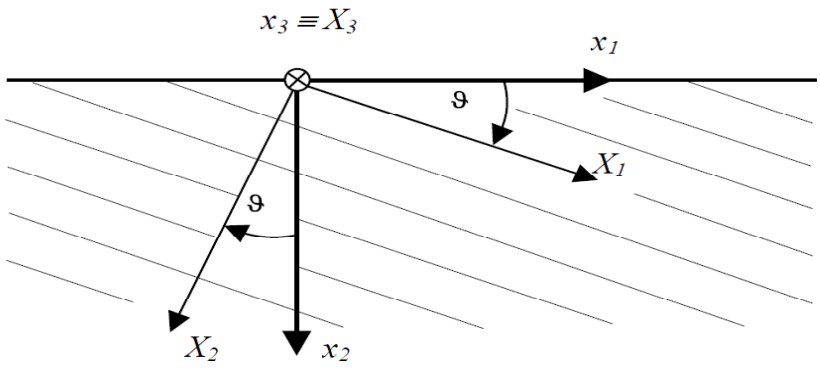

Figure 1. A thin semi-infinite orthotropic medium

The propagation of a Rayleigh wave along the free edge of a semiinfinite 2D orthotropic medium is modeled. It is supposed that corresponding displacement field has the form

$$u_j(x_1, x_2, t) = U_j(k \cdot x_2) \cdot e^{i \cdot k(x_1 - c \cdot t)}, \ (j = 1,2), \tag{1}$$

where k is the wave number and c is the wave velocity. It means that the wave is propagated in the direction of x_1 and its variation in the direction x_2 is not stated explicitly. The boundary conditions of the problem are: the edge $x_2=0$ is free of tractions, vanishing displacement (or stress) components at infinity, i.e. at $x_2 \to \infty$.

Solution

Classical method of the analytic solution leads to an implicit secular equation for Rayleigh wave velocity c_R. For the solution of implicit equation $F(c, p_j(c, \vartheta), \vartheta) = 0$ it is necessary for any ϑ to precompute some roots $p_j(c)$ of characteristic quartic equation. It is rather tedious work. The method based on the Stroh formalism leads to explicit quartic secular equation that depends on material constants only.

Results

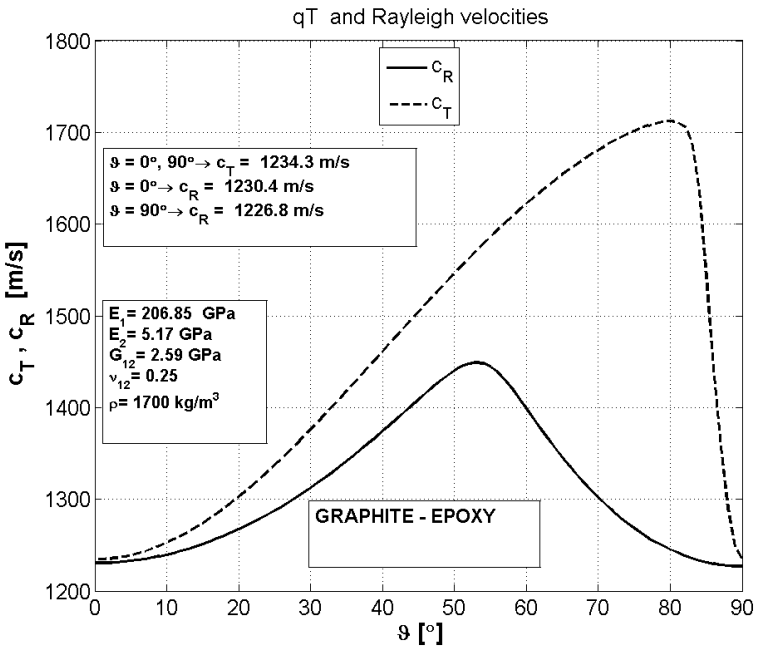

Figure 2. Wave velocities c_R (solid line) and c_T (dashed) versus orientation ϑ of principal material axes

Acknowledgement

This work was supported by the grant agency GA CR, projects P101/11/0288 and 101/09/1630 within the framework of project AV0Z20760514.

References

[1] J.Cerv, T.Kroupa, J.Trnka. Influence of principal material directions of thin orthotropic structures on Rayleigh-edge wave velocity. *Composite Structures,* **92**: 568-577, 2010.
[2] J.D. Achenbach. *Wave Propagation in Elastic Solids.* North Holland, Amsterdam, 1975.
[3] K. Tanuma. Stroh Formalism and Rayleigh Waves. *Journal of Elasticity,* **89**: No 1-3, 5-154, 2007.

A NEW FAST MULTIPOLE METHOD FOR 3D ELASTODYNAMICS USING THE HALF-SPACE FUNDAMENTAL SOLUTIONS

Stéphanie Chaillat, Marc Bonnet

POEMS, ENSTA, Paris, France; e-mail: {stephanie.chaillat; marc.bonnet}@ensta-paristech.fr

Keywords: elastodynamics, boundary element method, fast multipole method

The boundary element method (BEM) is well suited to the computation of seismic wave propagation in that only the domain boundaries (and possibly interfaces) are discretized, leading to a reduced number of degrees of freedom (DOFs). In traditional BE implementation the dimensional advantage with respect to domain discretization methods is offset by the fully-populated nature of the BEM coefficient matrix, with set-up and solution times rapidly increasing with the problem size N. Considerable speedup of solution time and decrease of memory requirements have been achieved through the development of the Fast Multipole Method (FMM). The goal of the FMM is to speed up the matrix-vector product computation at each GMRES iteration. This is achieved by (i) using a multipole expansion of the relevant fundamental solution, which (unlike in the standard BEM) allows to re-use element integrals for all collocation points, and (ii) defining a (recursive, multi-level) partition of the region of space enclosing the domain boundary of interest into cubic cells, allowing to optimally cluster influence computations according to the ratio between cluster size and distances between two such clusters. The FMM-accelerated BEM achieves substantial savings in both CPU time and memory.

Methodology. This contribution is concerned with improving the efficiency of the frequency-domain elastodynamic FM-BEM applied to semi-infinite media. The idea is to formulate the boundary integral equation with the elastic half-space fundamental solutions that satisfy a traction-free boundary condition, instead of the usual elastic full-space fundamental solutions as in [2], thus avoiding any BEM discretization on the free surface. The integral equation for $\boldsymbol{x} \in \partial\Omega$ has the form

$$c_{ik}(\boldsymbol{x})u_i(\boldsymbol{x}) = \int_{\Gamma_1} \left[(\boldsymbol{U}^{\mathrm{HS}})_i^k(\boldsymbol{x},\boldsymbol{y})t_i(\boldsymbol{y}) - (\boldsymbol{T}^{\mathrm{HS}})_i^k(\boldsymbol{x},\boldsymbol{y})u_i(\boldsymbol{y}) \right] \mathrm{d}S_y, \tag{1}$$

where Γ_1 is a surface embedded in the lower half-space $y_3 \leq 0$ (see Fig. 1), $\boldsymbol{u}$ and $\boldsymbol{t}$ denote the displacement and traction vector on the boundary, $\boldsymbol{U}^{\mathrm{HS}}(\boldsymbol{x},\boldsymbol{y})$ and $\boldsymbol{T}^{\mathrm{HS}}(\boldsymbol{x},\boldsymbol{y})$ denotes the half-space elastodynamic fundamental solutions, which satisfies a traction-free condition on the free surface $y_3 = 0$ and the free term $c_{ik}(\boldsymbol{x})$ is equal to $0.5\delta_{ik}$ in the usual case where $\partial\Omega$ is smooth at $\boldsymbol{x}$. However, unlike

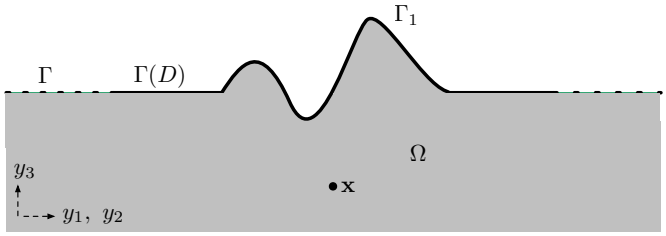

Figure 1: Notations related to the considered elastic wave propagation problem

the full-space fundamental solution, the elastic half-space fundamental solution cannot be expressed using derivatives of the Helmholtz fundamental solution or of $1/r$. As a result, multipole expansions of the elastic half-space fundamental solution cannot be obtained in a simple way, and are not currently known. In this work, an expansion of the elastic half-space fundamental solution is formulated in a form which achieves the separation of variables required by the FMM, thus enabling fast computations.

Formulation and fast evaluation of the multipole expansions. The starting point is to decompose $\boldsymbol{U}^{\mathrm{HS}}(\boldsymbol{x},\boldsymbol{y})$ (resp. $\boldsymbol{T}^{\mathrm{HS}}(\boldsymbol{x},\boldsymbol{y})$) as the sum of the elastic full-space fundamental solution $\boldsymbol{U}_\infty$ (resp. $\boldsymbol{T}_\infty$), the image full-space fundamental solution $\bar{\boldsymbol{U}}_\infty$ (resp. $\bar{\boldsymbol{T}}_\infty$) corresponding to a point force located at the mirror image $\bar{\boldsymbol{x}}$ of $\boldsymbol{x}$, and a complementary term $\boldsymbol{U}_{\mathrm{C}}$ (resp. $\boldsymbol{T}_{\mathrm{C}}$)(so that $\boldsymbol{U}^{\mathrm{HS}} = \boldsymbol{U}_\infty + \bar{\boldsymbol{U}}_\infty + \boldsymbol{U}_{\mathrm{C}}$ and $\boldsymbol{T}^{\mathrm{HS}} = \boldsymbol{T}_\infty + \bar{\boldsymbol{T}}_\infty + \boldsymbol{T}_{\mathrm{C}}$). The contributions corresponding to $\boldsymbol{U}_\infty$ and $\bar{\boldsymbol{U}}_\infty$ (resp. $\boldsymbol{T}_\infty$ and $\bar{\boldsymbol{T}}_\infty$) can be evaluated using the "standard" FMM associated with the diagonal form-based decomposition of the full-space fundamental solution [2].

Attention is therefore directed towards the contribution involving the complementary fundamental solution. A Fourier transform with respect to the two spatial coordinates parallel to the free-space is performed (similarly to that used for defining low frequency FMMs [3, 4]). A key numerical issue is concerned with the definition of an efficient numerical quadrature in Fourier space to perform the integration. Because the integrand is both singular and oscillatory, classical Gaussian quadratures would perform poorly, fail or require a large number of points. Bremer et al. [1] defined an algorithm to compute Generalized Gaussian quadratures which are well suited to integrands with more than one type of singular behavior. This procedure is used to define a new FMM for the elastic half-space fundamental solutions. The main advantage is that this quadrature is pre-computed once for all the FMM computations since the number of points depends only on the dimension of the cubic cells.

Fast Multipole Method. The product form achieved by the Fourier-space representation permits a decomposition reminiscent of the "standard" FMM associated with the diagonal form ($\boldsymbol{x}^0$ and $\boldsymbol{y}^0$ denote local origins of $\boldsymbol{x}$-clusters and $\boldsymbol{y}$-clusters):

$$\boldsymbol{U}_{\mathrm{C}}(\boldsymbol{x},\boldsymbol{y}) = \frac{1}{\mu k_{\mathrm{S}}^2} \sum_{a,b=\mathrm{L,T}} \int_0^{+\infty} \int_0^{2\pi} e^{\mathrm{i}k(\cos\alpha(y_1-y_1^0)+\sin\alpha(y_2-y_2^0))} e^{s_a(y_3-y_3^0)}\, \boldsymbol{\mathcal{U}}_{ab}(k,\alpha,\boldsymbol{x}^0,\boldsymbol{y}^0)$$
$$e^{\mathrm{i}k(\cos\alpha(x_1^0-x_1)+\sin\alpha(x_2^0-x_2))} e^{s_b(x_3-x_3^0)}\ \mathrm{d}\alpha\mathrm{d}k \quad (2)$$

where the $\boldsymbol{\mathcal{U}}_{ab}(k,\alpha,\boldsymbol{x}^0,\boldsymbol{y}^0)$ are transfer (tensor) functions. Similar expressions are obtained for $\boldsymbol{T}_{\mathrm{C}}$. The evaluation of single-layer potentials involves three successive typical operations: (i) computation of multipole moments, (ii) transfer and (iii) evaluation at observation points.

Results. The accuracy and numerical efficiency of the Generalized Gaussian quadratures to compute (2) is shown. Then, the accuracy and numerical efficiency of the complete FMM based on the elastic half-space fundamental solution (which does not require meshing the free surface) is compared to the accuracy and efficiency of the FMM based on the elastic full-space fundamental (which requires meshing the free surface) solutions on seismic-oriented canonical problems.

References

[1] J. Bremer, Z. Gimbutas, V. Rokhlin. A nonlinear optimization procedure for generalized gaussian quadrature. *SIAM J. Sci. Comput.*, **32**: 1761-1788, 2010.

[2] S. Chaillat, M. Bonnet, J. F. Semblat. A multi-level fast multipole BEM for 3-D elastodynamics in the frequency domain. *Computer Methods in Applied Mechanics and Engineering*, **197**: 4233-4249, 2008.

[3] E. Darve, P. Havé. Efficient fast multipole method for low-frequency scattering. *Journal of Computational Physics*, **197**: 341-363, 2004.

[4] L. Greengard, J. F. Huang, V. Rokhlin, S. Wandzura. Accelerating fast multipole methods for the Helmholtz equation at low frequencies. *IEEE Computational Science Engng.*, **5**: 32-38, 1998.

A METHOD FOR COMPUTATION OF WAVE PROPAGATION: EXTENSION TO TWO AND THREE-DIMENSIONAL PROBLEMS

S. S. Cho[1], K. C. Park[2,3], H. Huh[4]

[1]Korea Atomic Energy Research Institute, 989-111 Daedeok-daero, Yuseong-gu, Daejeon 305-353, Korea
[2]Department of Aerospace Engineering Sciences, University of Colorado at Boulder, CO 80309-0429, USA, and
[3]Department of Ocean Systems Engineering, KAIST, Daejeon 305-701, Republic of Korea, e-mail: kcpark@colorado.edu
[4]Department of Mechanical Engineering, KAIST, Daejeon 305-701, Republic of Korea

Keywords: explicit time integrator, wave propagation, spurious oscillations

Introduction

The present work presents an extension of the previously presented algorithm [1] for computations of discontinuous wave propagation in one-dimensional heterogeneous solids to two and three-dimensional heterogeneous problems. In the present extension of the algorithm [1] for two and three-dimensional problems, two-level integration operations are carried out. An element level integration is first carried out for treating different wave speeds within each element as two and three-dimensional elements solids admit shear waves, bending waves and extension waves propagating with different speeds. Waves propagating across different heterogeneous materials are then treated afterwards.

Specifically, we partition the total displacement into the longitudinal and shear wave components as

$$\mathbf{u} = \mathbf{u}_L + \mathbf{u}_S, \quad \mathbf{u}_L = \mathbf{D}_L \mathbf{u}, \quad \mathbf{u}_S = \mathbf{D}_S \mathbf{u} \tag{1}$$

where the subscripts (L,S) designate the longitudinal and shear components, respectively.

A key idea of the present extension of the method [1] to multidimensional wave propagation problems is that the decomposition operators $(\mathbf{D}_L, \mathbf{D}_S)$ are derived to satisfy the following properties for rectangular elements:

$$\begin{aligned}
\text{Partition of unity: } & \mathbf{D}_L + \mathbf{D}_S = \mathbf{I}, \\
\text{Projector property: } & \mathbf{D}_S^T \mathbf{D}_S = \mathbf{D}_S, \quad \mathbf{D}_L^T \mathbf{D}_L = \mathbf{D}_L \\
\text{Symmetry: } & \mathbf{D}_L^T = \mathbf{D}_L, \quad \mathbf{D}_S^T = \mathbf{D}_S \\
\text{Orthogonality: } & \mathbf{D}_L \, \mathbf{D}_S = \quad \mathbf{D}_S \, \mathbf{D}_L = \mathbf{0} \\
\text{Element mass commutability: } & \mathbf{D}_L^T \mathbf{M} = \mathbf{M}\mathbf{D}_L, \quad \mathbf{D}_S^T \mathbf{M} = \mathbf{M}\mathbf{D}_S \\
\text{Element mass orthogonality: } & \mathbf{D}_L^T \mathbf{M}\mathbf{D}_S = \mathbf{M}\mathbf{D}_L \mathbf{D}_S = \mathbf{0} \\
\text{Element stiffness orthogonality: } & \mathbf{D}_L^T \mathbf{K}\mathbf{D}_S = \mathbf{D}_S^T \mathbf{K}\mathbf{D}_L = \mathbf{0} \\
\text{Element stiffness decomposition: } & \mathbf{K} = \mathbf{K}_L + \mathbf{K}_S, \\
& \mathbf{K}_L = \mathbf{D}_L^T \mathbf{K}\mathbf{D}_L, \quad \mathbf{K}_S = \mathbf{D}_S^T \mathbf{K}\mathbf{D}_S
\end{aligned} \tag{2}$$

where $(\mathbf{M}, \mathbf{K})$ are elemental mass and stiffness matrices, respectively.

The first example problem is a rectangular plane strain problem subjected to shear impulse as shown in Fig. 1. Note the significantly improved performance with the decomposed stiffness matrices for which the spurious oscillations are almost gone, thus illustrating the importance of decomposing the longitudinal and shear waves.. The second example problem is a plane strain domain with a crack in the middle subjected to a uniform Heaviside initial velocity as shown on the left in Fig. 2.

When the initial P-wave reaches the symmetry line, the reflection gives rises to the reflected P-wave, the S-wave, the von Schmidt wave and the R-wave as illustrated in Fig. 2. Also shown in Fig. 2 are the contour plots of the principal shear stresses at a time when the principal shear stress at the crack tip is at its peak. The result yielded by the central difference method (shown at the second to the far right) with the time step corresponding to the half of the Courant stability limit is accompanied with ripples, a clear sign of spurious oscillations. On the

other hand, with the same time step, the principal shear stress contour plot yielded by the present method (shown on the far right) shows no detectable spurious oscillations as evidenced by smooth contour surface.

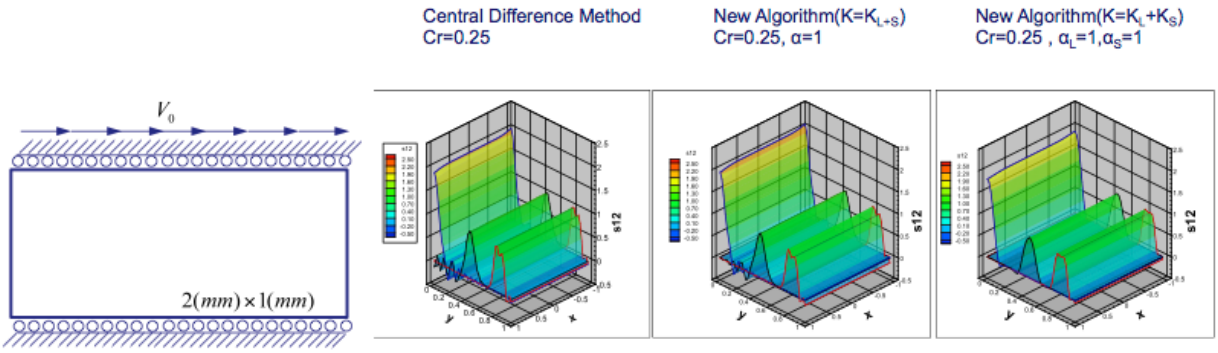

Figure 1: Performance of three algorithms for pure shear wave propagation. *Left:* Central difference method. *Center:* New algorithm without decomposition. *Right:* New algorithm with decomposition stiffness matrices

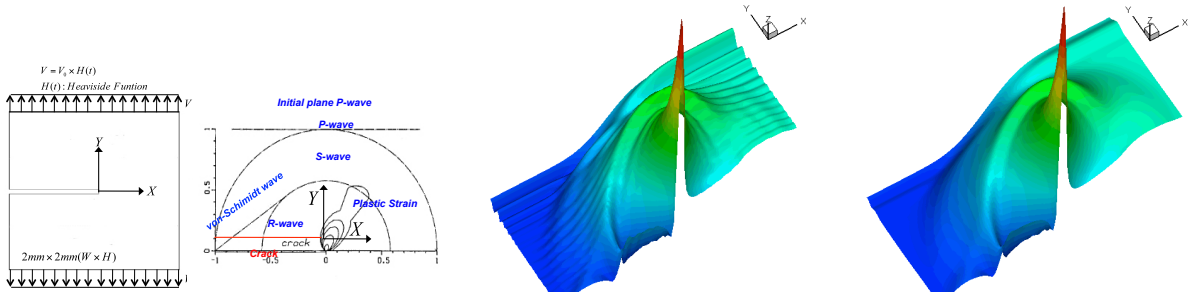

Figure 2: Plane strain rectangular model problem with initial crack tip subjected to a Heaviside initial velocity input. *Far right:* the model problem. *Second to the far right:* Representative reflecting waves consisting of P, S, R and von Schmidt wave components. *Second to the the far right:* Principal shear stress contour plot obtained by the central difference method with $\Delta t = 0.5\Delta x/c$ where c is the longitudinal wave speed. *Far right:* Principal shear stress contour plot obtained by the present method with $\Delta t = 0.5\Delta x/c$.

Details of the new algorithm and its performance will be presented at the Colloquium.

Acknowledgement

The present study has been partially supported by WCU (World Class University) Program through the Korea Science and Engineering Foundation funded by the Ministry of Education, Science and Technology, Republic of Korea (Grant Number R31-2008-000-10045-0). The third author has been partially supported by the Brain Korea 21 Program (KAIST Valufacture Institute of Mechanical Engineering), Ministry of Education, Science and Technology.

References

[1] K. C. Park, S. J. Lim, H. Huh. A method for computation of discontinuous wave propagation in heterogeneous solids: basic algorithm description and application to one-dimensional problems. International Journal for Numerical Methods in Engineering, Published online: 8 FEB 2012. DOI: 10.1002/nme.4285

SURFACE AND INTERFACE WAVES IN PIEZOELECTRICS WITH SPATIAL DISPERSION

Bernard Collet

Institut Jean le Rond d′Alembert, CNRS UMR 7190,
Université Pierre et Marie Curie, 4 place Jussieu 75252 Paris Cedex 05, France;
e-mail: bernard.collet@upmc.fr

Keywords: shear horizontal surface waves, electric field gradient, piezoceramics, dispersion relation, very high-frequency

In general, piezoelectrics modeling needs the consideration of an additional state variable to the strain, which usually is taken to be the electric field vector. Its energetically conjugate quantity is the electric displacement. An other possibility is to choose the (diplole) polarization vector as independent variable, in this case the conjugate variable is a local electric field. A standard extension to the direction the weak nonlocality concists in the inclusion in the stored energy density of the first gradient of electric field or polarization vector. In the first case, the conjugate to the electric field gradient quantity is the electric quadrupole symmetric tensor [1, 2], a well-defined variable in solid state physics.

According to lattice dynamics gradient theories are closer to lattice dynamics than classical continuum approach. They are still applicable when the characteristic length of a problem is so small that classical theories are not valid. In elastodynamics, different from classical theories, first gradient theories predict that short bulk and surface waves are dispersive, which agrees with lattice dynamics. The resulting theories are called dielectrics (or piezoelectrics) with spatial dispersion. Gradient theories also have important consequences in elastostatics with singularities, eg., defects,

The motivation of this work is to explore the effects of the electric field gradient into the constitutive laws for piezoelectric crystals by analyzing the shear horizontal waves propagating over a half-space or at interface between two half-spaces. Specifically, the piezoelectric materials possess 2mm, 4mm or 6mm symmetry and the boundary (or interface) is orthogonal at basal plane. The secular equations are obtained explicitly not only for metallized boundary conditions, but also for others types such as: unelectroded surface and air gap boundary conditions.

The obtained frequency equations show clearly that the gradient effects makes the surface and interface waves dispersive. In contrast to these, the well known Bleustein-Gulyaev [3] surface waves and Maerfeld-Tournois [4] interface surface waves are non-dispersive according to the classical modeling of linear piezoelectricity which neglects the gradient effects. The generalized slowness curves and dispersion curves for a set of ferroelectric crystals and piezoceramics as well as fields spatial distributions in half spaces are obtained and discussed. In particular, the results show as for others gradient theories a characteristics length exists which may have significant size effects for microacoustic-devices operating at very high-frequency and short wavelength.

References

[1] C.B. Kafadar. Theory of multipoles in classical electromagnetism. *International Journal of Engineering Science*, **9**: 853–881, 1971.

[2] H. Demiray, A.C. Eringen. On the constitutive relations of polar elastic dielectrics. *Letters in Applied Engineering Science*, **1**: 517–527, 1973.

[3] D. Royer, E. Dieulesaint. *Elastic waves in solids I, free and guided propagation*. Springer-Verlag, Berlin, 2000.

[4] C. Maerfeld, P. Tournois Pure shear surface wave guided by the interface of two semi-infinite media. *Applied Physics Letters*, **19**: 117–118, 1971.

THE FORMATION OF NONLINEAR MAGNETOELASTIC WAVES

Vladimir I. Erofeyev[1], Alexey Malkhanov[2]

[1,2]A.A. Blagonravov Mechanical Engineering Institute RAS., Nizhny Novgorod, Russia;
e-mail: [1]erf04@sinn.ru, [2]alexey.malkhanov@gmail.com

Keywords: magnetoelasticity, deformation, magnetic field

Electromagnetoelasticity which studies the interaction of deformation and electromagnetic fields in materials and constructions is a positive example of the development of the theory of conjugate fields of various physical natures. The first researches were initiated by the problems of geophysics. There was the need to describe the wave dynamics of the deep layers of the Earth taking into account its conductivity and interaction with geomagnetic field. In the modern electromagnetoelasticity which has various physical, technical and technological applications the following branches can be underlined: magnetoelasticity and magnetothermoelasticity of conductive non-ferromagnetic body in a constant magnetic field; magnetoelasticity of magnetoactive medium and electroelasticity of piezoelectricand electrostrictive medium. The current research was carried out in frames of the first branch. The main attention was paid to the problem of nonlinear waves formation under influence of a constant magnetic field.

The system of magnetoelasticity equations looks as follows [1]:

$$\rho \frac{\partial^2 \mathbf{u}}{\partial t^2} = \left(K + \frac{1}{3} G \right) \text{grad div } \mathbf{u} + G\Delta \mathbf{u} + \mathbf{F}_{nonlinear} + \mu_e \left(\text{rot } \mathbf{H} \times \mathbf{H} \right),$$

$$\frac{\partial \mathbf{H}}{\partial t} = \text{rot} \left[\frac{\partial \mathbf{u}}{\partial \tau} \times \mathbf{H} \right] + \frac{1}{\mu_e \sigma} \Delta \mathbf{H}.$$

Where $\mathbf{u}$ – displacements vector; K, G – compression and shear constants; ρ – density of a material; t – time, $\mathbf{H}$ – intensity of magnetic field, σ – conductivity, μ_e – permeability, $\mathbf{F}_{nonlinear}$ – includes items resulted from considering of elastic non-linearity.

In the research we studied the longitudinal wave formation in a rod (1 – dimensional media), the wave formation in a plate (2 – dimensional media) as well as magnetoelastic wave formation in 3 – dimensional media. For each particular case we obtained evolutionary equations by introducing small parameter into the magnetoelasticity system. In some cases the evolutionary equations represent well known model equations of nonlinear wave dynamics. Thus, in case of a rod the system reduces to one of the following equations: Korteweg-de Vries-Burgers equation for a rod with finite conductivity, Korteweg-de Vries equation for ideal conductive rod and Riemann equation for ideal conductive rod when we does not take into account the kinetic energy of transverse deformations. For the magnetoelastic Riemann wave we found that the external magnetic field stabilizes the wave, increasing the time of formation of a sharp front.

If the object is considered a plane then evolutionary equation combines the 2-dimentional model equations of Khokhlov-Zabolotskaya-Kuznetsov and Kodomtsev-Petviashvili.

For 3-dimentional media the evolutionary equation represents 3-dimentional Khokhlov-Zabolotskaya-Kuznetsov equation.

As a result of the analytical studies and numerical simulations we demonstrated the possibility of the formation of intense space-localized magnetoelastic waves: strain solitary waves in a rod, quasiplanar two-dimensional wave beams in a plate and quasiplanar three-dimensional wave beams in an elastic conductive medium.

The dependences of wave parameters (amplitude, velocity, and width) on the magnitude and spatial orientation of the external magnetic field were identified. They show that the properties of localized waves can be controlled with the help of a magnetic field.

Acknowledgement

This work was supported by the grant project RFBR # 11-08-97066.

References

[1] V.I. Erofeyev. *Wave Processes in Solids with Microstructure*, World Scientific, Singapore, 2003.

SPECTRAL MEASURES, DISPERSIVE ESTIMATES AND PROPAGATION OF ACOUSTIC WAVES IN INCOMPRESSIBLE LIMITS

Eduard Feireisl

Institute of Mathematics AS CR, v.v.i., Prague, Czech Republic; e-mail: feireisl@math.cas.cz

Keywords: spectral measure, dispersive estimates, incompressible limit

Many well accepted models in continuum mechanics arise as a result of scaling of more complicated primitive systems, see Klein et al. [4], Sideris and Thomases [6], among others. A typical example is the so-called *incompressible limit*, where, roughly speaking, the acoustic waves present in the original primitive system are suppressed (filtered) in the course of the limit process. In many cases it is customary to say that the acoustic effects "disappear" because the speed of sound in the media becomes very high, or, equivalently, the characteristic speed is very low, and dispersion prevails. In rigorous analysis of this process, we are interested in the way how this phenomena really occur, and what is the rate in which the acoustic wave are anihilated. This leads to the study of *acoustic equations* in the general form

$$\varepsilon \partial_t r + \nabla \cdot \vec{v} = f_1,$$
$$\varepsilon \partial_t \vec{v} + \nabla r = \vec{f_2},$$

where ε is a positive small parameter. Writing the Helmholtz decomposition of $\vec{v} = \vec{w} + \nabla \Phi$, where $\vec{w}$ is a solenoidal field, we obtain a wave equation

$$\varepsilon \partial_t r + \Delta \Phi = g_1, \tag{1}$$

$$\varepsilon \partial_t \Phi + \Phi = g_2 \tag{2}$$

for the *acoustic potential* Φ. The problem is supplemented with the Neumann condition

$$\nabla \Phi \cdot \vec{n}|_{\partial \Omega} = 0$$

imposed on the boundary of the physical space $\Omega \subset R^3$.

A short inspection of Duhamel's formula yielding solutions of system (1), (2) reveals that all information is provided by the quantity

$$\exp\left(\mathrm{i} \frac{t}{\varepsilon} \sqrt{-\Delta_N} \right),$$

where the symbol $-\Delta_N$ denotes the self-adjoint realization of the Neumann Laplacean in the Hilbert space $L^2(\Omega)$. In the incompressible limits, the property of interest is local decay of acoustic waves provided by the so-called dispersive estimates. Here "local" means in both physical and frequency space. This amounts to showing decay, for $\varepsilon \to 0$, of

$$\varphi G(-\Delta_N) \exp\left(\mathrm{i} \frac{t}{\varepsilon} \sqrt{-\Delta_N} \right),$$

where the function φ has compact support in the physical domain Ω, while G is compactly supported in the frequency space, meaning in the interval $[0, \infty)$ that contains the spectrum of $-\Delta_N$. As a necessary condition for dispersion is the absence of point spectrum - true eigenvalue and eigenfunctions - we focus on the analysis on *unbounded* domains.

In this contribution we discuss the spectral properties of the operator $-\Delta_N$ that influence the dispersive decay. Qualitatively, we may distinguish several level of decay, related to the properties of the associated family of *spectral measures* (cf. [2], Last [5]):

- *Strichartz estimates* provide a global information and local decay of optimal order $\sqrt{\varepsilon}$ without cutting the frequency domain. They require very restrictive conditions to be imposed on the underlying spatial domain, if available, see Chemin et al. [1].
- Estimates based on *Limiting Absorption Principle* provide local decay of optimal order $\sqrt{\varepsilon}$ based on some information on the resolvent operator. They are local with respect to the spectrum of $-\Delta_N$.
- Estimates based on *RAGE theorem* are optimal from the point of view of necessary hypotheses, however, provide only *uniform* decay without explicit knowledge of the rate in terms of ε.

We shall discuss the above phenomena from the point of view of the family of spectral measures associated to the Neumann Laplacean Δ_N. In particular, we are interested in the explicit dependence of the decay rate on the geometrical properties of the underlying spatial domain. We discuss several applications of the method to singular limits arising in fluid mechanics. We focus on problems, where the geometry of the underlying physical space changes in the limit process, for instance, the domain contains a number of small holes with radius tending to zero in the asymptotic limit. In such a way, we derive a correct formulation of several well established models, like the so-called Oberbeck-Boussinesq approximation, on unbounded domains, cf. [3].

Further applications of the results to problems arising in homogenization, optimal shape design, and problems involving more complex systems will be addressed.

Acknowledgement

This work was supported by the grant project GAČR 201/09/0917.

References

[1] J.-Y. Chemin, B. Desjardins, I. Gallagher, E. Grenier. *Mathematical geophysics*, volume 32 of *Oxford Lecture Series in Mathematics and its Applications*. The Clarendon Press Oxford University Press, Oxford, 2006.

[2] E. Feireisl. Incompressible limits and propagation of acoustic waves in large domains with boundaries. *Commun. Math. Phys.*, **294**:73–95, 2010.

[3] E. Feireisl, A. Novotný. *Singular limits in thermodynamics of viscous fluids*. Birkhäuser-Verlag, Basel, 2009.

[4] R. Klein, N. Botta, T. Schneider, C.D. Munz, S. Roller, A. Meister, L. Hoffmann, T. Sonar. Asymptotic adaptive methods for multi-scale problems in fluid mechanics. *J. Engrg. Math.*, **39**:261–343, 2001.

[5] Y. Last. Quantum dynamics and decomposition of singular continuous spectra. *J. Funct. Anal.*, **142**:406–445, 1996.

[6] T. C. Sideris, B. Thomases. Global existence for three-dimensional incompressible isotropic elastodynamics. *Comm. Pure Appl. Math.*, **60**(12):1707–1730, 2007.

SUBWAVELENGTH FOCUSING OF BROADBAND TIME-REVERSED WAVES

Mathias Fink

Institut Langevin, Ecole Supérieure de Physique et de Chimie Industrielles de la Ville de Paris,
10 rue Vauquelin, Paris, 75005, France; e-mail : mathias.fink@espci.fr

Keywords:

The origin of diffraction limit in wave physics, and the way to overcome it, can be revisited using the time-reversal mirror concept. According to time-reversal symmetry, a broadband wave can be focused both in time and space regardless of the complexity of a scattering medium. In a complex environment a time-reversal mirror acts as an antenna that uses complex environments to appear wider than it is, resulting in a refocusing quality that does not depend on the time-reversal antenna aperture. The broadband nature of time-reversed waves distinguishes them from continuous phase-conjugated waves and allows revisiting the origin of diffraction limits, suggesting new ways to obtained subwavelength focusing for broadband waves.

Two approaches will be discussed. One is related to the concept of a perfect time-reversal experiment that needs, not only to time-reverse the wavefield but also to time-reverse the source. It is the concept of an acoustic or electromagnetic "sink" that is related to the perfect absorber theory. Different strategies to build a sink have been investigated. They show the fundamental differences between a monochromatic and a broadband sink.

Another approach for broadband sub-wavelength focusing will be discussed. It consists in introducing the initial source inside a micro structured medium made of subwavelength resonators with a mean distance smaller than the used wavelengths. It will be shown that, for a broadband source located inside such metamaterials, a time-reversal mirror located in the far field radiated a time-reversed wave that interacts with the random medium to regenerate not only the propagating but also the evanescent waves required to refocus below the diffraction limit. This focusing process is very different from the one developed with superlenses made of negative index material only valid for narrowband signals. We will emphasize the role of the frequency diversity in time-reversal focusing and a modal description of the spatiotemporal focusing will be presented. It shows the super-resolution properties obtained with acoustic, elastic and electromagnetic waves.

APPLICATION OF EXPLICIT CONTACT-IMPACT ALGORITHM TO THE FINITE ELEMENT SOLUTION OF WAVE PROPAGATION PROBLEMS

Dušan Gabriel[1], Ján Kopačka[1], Jiří Plešek[1], Miran Ulbin[2]

[1]Institute of Thermomechanics AS CR, Prague, Czech Republic; e-mail: {gabriel,kopacka,plesek}@it.cas.cz
[2]Faculty of Mechanical Engineering, University of Maribor, Slovenia; e-mail: ulbin@uni-mb.si

Keywords: FEM, contact-impact, wave propagation, explicit dynamics, local contact search

In the context of the finite element method, a frictionless three-dimensional contact-impact algorithm using pre-discretization penalty formulation was proposed [1]. The method was shown to be consistent with the variational formulation of a continuum problem, which enabled easy incorporation of higher-order elements with mid-side nodes to the analysis. Local search and the penalty constraint enforcement were performed on the Gauss point level of linear/quadratic serendipity elements rather than the nodal level of a finite element mesh. Owing to a careful description of kinematics of contacting bodies when the non-linearized definition of penetration has been introduced, the displacement increments in the course of one load step were permitted to be large. Thus, the extension of the algorithm to geometrically nonlinear problems was straightforward. The algorithm proved to be robust, accurate and symmetry preserving—no master/slave surfaces had been introduced.

The indispensable part of the contact algorithm is the local search procedure which represents measuring penetration of a Gauss point through the counterpart's object surface. It is necessary first to define the outward normal and then to compute its intersection with a curved surface, establishing distance. Although appearing trivial at first glance the numerical solution process is far from being easy, especially when dealing with severely distorted surfaces. In Ref. [2] several methods for the solution of non-linear algebraic systems were thoroughly tested: the Newton-Raphson method, the least square projection, the steepest descent method, Broyden's method, BFGS method and the simplex method. The effectiveness of these methods was performed by means of the benchmark configuration of distorted contact segment from the static solution of bending of two rectangular plates over a cylinder [1]. The most fitting method turned out the modification of the Nealder-Mead simplex method [3], which belongs to very popular and simple direct search technique that had been widely used in unconstrained optimization problems.

In this work, the attention was focused on the application of contact algorithm in wave propagation problems. It is obvious that the local search technique strongly influences the robustness, accuracy and computational cost of the transient dynamic analysis. Therefore, an emphasis was laid on the performance of the Nealder-Mead simplex method implemented in local search procedure by means of a contact-impact problem of two colliding thick plates, for which the analytical solution was available [4]. Apart from this, the influence of the numerical dispersion was taken into account.

The plates made contact with initial velocity $v_0 = 1$ m/s prescribed at time $t = 0$ s. The dimensions were: thickness $2d = 5$ mm, length 2.5 mm. Young's modulus, Poisson's ratio and density, respectively, were $E = 2.1 \times 10^5$ MPa, $\nu = 0.3$, $\rho = 7800\,\mathrm{kg/m^3}$. In view of symmetry, only one half of the plates was discretized using 100×100 eight-node linear brick elements per each plate. The contact algorithm is fully compatible with the explicit time integration methods. Thus, for the integration of equilibrium equations, the central difference with the lumped mass matrix was employed. The time step was chosen very small corresponding to the dimensionless Courant number $Co = 0.125$.

The normalized longitudinal stress distribution σ_x^* along x-axis is drawn in Fig. 1 (left). The results are plotted for normalized time $t^* = 0.56$ and coordinate $z/d = 0$, for which no reflections from boundaries occur. Except the contact analysis a symmetric reference calculation was performed, where the longitudinal displacements of the front-end nodes of the plate were fixed. The contact solution is plotted by red line while the solution based on the reference calculation is denoted by blue

line. In addition, the theoretical solution corresponding to uniaxial strain condition is plotted by the black line. Quite a good agreement between the contact and reference calculation was observed. It should be emphasized that the symmetry of longitudinal stress distributions was perfectly preserved in contact analysis. Thus, the capability of the Nealder-Mead simplex method implemented in local search procedure was confirmed. It is clear that the numerical solution was influenced by dispersion errors caused by both FE spatial and time discretization. In comparisons with the continuum solution the speed of the longitudinal wave was slower. This fact follows from the theoretical dispersion diagrams derived in Ref. [5].

The normalized transversal stress distribution σ_z^* along z-axis is drawn in Fig. 1 (right). In contrast to previous figure these distributions are strongly influenced by the longitudinal and transversal waves reflected from the boundary of plate. Before the arrival of these waves the solution is identical to the constant values $\sigma_z^* = -1$ corresponding to a half-space impact problem. It should be pointed out that the accuracy of analytical solution using the Laplace transform is strongly influenced by the number of terms included in the series of improper integrals [4]. The analytical solution plotted in this figure was derived from the summation of the first 300 terms of this series.

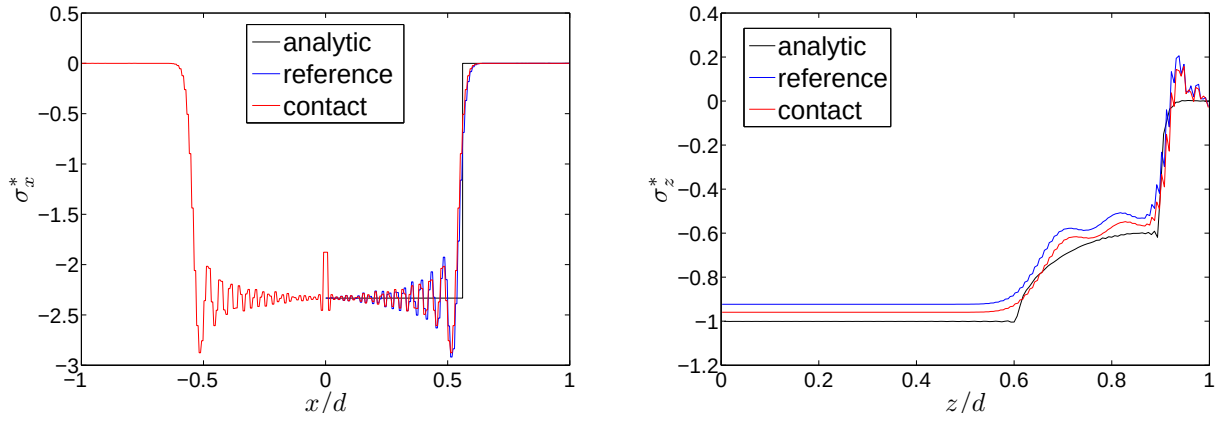

Figure 1: Longitudinal and transversal stress distribution for normalized time $t^* = 0.56$ and Courant's number $Co = 0.125$: σ_x^* for $z/d = 0$ (left); σ_z^* for $x/d = 0.4$ (right).

Acknowledgement This work was supported by the grant projects ME10114, GAP101/12/2315 and GA101/09/1630 in the framework of AV0Z20760514.

References

[1] D. Gabriel, J. Plešek, M. Ulbin. Symmetry preserving algorithm for large displacement frictionless contact by the pre-discretization penalty method. *Int. J. Num. Met. Engng*, **61**: 2615–2638, 2004.

[2] D. Gabriel, J. Kopačka, J. Plešek, M. Ulbin. Assesment of methods for calculating the normal contact vector in local search. *4th European Conference on Computational Mechanics (ECCM 2010)*, Paris, Computational Structural Mechanics Association, CD-ROM, 2010.

[3] J. A. Nelder, R. Mead. A simplex method for function minimization. *The Computer Journal*, **7**: 308–313, 1965.

[4] R. Brepta, F. Valeš. Longitudinal impact of bodies. *Acta Technica ČSAV*, **32**: 575–602, 1987.

[5] J. Plešek, R. Kolman, D. Gabriel. Dispersion error of finite element discretizations in elastodynamics, *Computational Technology Reviews*, B.H.V. Topping, J.M. Adam, F.J. Pallarés, R. Bru, M.L. Romero (eds.), Saxe-Coburg Publications, 251–279, 2010.

WAVES IN HALF-SPACES OF MICROSTRUCTURED MATERIALS CHARACTERIZED BY GRADIENT ELASTICITY

H.G. Georgiadis[1], P.A. Gourgiotis[2]

[1]Mechanics Division, National Technical University of Athens, Zographou, Greece; e-mail: georgiad@central.ntua.gr
[2]Mechanics Division, National Technical University of Athens, Zographou, Greece; e-mail: pgourgiotis@yahoo.gr

Keywords: reflection of plane waves, surface waves, microstructure, micro-inertia, gradient elasticity

Classical continuum theories possess no intrinsic length scale and thus fail to predict the scale effects observed experimentally in problems with geometrical lengths comparable to the lengths of material microstructure [1]. It is also well known that the classical theory of elasticity does not predict dispersion of Rayleigh-wave motions at any frequency. Of course, at high frequencies (small wavelengths), this is a result that contradicts experimental data and also does not agree with results of the discrete particle theory (atomic-lattice approach). In these situations, dispersion phenomena at high frequencies can only be explained on the basis of generalized continuum theories (see e.g. [2,3]). In particular, gradient theories enrich the classical continuum with additional material lengths (characteristic lengths) in order to describe the scale effects resulting from microstructure. In this way, gradient theories extend the range of applicability of the 'continuum' concept in an effort to bridge the gap between classical continuum theories and atomic-lattice theories.

The present work studies the propagation and reflection of plane waves in a body having the form of a half-space. It is assumed that the mechanical response of this body is governed by dipolar gradient elasticity. Our goal is to investigate the effect of boundaries on the elastic wave motion in a medium with microstructure and, thus, to determine possible deviations from the predictions of classical linear elastodynamics. By using gradient elasticity, size effects are taken into account in a manner that the classical theory cannot afford. Here, a simple but yet rigorous version of the generalized continuum theories of Toupin [4] and Mindlin [5] is employed that also includes micro-inertial effects. It is noted that previous experience with gradient analysis of torsional and Rayleigh type waves indicated that micro-inertial effects are important at high frequencies [2,3,6].

Our results show departure from the ones of the classical elastodynamic theory. Indeed, it is observed that an incident dilatational or distortional wave at the traction-free plane boundary gives rise to four reflected waves, instead of the usual two waves predicted by the conventional theory. Two of these reflected waves are surface waves with exponentially decaying amplitudes, while the other two propagate with dispersion into the medium. In addition, contrary to the classical elasticity case, the amplitudes of the reflected waves are complex quantities, thus indicating a phase shift between the incident and reflected waves. It is shown that this phase shift increases as the wavelength of the incident wave becomes comparable with the intrinsic material lengths. In view of the above, it appears that the material microstructure plays an important role in the propagation and reflection of plane waves in the presence of boundaries.

Acknowledgement

The research leading to these results has received funding from 'PEVE 2011' programme of NTU Athens, title of the individual project: 'Dynamic Fracture and Contact within the Framework of Generalized Continuum Theories'.

References

[1] N.A. Fleck, J.W. Hutchinson. Strain gradient plasticity. *Advances in Applied Mechanics*, Vol. 33, Academic Press, New York, 295–361, 1997.

[2] H.G. Georgiadis, I. Vardoulakis, E.G. Velgaki. Dispersive Rayleigh-wave propagation in microstructured solids characterized by dipolar gradient elasticity. *Journal of Elasticity,* **74**: 17–45, 2004.

[3] H.G. Georgiadis, E.G. Velgaki. High frequency Rayleigh waves in materials with micro-structure and couple-stress effects. *International Journal of Solids and Structures,* **40**, 2501-2520, 2003.

[4] R.A. Toupin. Perfectly elastic materials with couple stresses. *Archive for Rational Mechanics and Analysis,* **11**, 385-414, 1962.

[5] R.D. Mindlin. Micro-structure in linear elasticity. *Archive for Rational Mechanics and Analysis,* **16**, 51-78, 1964.

[6] H.G. Georgiadis, I. Vardoulakis, G. Lykotrafitis. Torsional surface waves in a gradient elastic half-space. *Wave Motion,* **31**, 333-348, 2000.

OPERATIONAL EQUATIONS OF STATE FOR MODELLING SHOCK WAVES PHENOMENA IN SOLIDS

Michael Grinfeld

US Army Research Laboratory, Aberdeen Proving Ground, USA, e-mail: michael.greenfield4.civ@mail.mil

Keywords: shock waves, inverse problems, equations of state, hydrocode

Operational Equations of State (EoS) can be defined as the EoS which have the form of different operators. For the shock-wave community, the classical example of the operational EoS is the famous Mie-Gruneisen equation [1,2]:

$$P_{MG}\left(V,E\right)=P_{ref}\left(V\right)+\frac{\Gamma\left(V\right)}{V}\left(E-E_{ref}\left(V\right)\right),$$

where $P_{MG}\left(V,E\right)$ is the dependence of pressure upon the „hydrocode“ thermodynamic variables: a specific volume V and a specific internal energy density E; $\Gamma\left(V\right)$ is the so-called Gruneisen parameter; $P_{ref}\left(V\right)$ and $E_{ref}\left(V\right)$ are the values of the pressure and the specific energy on the so-called reference curve (see, Figure 1). Thus, the Mie-Gruneisen EoS is an ordinary function with respect to the hydrocode variables $\left(V,E\right)$ and an operator with respect to the functional variables $\left\{P_{ref}(V),E_{ref}\left(V\right)\right\}$.

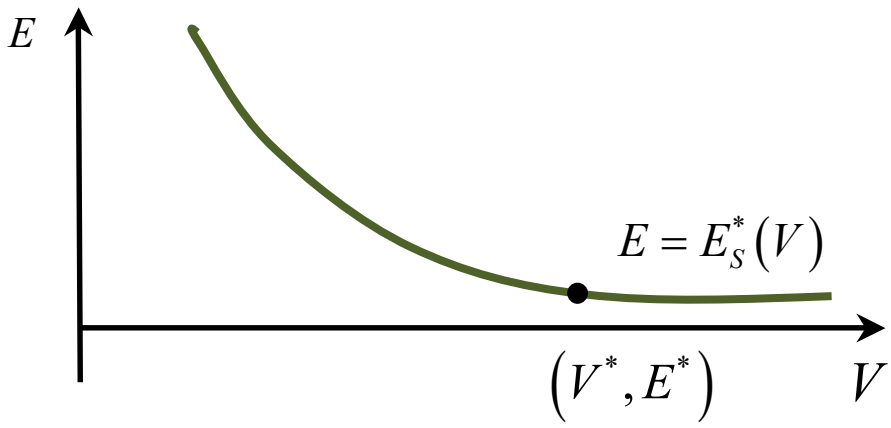

Figure 1: The reference curve in the “hydrocode” plan.

The EoS is a mandatory element for analyzing wave motion and shock waves, in particular [3,4]. At the same time, measuring various physical characterics of wave fields we can try to solve the inverse problem, i.e., the problem of recovery of the EoS from experimental data. When the reference curve coincides with the Hugoniot adiabat the Mie-Gruneisen equation appears to be

helpful for solving this inverse problem. Then, this EoS converts the experimentally determined Hugoniot adiabat data into the EoS for hydrocode. By definition, the recovered EoS is automatically fully compatible with those Hugoniot experimental data. After the conversion, the resulting EoS can be used also for modeling of a variety of high-rate problems (including those with and without shock waves).

With all its valuable features, the Mie-Gruneisen EoS suffers serious weaknesses as well. In particular, it is thermodynamically inconsistent with various widespread models of the heat capacity functions unless the substance's heat capacity depends solely on the specific entropy. In many applications the heat capacity is assumed constant. This assumption makes the Mie-Gruneisen EoS thermodynamically consistent but it does not always provide sufficient flexibility in modeling physical phenomena, for instance, when dealing with polymers.

In the paper, we discuss the concept of *operational* EoS, distinguishing between the *complete* and *incomplete* EoS as well as distinguishing between thermodynamically consistent and inconsistent models. We also suggest some simple examples of the operational EoS which are thermodynamical complete and consistent and can be recommended for modeling shock and blast phenomena. Presented results develop further the earlier publications [5,6].

References

[1] S. Eliezer, S., A. Ghatak, H. Hora. *Fundamentals of Equations of State*. World Scientific, Singapore, 2002.
[2] V.N. Zharkov, V.A. Kalinin, *Equations of State for Solids at High Pressures and Temperatures*. Consultants Bureau, 1971.
[3] R. Courant., K. O. Friedrichs, K.O. *Supersonic Flow and Shock Waves*. Interscience, New York, 1948.
[4] Ya.B. Zel'dovich, Yu.P. Raizer, *Physics of Shock Waves and High-Temperature Hydrodynamic Phenomena*, Dover, 2002.
[5] M.A. Grinfeld. *A Novel Equation of State for Hydrocode*. In Proceedings of the Conference of the Conference of the American Physical Society Topical Group on Shock Compression of Condensed Matter, M.L. Alert, W.T., Buttler et al. (eds), AIP, 804-807, 2012.
[6] M.A. Grinfeld. *The Generalized Courant-Friedrichs Equation of State for Condensed Matter*. In Proceedings of the Conference of the Conference of the American Physical Society Topical Group on Shock Compression of Condensed Matter, M.L. Alert, W.T., Buttler et al. (eds), AIP, 804-807, 2012.

EXPLICIT LOCAL TIME-STEPPING METHODS FOR TRANSIENT WAVE PHENOMENA

Marcus J. Grote[1], Michaela Mehlin[1], Teodora Mitkova[1]

[1]Institute of Mathematics, University of Basel, Switzerland;
e-mail: {marcus.grote, michaela.mehlin, teodora.mitkova}@unibas.ch

Keywords: finite element methods, high-order methods, explicit time integration, local time-stepping

The efficient simulation of time-dependent wave phenomena is of fundamental importance in a wide variety of applications from acoustics, electromagnetics and elasticity, for which the scalar damped wave equation

$$u_{tt} + \sigma u_t - \nabla \cdot (c^2 \nabla u) = f \qquad \text{in } \Omega \times (0,T)\,, \tag{1}$$

often serves as a model problem. Here, Ω is a bounded domain, $f(x,t)$ is a (known) source term, whereas the damping coefficient $\sigma(x) \geq 0$ and the speed of propagation $c(x) > 0$ are piecewise smooth.

We discretize (1) in space by using either standard continuous (H^1-conforming) finite elements with mass lumping [1], a symmetric IP-DG discretization [5], or a nodal DG discretization [6]. All three discretizations lead to a system of ordinary differential equations with an essentially diagonal mass matrix. Thus, when combined with explicit time integration, the resulting time scheme for the solution of (1) will be truly explicit.

Locally refined meshes impose severe stability constraints on explicit time-stepping methods for the numerical solution of (1). Local time-stepping (LTS) methods overcome that bottleneck by using smaller time-steps precisely where the smallest elements in the mesh are located. In [2, 3], explicit second-order LTS integrators for transient wave motion were developed, which are based on the standard leap-frog scheme. In the absence of damping, i.e. $\sigma = 0$, these time-stepping schemes, when combined with the modified equation approach, yield methods of arbitrarily high (even) order. By blending the leap-frog and the Crank-Nicolson methods, a second-order LTS scheme was also derived there for (damped) electromagnetic waves in conducting media, i.e. $\sigma > 0$, yet this approach cannot be readily extended beyond order two. To achieve arbitrarily high accuracy in the presence of damping, while remaining fully explicit, explicit LTS methods for (1) based on Adams-Bashforth multi-step schemes were derived in [4].

Here we propose explicit LTS methods based either on classical or low-storage Runge-Kutta schemes. In contrast to Adams-Bashforth methods, Runge-Kutta methods are one-step methods; hence, they do not require a starting procedure and easily accommodate adaptivity in time. Although Runge-Kutta methods require more computational work per time-step, that additional work is compensated by a less stringent CFL stability restriction.

To illustrate the versatility of our approach, we now consider a computational rectangular domain of size $[0,2] \times [0,1]$ with two rectangular barriers inside forming a narrow gap. We use continuous P^2 elements on a triangular mesh, which is highly refined in the vicinity of the gap, as shown in Fig. 1. For the time discretization, we choose an LTS method based on an explicit third-order low-storage Runge-Kutta scheme. Thus, the numerical method is third-order accurate both in space and time with respect to the L^2-norm. Since the typical mesh size inside the refined region is about $p = 7$ times smaller than that in the surrounding coarser region, we take p local time steps of size $\Delta\tau = \Delta t/p$ for every time step Δt. In Fig. 2, a Gaussian pulse initiates two plane waves which propagate horizontally in opposite directions. As the right-moving wave impinges upon the obstacle, a small fraction of the incoming wave penetrates the gap and generates multiple circular waves on both sides of the obstacle, which further interact with the wave field.

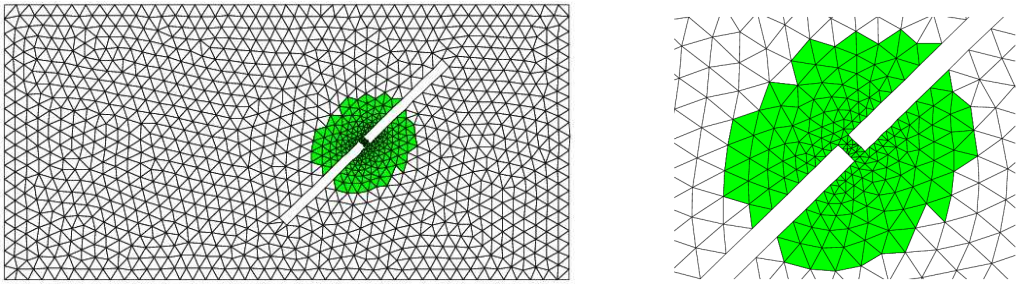

Figure 1: The initial triangular mesh (left); zoom on the "fine" mesh indicated by the darker (green) triangles (right).

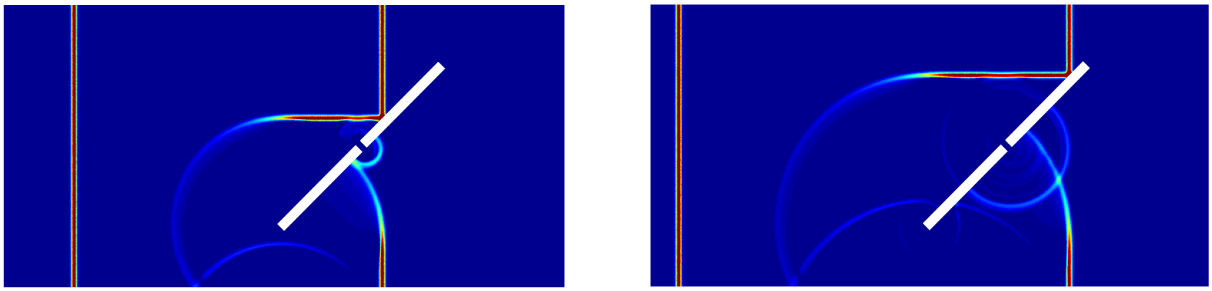

Figure 2: The solution at times t =0.55 and 0.7.

References

[1] G. Cohen. *High-Order Numerical Methods for Transient Wave Equations*. Springer, 2002.

[2] J. Diaz, M. Grote. Energy conserving explicit local time-stepping for second-order wave equations. *SIAM Journal on Scientific Computing*, **31**: 1985–2014, 2009.

[3] M. Grote, T. Mitkova. Explicit local time-stepping for Maxwell's equations. *Journal of Computational and Applied Mathematics*, **234**: 3283–3302, 2010.

[4] M. Grote, T. Mitkova. High-order explicit local time-stepping methods for damped wave equations. Preprint arXiv:1109.4480v1, 2011.

[5] M. J. Grote, A. Schneebeli, D. Schötzau. Discontinuous Galerkin finite element method for the wave equation. *SIAM J. Numer. Anal.*, 44 (2006) 2408–2431. **44**: 2408–2431, 2006.

[6] J.S. Hesthaven, T. Warburton. *Nodal Discontinuous Galerkin Methods*. Springer, 2008.

COUPLED THERMAL AND VISCOELASTIC 1–D WAVES

Harry H. Hilton

Aerospace Engineering Department in the College of Engineering and
Private Sector Program Division at the National Center for Supercomputing Applications
University of Illinois at Urban-Champaign, Urbana, IL 61801-2935 USA, e-mail: h-hilton@illinois.edu

Keywords: material temperature sensitivity, longitudinal and thermal waves, variable coefficient DEs

General Considerations

Propelled by intense needs for the development of structural applications of high polymers, solid propellants, elevated temperature metals, composites, etc., fundamental research efforts during the last seventy plus years starting with [1] have moved linear viscoelasticity into the realm of mature sciences [2]. However, there remain a number of problems areas that need further research refinements, such as improved linear characterization, coupled dynamic problems, analysis and computational protocols and practically the entire nonlinear viscoelasticity area. Analyses in the presence of temperature fields, whether static $T(x)$ or fully dynamic $T(x,t)$ with $x = \{x_1, x_2, x_3\}$, generate their own set of intrinsic difficulties. Because of the extreme temperature sensitivities of viscoelastic material properties (Fig. 1), the following phenomena arise:

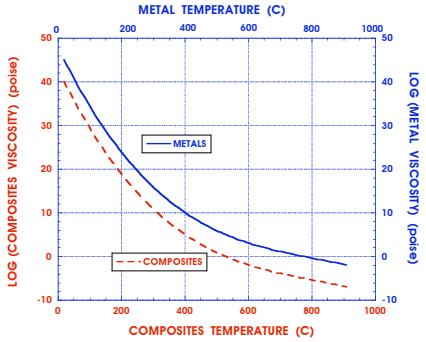

Figure 1: Material property temperature dependence

- for $T(x)$ material properties become non-homogeneous resulting in governing integral partial differential relations (IPDE) with preserved convolution properties and with spatially variable coefficients
- for $T(t)$ homogeneous material properties remain but constitutive relation time integrals are of the non-convolution type destroying possibilities of formulating elastic-viscoelastic correspondence principles (EVCP)
- for $T(x,t)$ the worst case scenario ensues where viscoelastic materials become non-homogeneous without convolution integral properties
- in all cases where material properties are considered temperature dependent, the analysis of coupled temperature-displacement problems entails solutions of nonlinear governing relations (see Table 1) and, consequently, the elastic-viscoelastic correspondence principle is inapplicable

Solution protocols are formulated and illustrative examples are presented.

Solution Protocols

1. If the density and material and thermodynamic properties are approximated as temperature independent, then the resulting linear constant coefficient integro-differential equations are linear and can be solved by standard procedures, such as for instance Laplace (LT) or Fourier (FT) transforms or by series of separable terms

$$\rho(x_1,t) = \text{const.} \qquad u_1(x_1,t) = \sum_{n=1}^{N^*} F_n(t) u_n^*(x_1) \qquad T(x_1,t) = \sum_{n-1}^{N^*} F_n(t) T_n^*(x_1) \qquad (1)$$

Material	Temperature	Modulus	Coupling	Governing relations	Convolution in t space	EVCP
elastic	$T(x)$	$E_0(x)$	weak	linear	no	n/a
elastic	$T(x,t)$	$E_0(x)$	strong	linear	no	n/a
viscoelastic	$T(x)$	$E\left[x, t-t', T(x)\right]$	strong	nonlinear	yes	no
viscoelastic	$T(x,t)$	$E\left[x,t,t', T(x,t')\right]$	strong	nonlinear	no	no

Table 1: Elastic and viscoelastic thermal coupling

Type of Uncoupling of Governing Relations	Conditions If and Only If
totally uncoupled	time independent temperature spatially independent temperature temperature independent material properties time independent displacements
temperature uncoupled	constant temperature and temperature independent material properties
displacements uncoupled	time independent displacements

Table 2: Temperature–displacement coupling

Such a formulation may be considered as a "poor" first approximation to the more realistic development in 3. below.

2. Since for the identical thermo-elastic problem where the temperature influence on material properties is marginally weak compared to viscoelastic media, the same integral transform protocols as above can be employed.
3. If material and/or thermodynamic properties are inclusively prescribed as temperature dependent, then the governing relations are nonlinear and currently there is no hope for an analytical solution. Numerical procedure involving finite element and finite difference approaches are then useful.
4. If boundary conditions corresponding to say absorbing or reflecting boundaries at $x_1 = 0$ and/or $x_1 = L$ are introduced, then Galerkin's method may be applied to spatial dependences and thus resulting in ordinary, rather than partial, temporal integro-differential nonlinear equations.
5. For the nonlinear governing relations the Poincaré-Kuo method of successive approximations [3] may be used to linearize the simultaneous PIDEs.
6. A Runge-Kutta approach may also be employed.

Acknowledgement

Support by the Private Sector Program Division (PSP) of the National Center for Supercomputing Applications (NCSA) at the University of Illinois at Urbana-Champaign is gratefully acknowledged.

References

[1] T. Alfrey, Jr. Non-homogeneous stress in viscoelastic media. *Quarterly of Applied Mathematics* **2**:113–119, 1944.

[2] H.H. Hilton. Equivalences and contrasts between thermo-elasticity and thermo-viscoelasticity: a comprehensive critique. *Journal of Thermal Stresses*, **34**:488–535, 2011.

[3] A.H. Nayfeh. *Perturbation Methods.* Wiley, New York, 2000.

ELASTIC WAVES REVERBERATIONS AND ELASTIC LOAD IN LONG ROD PENETRATION

Eitan Hirsch

Private consulter, Tachkemony St. 6, Netanya, 42611 Israel; e-mail: heitanon@bezeqint.net

Keywords: elastic energy, high strain rates, shear-bands

The simulation of the head-on collision of two long rods along their common axis of symmetry reveals that the rod's material loses its strength long before reaching the interface between the two rod's materials. The process by which the strength is lost is the fast formation of shear bands as indicated by the analysis of the head of a recovered long rod that penetrated a finite thickness target. The pressure due to which this strength failure process occurs is the Bernoulli pressure that is created by the elastic wave reverberations between the interface and the location where the rod loses its strength. Also, the shear bands are formed because of the fast accumulation of elastic energy in the rods while they reach the place where the shear bands form. In this shear bands formation process the elastic energy is released in a process that reminds of how lasers perform or how an explosion can proceed supersonically in an explosive.

The energy Ed that the rod material accumulates before it gets released is a major parameter in the penetration mechanics, because it determines by how much the rod diameter increases before the plastic penetration process actually starts. The comparison of measured long rods penetration data, with predictions made by a computer code written especially for the above described penetration mechanism model, shows that the accumulated energy Ed may reach values above 1 KJoul/cc. Such values are much larger than the value of 100 Joul/cc reached typically at low strain rates in experiments where plastic deformation is measured.

The direct measurement of Ed has been suggested [1] but not yet performed, while its indirect measurement via penetration measurements demands that all the parameters involved in the experiments are measured with the utmost accuracy. This parameter tells up to which energy density values the material can be loaded temporarily. At low strain rates this load is released by plastic deformation rather than by shear banding. What are threshold conditions between the two channels? This is open for discussion. We postulate that in the case of long rod penetration the strain rate at the location where the material loses its strength times the rod diameter should be smaller than the velocity of the dislocations in order that the plastic deformation will dominate rather than the elastic energy accumulation that leads to the shear bands formation. (The attached pictures are not new but their interpretation took time to mature).

Experiments where several layers of fragments were launched with high explosive confirmed that the elastic energy that is accumulated by steel fragments for a very short time can have a very strong effect on the velocity distribution of the fragments. This observation gives another support to the phenomenon of the short duration elastic energy accumulation in metals, a phenomenon that is responsible for the fast shear bands formation failure mode. This failure mode probably stands behind the metallic flow in shaped charge jet formation and long rods penetration.

Head on collision between two identical rods, reveals the Strength Failure Surface location#.

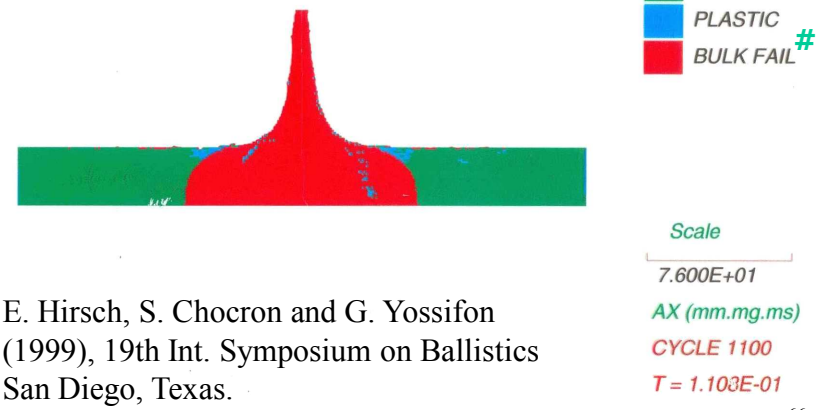

E. Hirsch, S. Chocron and G. Yossifon (1999), 19th Int. Symposium on Ballistics San Diego, Texas.

66

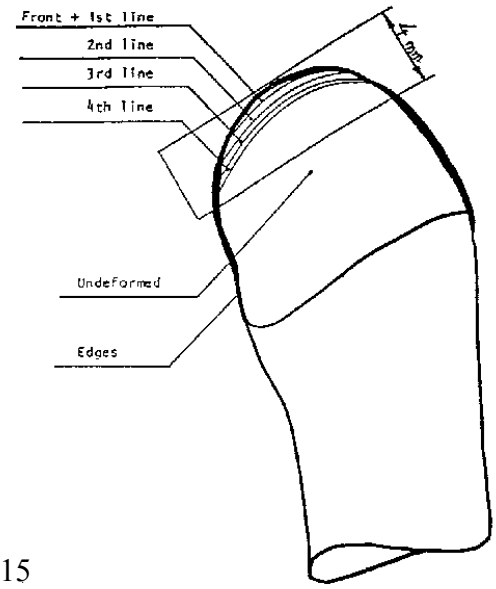

Shear bands at the end of a retrieved rod.

From Ref. 15

71

References

[1] E. Hirsch, D. Mordechai. A Test for Measuring the Energy Density lost in Two Flow Metallic Collision. In *20th International Symposium on Ballistics,* Orlando Florida, 23–27, 2002.

STRESS WAVE RADIATION FROM BRITTLE CRACK EXTENSION BY MD AND FEM

Petr Hora[1], Olga Červená[2], Alena Uhnáková[3], Anna Machová[4]

Institute of Thermomechanics AS CR, v.v.i., Prague, Czech Republic
e-mail: [1]hora@cdm.it.cas.cz, [2]cervena@cdm.it.cas.cz,
[3]uhnakova@it.cas.cz, [4]machova@it.cas.cz

Keywords: molecular dynamic, finite element simulation, bcc iron crystal

We present results for molecular dynamic (MD) and finite element (FEM) simulations in 3D bcc iron crystals, with embedded central through crack (001)[110] of Griffith type, loaded in mode I. The sample geometry and border conditions in MD were chosen in such a way as to invoke a cleavage crack extension. Acoustic emission (AE) sources caused by the crack were analysed on both the atomistic and continuum level with FEM.

Crack (001)[110] (crack plane/crack front) can extend in a brittle manner, as atomistic simulations under plane strain conditions (e.g.[1]), but also fracture experiments on iron crystals [2, 3] have shown. However, behaviour at the crack front depends not only on the stress intensity K_I, but also on the so–called T-stress acting parallel to crack plane [4]. Change of the T-stress from negative to positive values may recall the ductile–brittle transition, as indicated in atomistic simulations under bi–axial loading, as well as continuum predictions [4]. The change of T-stress can also be recalled due to the geometry of a cracked sample under uni–axial tension, as follows from [5]. It was utilized in 3D atomistic MD simulations [6] together with special boundary conditions to invoke cleavage fracture. As mentioned in [6], AE sources from MD are well visible in the planes perpendicular to the crack front, but not in the crack plane due to a continuous bond breakage in the atomistic sample. It is a reason why surface Rayleigh waves cannot be recognised in the crack plane from MD.

In this paper we repeat 3D atomistic simulations from [6] where cleavage crack extensions have been invoked along the whole crack front. Acoustic emission sources in 3D, recalled by the brittle fracture, are analysed on both the atomistic and FEM level utilizing information from MD on residual forces in the crack plane during crack propagation.

At MD and FEM simulations we consider a pre–existing central crack of $2l_0 = 2a$ length, embedded in a rectangular sample. The crack surfaces lie on (001) planes, the crack front is oriented along the z–direction [110] and the potential crack extension is in the $x = [\bar{1}10]$ direction. The crack is loaded uni–axially in mode I, i.e. the sample borders are loaded in y $\langle 001 \rangle$directions. Due to the symmetry of the problem, we simulate only one half of the sample in the x–direction. To maintain the symmetry, the atoms lying on the left border plane are fixed in the x–direction. The other atoms are free to move in the x–, y– and z–directions, excepting surface atoms on $\{110\}$ surfaces that are fixed in the z–direction. This serves to decrease stress concentration and prevent the plastic process at the corners, where the crack front penetrates the free surfaces. We utilize an N–body potential for bcc iron of Finnis–Sinclair type [7]. Interatomic interactions across initial crack faces are prevented, in order to simulate a pre–existing crack occurring in continuum models and in linear fracture elastic mechanics.

The half crack length is $l_0 = 178 d_{110}$, where $d_{110} = a_0\sqrt{2}/2$ and $a_0 = 2.8665$ Å is the lattice parameter and the initial half crack opening is $c_0 = d_{001}/2 = a_0/4$. The thickness of the crystal corresponds to 30 layers (110) in the z–direction parallel to the crack front. Crystal consists of 300 planes $[\bar{1}10]$ in the x–direction and 300 planes (001) in the y–direction.

Newtonian equations of motion for individual atoms are solved by a central difference method, using time integration step $h = 1 \times 10^{-14}$ s. We use a ramp loading, i.e. the sample is loaded up to a level

σ_A gradually (linearly) during 4000 time steps, as in [6]. When a prescribed stress level σ_A is reached, the applied stress is held constant.

Prior to external loading, the atomistic samples are relaxed to avoid the influence of surface relaxation on the microscopic processes at the crack front. At selected time steps, the local number of interactions, the local kinetic energies and the coordinates of individual atoms are monitored for purposes of graphic treatment of the MD results. When bond breakage occurs in the atomistic system, residual atomic forces in the middle of the crack plane are monitored each time step for purposes of FEM.

The wave motion modelling in the sample was carried out by using the finite element (FE) code COMSOL [8]. The FE sample of width $150a_0\sqrt{2}$, height $150a_0$ and thickness $15a_0\sqrt{2}/2$ (half of the MD sample) was considered as a linear anisotropic elastic medium with cubic symmetry. Plane strain conditions inside the sample together with zero displacements in the z–direction have been utilized in the anisotropic FE model of the same orientation as in MD. The FE sample is supposed to be without any initial stress/strain. For the time integration the full mass matrix and integration time step Δt was 1×10^{-13} s were used.

At higher applied loads, positive T–stress contributes to cleavage crack extension in MD. Under the ramp loading during 4000 time steps, the crack was initiated at the critical Griffith stress intensity.

MD simulations show that cleavage crack initiation in the 3D bcc iron crystal forms an AE–source, where qL–waves dominate. However, qT–waves are also generated during a continuous bond breakage in the crystal, which is new knowledge from 3D modelling. The strongest pulse emission comes from stress relaxation at the crack front, after the crack initiation.

Simplified modelling of the pulse emission by FEM shows that, besides the qL and qT–waves, Rayleigh waves can also be generated at the (001) free crack faces, in agreement with expectations according to continuum analysis.

Acknowledgement

The work was supported by the grant GA CR No 101/09/1630 and by the Institute Research Plan AV0Z20760514.

References

[1] A. Machová, G.E. Beltz, M. Chang. Atomistic simulation of stacking fault formation in bcc iron. *Modelling Simul. Mater. Sci. Eng.*, **7**: 949–974, 1999.

[2] A. Spielmannová, M. Landa , A.Machová, P. Haušild, P.Lejček. Influence of crack orientation on the ductile–brittle behavior in Fe–3wt%Si single crystals. *Materials Characterization*, **58**: 892–900, 2007.

[3] J. Prahl, A. Machová, M. Landa, P. Haušild, M. Karlík, A. Spielmanová, M. Clavel, P. Haghi-Ashtiani. Fracture of Fe–3wt%Si single crystals. *Mater. Sci. Eng.*, **A 462**: 178–182, 2007.

[4] G.E. Beltz, A. Machová. Effect of T-stress on dislocation emission in iron. *Scripta Mater*, **50**: 483–487, 2004.

[5] T. Fett, *A compendium of T-stress solutions*. Forschungscentrum Karlsruhe GmbH, 1998.

[6] A.Uhnáková, A. Machová, P. Hora, J. Červ, T. Kroupa. Stress wave radiation from cleavage crack extension in 3D bcc iron crystals. *Computational Materials Science*, **50**: 678–685, 2010.

[7] G.J. Ackland, D.J. Bacon, A.F. Calder, T. Harry. Computer simulation of point defect properties in dilute Fe–Cu alloy using a many–body potential, *Phil. Mag.*, **A 75**: 713–732, 1997.

[8] http://www.comsol.com

AN ANALYTICAL AND NUMERICAL STUDY ON IMPACT WAVES IN A NONLINEARLY ELASTIC COMPOSITE BAR

Shou-Jun Huang[1], Hui-Hui Dai[2], Zhen Chen[3] and De-Xing Kong[4]

[1]Department of Mathematics, Anhui Normal University, Wuhu, 241000, China
[2]Department of Mathematics, City University of Hong Kong, Hong Kong, China; e-mail: mahhdai@cityu.edu.hk
[3]Department of Civil and Environmental Engineering, University of Missouri, Columbia, MO 65211-2200, USA
[4]Department of Mathematics, Zhejiang University, Hangzhou 310027, China

Keywords: impact waves, composite bar, material nonlinearity

Composite materials have been extensively used for the purpose of impact-resistant design. As an important ongoing research area, many works have been done to address various aspects of wave behavior in nonlinearly elastic composite materials. One focus is on the influences of the cell structure on waves. For example, the homogenization method was used to study the dynamical properties of layered composite Murnaghan materials ([1]) and the effective incremental response in a pre-stressed nonlinearly elastic composite bar was considered in [2]. Numerical computations by a finite volume method also revealed some interesting behavior (see [3]). In this talk, we concentrate on a different aspect: How material nonlinearity can be utilized to undermine the strength of tensile waves. When a compressive impact is exerted on a composite bar, tensile waves can arise due to multiple reflections at interfaces, which can, in turn, induce cracks. As a result, the strength of the structure can be significantly reduced. Thus, it is an important issue to reduce the magnitude of a tensile wave.

The object of our study is a two-layer composite bar, with the first layer composed of a linearly elastic material of finite length h (called material 1) and the second layer composed of a nonlinearly elastic material of infinite length (called material 2). We consider the problem that a compressive impact with stress amplitude A and duration T is exerted on the left end of the first layer. The aim is to conduct an analytical and numerical study to show that under certain conditions a tensile wave will be transmitted into the second layer and it can catch the first transmitted compressive wave (so the strength of the former can be reduced.)

The mathematical formulation (in a Lagrangian description) is given below:

$$\rho v_t = \sigma_x, \quad \gamma_t = v_x, \tag{1}$$

where γ, v, σ are smooth functions and denote the strain, particle velocity and nominal stress respectively. At a moving strain discontinuity $x = s(t)$, the jump conditions are

$$\dot{s}[\gamma] + [v] = 0, \quad \dot{s}\rho[v] + [\sigma] = 0, \tag{2}$$

where $[f] = f(t, s(t) + 0) - f(t, s(t) - 0)$. The constant density ρ and the stress-strain relation are defined as

$$\rho = \begin{cases} \rho_1, & 0 \leqslant x < h \\ \rho_2, & h < x < \infty \end{cases} \qquad \sigma = \begin{cases} E_1\gamma, & 0 \leqslant x < h,\ \gamma > -1 \\ E_2 f(\gamma), & h < x < \infty,\ \gamma > -1. \end{cases} \tag{3}$$

The initial-boundary value conditions are given by

$$v(0, x) = 0,\ \gamma(0, x) = 0 \ \text{ for } \ x > 0 \ \text{ and } \ \sigma(t, 0) = \begin{cases} A, & 0 < t \leqslant T, \\ 0, & t > T. \end{cases} \tag{4}$$

We show that, when material 2 is linear and the impedance ratio of two materials is less than 1, a tensile wave will be transmitted into the second layer but it can never catch the first transmitted compressive wave. Then, we consider the case that material 2 is nonlinearly elastic. By using the theory of nonlinear hyperbolic equations, we are able to show that if material 2 is convex there are two wave patterns (see Figure 1) for which the tensile wave can catch the first transmitted compressive wave. Depending on whether the time interval T of the impact is larger or smaller than a critical value T^*, the tensile shock wave S_1 catches first the compressive shock wave S_0 or S_0 first penetrates the rarefaction wave and then is caught by the tensile shock wave S_1.

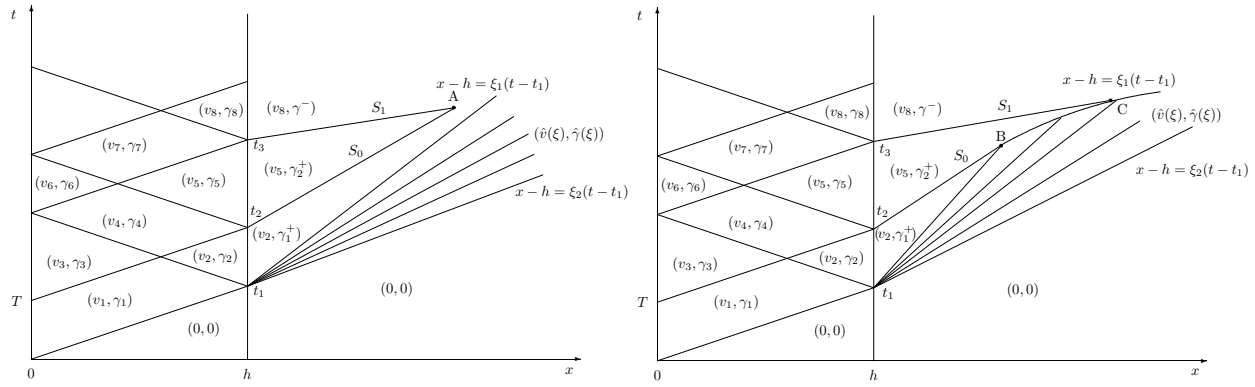

Figure 1: *The catching-up phenomenon in the composite bar. Case I: $T \geqslant T_*$ (left); Case II: $T < T_*$ (right), where $T_* \doteq 2t_1 s_1(s_0 - c(\gamma_1^+))/[s_0(s_1 - c(\gamma_1^+))], c(\gamma) = (\sigma'(\gamma)/\rho_2)^{1/2}, t_1 = h/c_1, t_2 = T + t_1 = (1+\theta)t_1, t_3 = 3t_1$.*

We also manage to construct the explicit asymptotic solutions when $\varepsilon = -2A/E_2 > 0$ is small. For example, we have the following formulas for some quantities shown in Figure 1.

$$\gamma_1^+ \approx -\frac{1}{\beta+1}\varepsilon,\ \gamma_2^+ \approx -\frac{\beta\left[f''(0)\right]^2}{96(1+\beta)^4}\varepsilon^3,\ \gamma^- \approx \frac{1-\beta}{(1+\beta)^2}\varepsilon,\ \frac{s_0}{c_2} \approx 1 - \frac{f''(0)}{4(1+\beta)}\varepsilon,\ \frac{s_1}{c_2} \approx 1 + \frac{(1-\beta)f''(0)}{4(1+\beta)^2}\varepsilon. \tag{5}$$

Here, $c_i = (E_i/\rho_i)^{1/2} (i = 1, 2)$ are the speeds of sound waves in materials 1 and 2, $\alpha \doteq c_1/c_2, \beta \doteq \rho_1 c_1/\rho_2 c_2$. One can see that γ^- is positive when $\beta < 1$, thus the shock S_1 is tensile. Also, since $f''(0) > 0$, the tensile wave S_1 is faster than the compressive shock S_0 ($s_1 > s_0$). All the other quantities can then be determined.

For example, the time and location (point C in Figure 1) at which the tensile wave S_1 catches the varying-speed compressive shock (the curve BC) are given by

$$t_{_C}/t_1 \approx 1+X/\varepsilon,\ x_{_C}/h \approx 1+X/(\alpha\varepsilon),\ X = 8(\beta+1)/[f''(0)(\theta+(1-\beta)/(\beta+1)+\sqrt{\theta^2+2\theta(1-\beta)/[(\beta+1)]})]. \tag{6}$$

The roles played by the constitutive relation, the strength of the initial impact and the material and geometrical parameters can be clearly observed from these expressions. We also conduct some numerical simulations, which confirm that the analytical results are valid as long as $\varepsilon < 0.3$ (so actually we do not need ε to be very small).

It is hoped that the analytical and numerical study presented here may provide a new way (by exploring material nonlinearity) for designing certain structures for impact protection purpose.

Acknowledgement

Some of the results presented here have been or may be reported in other meetings. A full paper will be submitted to a journal shortly.

References

[1] I.V. Andrianov, V.V. Danishevs'kyy, H. Topol, D. Weichert. Homogenization of a 1D nonlinear dynamical problem for periodic composites. *ZAMM* **91**: 623-54, 2011.

[2] W.J.Parnell. Effective wave propagation in a pre-stressed nonlinear elastic composite bar. *IMA Journal of Applied Mathematics***72**: 223-244, 2007.

[3] A. Berezovski, M. Berezovski, J. Engelbrecht. Numerical simulation of nonlinear elastic wave propagation in piecewise homogeneous media. *Materials Science and Engineering A* **418**: 364-369, 2006.

DISSIPATION AND TRANSMISSION OF STRESS WAVE ENERGY AT A PERCUSSIVE DRILL ROD JOINT

T. Jansson[1], B. Lundberg[1,2]

[1]Sandvik Mining AB, SE-811 34 Sandviken, Sweden; e-mail: tomas.sh.jansson@sandvik.com
[2]The Ångström Laboratory, Uppsala University, Box 534, SE-751 21 Uppsala, Sweden;
e-mail: bengt.lundberg@angstrom.uu.se

Keywords: Drill rod joint, stress wave energy, dissipation, transmission, simulation, experiment

In percussive top hammer drilling of deep holes in rock, stress wave energy is transferred through joined drill rods to a drill bit, where a part of the energy is converted into work as the rock is crushed. Through the chain of drill rods there is a central hole for transport of flushing fluid to the bottom of the hole.

In the common type of drill rod joint shown in Fig. 1, the threaded ends of two drill rods are screwed into a coupling sleeve with internal thread. When a stress wave arrives at the joint, one part of its energy is transmitted, a second part is reflected and the remaining part is dissipated as heat due to slip and resulting frictional work in the threads. It has been found experimentally [1] that the dissipated energy may constitute from a few percent to as much as 15 percent of the incident wave energy depending on the conditions. For a supplied power of 20 kW, this means heat losses in the threads up to 3 kW and corresponding temperature rises.

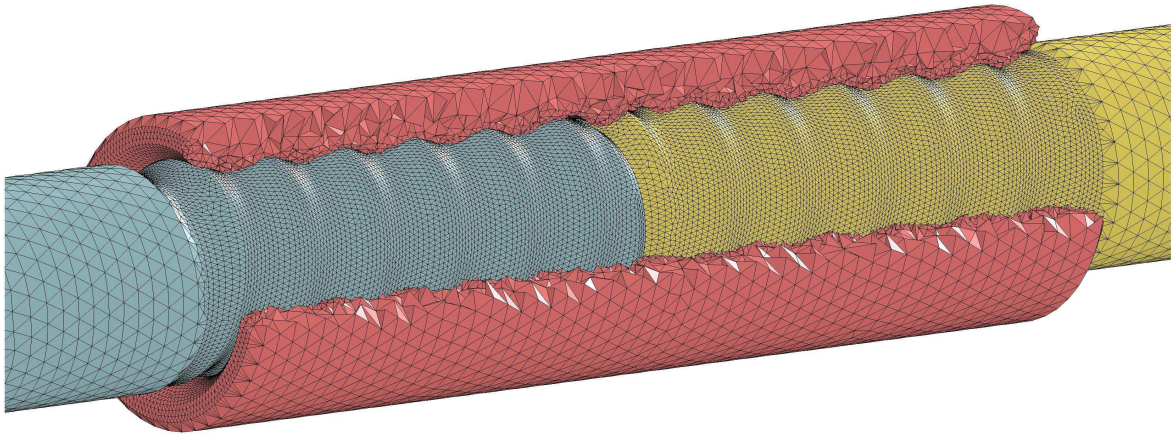

Fig. 1: Drill rod joint with a sector of the coupling sleeve removed.

A drill rod joint model comprising a rigid coupling sleeve, whose interaction with two elastic drill rods considered to be 1D is represented by two stiffness parameters and one friction parameter, has given results for wave energies and dissipated energy that agree well with experimental results [2]. However, it is a weakness of this model that its three thread parameters must normally be estimated from experimental tests, which means that it cannot be used without the existence of a prototype. Here, therefore, we have tested a 3D FE model for the drill rod joint used in [1].

The total length of the joined drill rods was 7 580 mm, and their external and internal diameters were 32.0 and 12.5 mm, respectively. The length of the coupling sleeve was 150 mm, and its external diameter was 44.0 mm. The material was steel with Young's modulus 210 GPa, Poisson's ratio 0.3 and density 7 800 kg/ m^3 .

Simulations were carried out with LS-DYNA in two steps. First the drill rods were screwed into the coupling sleeve quasi-statically until axial surface prestrains of 20, 120 and 360×10^{-6} were obtained at the mid-section of the sleeve. Then, an incident wave was generated by a rectangular pressure pulse applied at the end of the first drill rod. This pulse had amplitude 200 MPa and duration corresponding to impact by a cylindrical steel hammer with the same cross-sectional area as the drill rods, impact velocity about 10 m/s and length 0.3, 0.6 or 0.9 m (two transit times). In the simulations 994 917 4-node tetrahedal elements were used, corresponding to 231 185 nodes. In the drill rods, the element size varied from 4 mm outside the threaded parts to 1 mm on the surface of the threads. In the sleeve, the element size varied from 4 mm on the external surface to 1 mm on the surface of the internal thread. Explicit time integration was used and the time step was $0.024\ \mu s$.

Dissipated and transmitted energy, normalized to the energy of the incident wave, are shown in Figs. 2 and 3 for prestrain 120×10^{-6} and coefficient of friction 0.3. Corresponding experimental results [1] are shown for comparison. The dissipated energy decreases and the transmitted energy increases with increasing hammer length. Similar results for the prestrains 20 and 360×10^{-6} show that these energies decrease and increase, respectively, with increasing prestrain. Generally, the results of simulation and experiment agree satisfactorily. The slight difference between the dissipated energies based on the deficit of wave energy and the frictional work in the contact area, respectively, is probably due to waves which are incomplete or slightly overlapping in the rod volumes outside the joint where the energies were computed. It is also found that dissipation mainly occurs just after the arrival at the joint of the front and the end of the incident wave. During these periods, the sleeve is accelerated and retarded, respectively, and therefore some slip occurs. Although the results are preliminary, it is concluded that 3D FE simulation should be an efficient tool in the design of drill rod joints and similar sub-structures or components used in percussive drills.

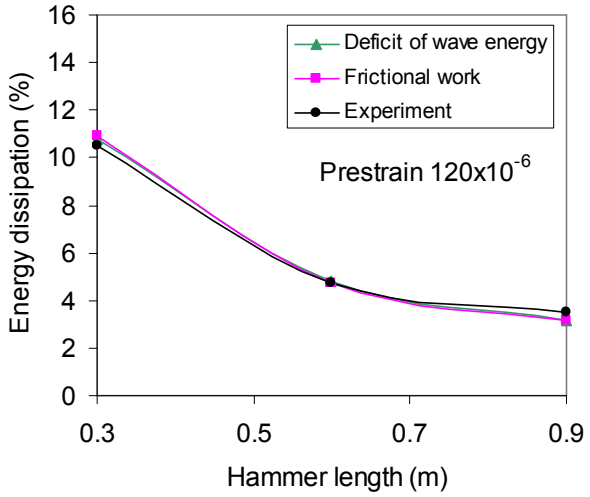

Fig. 2: Dissipated energy relative to the energy of the incident wave.

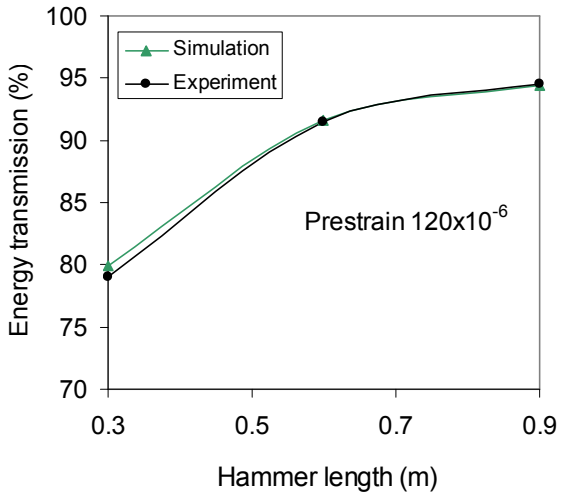

Fig. 3: Transmitted energy relative to the energy of the incident wave.

References

[1] R. Beccu, B. Lundberg. Transmission and dissipation of stress wave energy at a percussive drill rod joint. *Int. J. Impact Engng.,* **6:** 157-173, 1987.

[2] B. Lundberg, R. Beccu, A. Nilsson. Nonlinear dissipative spring mass model for a percussive drill rod joint of the coupling sleeve type. *Int. J. Impact Engng.,* **8:** 303-313, 1989.

IDENTIFICATION OF A HETEROGENEOUS MATERIAL PROPERTY FIELD USING A TIME-REVERSAL APPROACH

Shahram Khazaie[1], Régis Cottereau[2], D. Clouteau

Laboratoire MSSMat UMR8579, École Centrale Paris, CNRS, France;
e-mail: [1]shahramkhazaee@gmail.com, [2]regis.cottereau@ecp.fr

Keywords: Identification, Random medium, Time-reversal, Cross-correlation, Full-field measurement

There has been a lot of interest recently for three techniques of imaging in the context of heterogeneous media: (i) time-reversal techniques have shown to be very efficient in the identification of sources and scatterers in homogeneous and random media [2, 3]; (ii) noise cross-correlation has been widely used, in particular in geophysics [6, 4], to image smoothly varying heterogeneous media; and (iii) full-field measurement techniques have been developed to account for over-abundant data, in particular in the context of static material mechanics problems [5]. The objective of this presentation is to propose a new identification technique that incorporates some of the features of each of these three methods to allow for the identification of very heterogeneous material property field from the knowledge of a series of time signals at the surface of the medium.

More specifically, we consider the following two semi-discretized weak formulations:

1. *true time-reversed solution:* find $\tilde{u}(x,t)$ (in an appropriate functional space) such that

$$\int_\Omega \rho\ddot{\tilde{u}}(x,t)v(x)dx + \int_\Omega \tilde{k}(x)\nabla\tilde{u}(x,t)\nabla v(x)dx = \sum_{i=1}^{N} \tilde{f}(x_i, T-t)v(x_i), \quad \forall t, \forall v(x) \tag{1}$$

2. *surrogate time-reversed solution:* find $u(x,t)$ (in an appropriate functional space) such that

$$\int_\Omega \rho\ddot{u}(x,t)v(x)dx + \int_\Omega k(x)\nabla u(t,x)\nabla v(x)dx = \sum_{i=1}^{N} \tilde{f}(x_i, T-t)v(x_i), \quad \forall t, \forall v(x) \tag{2}$$

In these formulations, the loading fields $\tilde{f}(x_i,t)$ are recordings at N stations at the boundary of the medium. The true parameter field $\tilde{k}(x)$ is unknown in the identification problem, so the solution $\tilde{u}(x,t)$ of the first weak formulations can therefore not be approximated. The second weak formulation simulates a time-reversal experiment in which the model for the reversed experiment is different from the model for the direct experiment. The identification problem then consists in choosing a field $k(x)$ which is compatible with the information on $\tilde{k}(x)$ which is contained in the loading fields $\tilde{f}(x_i,t)$. Several approaches are possible, which bear similarities with full-field measurement techniques. However, the latter usually concentrate on space data rather than time recordings. Note that, for any chosen $k(x)$, the solution $u(x,t)$ can be computed, because $\tilde{f}(x_i,t)$ is given as data. Note also that an identification process for both parameters fields $k(x)$ and $\rho(x)$ would be possible, although we concentrate here on $k(x)$.

For very heterogeneous media, the parameterization of the field $k(x)$ becomes an issue, and the identification problem may become ill-posed. In particular, the values of the parameter field far from the sources may be little constrained by the data. For positions far-away from the recording locations, we therefore turn to a random field model for $k(x)$ and look for statistical information on it rather than its exact value at all points. Cross-correlation information will then be considered primarily.

Identification results will be presented for both 2D acoustic and 3D elastic models. For the later, we will use a spectral element code, originally based on RegSEM [1], for the resolution of equation (2) in a randomly heterogeneous medium [7].

References

[1] P. Cupillard, E. Delavaud, G. Burgos, G. Festa, J.-P. Vilotte, Y. Capdeville, J.-P. Montagner. RegSEM: a versatile code based on the spectral element method to compute seismic wave propagation at the regional scale. *Geophys. J. Int.*, **188**(3): 1203–1220, 2012.

[2] M. Fink. Time reversed acoustics. *Scientific American*, **281**(5): 91–97, 1999.

[3] J.-P. Fouque, J. Garnier, G. Papanicolaou, K. Solna. Wave propagation and time reversal in randomly layered media. *Springer*, 2007.

[4] J. Garnier, G. Papanicolaou. Passive sensor imaging using cross-correlations of noisy signals in a scattering medium. *SIAM J. Imaging Sciences*, **2**: 396–437, 2009.

[5] M. Grédiac, F. Hild. Mesures de champs et identification en mécanique des solides. *Lavoisier*, 2011.

[6] N. Shapiro, M. Campillo, L. Stelhy, M. Ritzwoller. High-resolution surface-wave tomography from ambient seismic noise. *Science*, **307**(5715): 1615–1618, 2005.

[7] Q.-A. Ta, D. Clouteau, R. Cottereau. Modeling of random anisotropic elas- tic media and impact on wave propagation. *Europ. J. Comp. Mech.*, **19**(1-3): 241–253, 2010.

SENSITIVITY GAUSSIAN PACKETS

Luděk Klimeš

Department of Geophysics, Faculty of Mathematics and Physics,
Charles University in Prague, Czech Republic; http://sw3d.cz

Keywords: elastic waves, elastic moduli, perturbation, Born approximation, heterogeneous media

We study how the perturbations of a generally heterogeneous isotropic or anisotropic structure manifest themselves in the wave field, and which perturbations can be detected within a limited aperture and a limited frequency band. We consider a smoothly varying heterogeneous generally anisotropic elastic background medium, and its arbitrarily varying generally anisotropic perturbations. We decompose the perturbations of elastic moduli and density into Gabor functions. The wave field scattered by the perturbations is then composed of waves scattered by the individual Gabor functions.

We assume a short–duration, broad–band, incident wave field with a smooth frequency spectrum. We approximate each wave scattered by one Gabor function by the *first–order Born approximation*, which describes the first–order sensitivity of the wave field to the infinitesimally small structural perturbations exactly. We make use of the *paraxial ray approximation* of the incident wave in the vicinity of the central point of the Gabor function, and of the *two–point paraxial ray approximation* of the Green tensor. The above–mentioned approximations enable us to calculate the waves scattered by the individual Gabor functions analytically [1].

The wave, scattered by one Gabor function, is composed of a few (i.e. 0 to 5 as a rule) Gaussian packets. Each of these "sensitivity" Gaussian packets has a specific frequency and propagates from the Gabor function in a specific direction, see Figures 1–3. Each sensitivity Gaussian packet is sensitive to just a single linear combination of the perturbations of elastic moduli and density, corresponding to the Gabor function. This information about the Gabor function is lost if the sensitivity Gaussian packet does not fall into the aperture covered by the receivers and into the legible frequency band. The situation improves with the increasing number of differently positioned sources. If we have many sources, the sensitivity Gaussian packets, propagating from a Gabor function, may be lost during the measurement corresponding to one source, but recorded during the measurement corresponding to another, differently positioned source. However, the problem is not only to record the Gaussian packets from a Gabor function, but to record them in as many different measurement configurations as to resolve the perturbations of all elastic moduli and density.

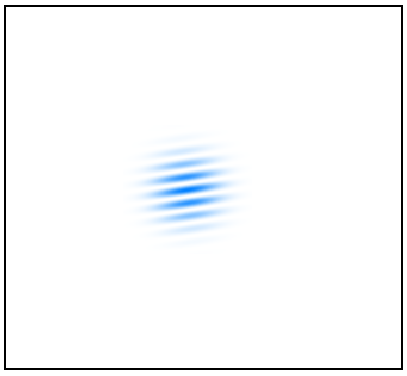

Figure 1: A single Gabor function.

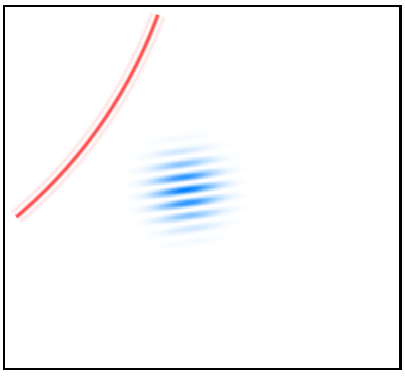

Figure 2: Broad–band wave incident at the Gabor function.

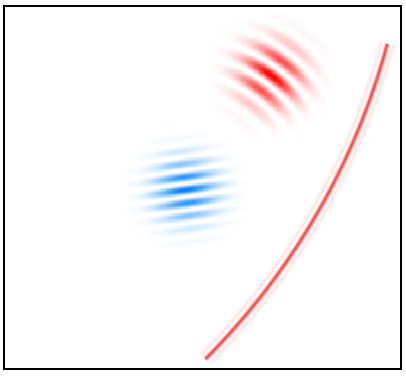

Figure 3: Gaussian packet scattered by the Gabor function.

In a numerical example, we consider the distribution of the P–wave velocity in the Marmousi structure. The velocity difference between the Marmousi structure and the smooth background medium is displayed in Figure 4. For the decomposition of the velocity difference, we generate the set of Gabor functions with their shapes optimized according to [2], see Figure 5. We then decompose the velocity difference from Figure 4 into the sum of Gabor functions. For each shot, we calculate the sensitivity Gaussian packets scattered by the individual Gabor functions. If a sensitivity Gaussian packet arrives at the receiver array within the registration time and frequency band, the recorded wave field contains

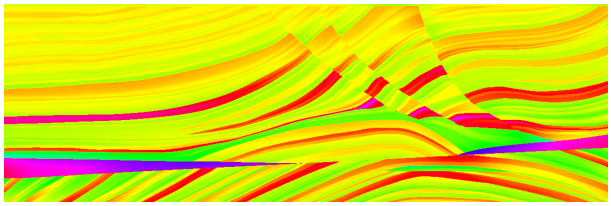

Figure 4: Velocity difference between the Marmousi structure and the velocity model.

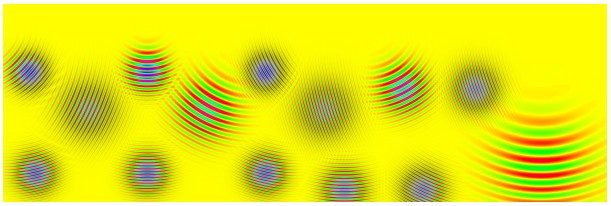

Figure 5: Example showing 14 ones of 67014 optimized Gabor functions used to decompose the velocity difference.

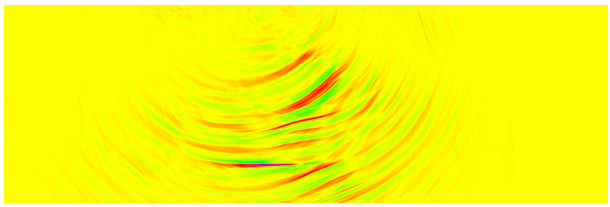

Figure 6: Sum of the Gabor functions influencing the seismograms recorded for shot 70.

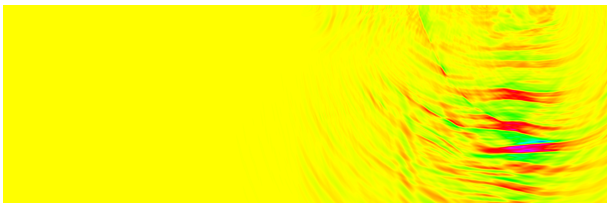

Figure 7: Sum of the Gabor functions influencing the seismograms recorded for shot 220.

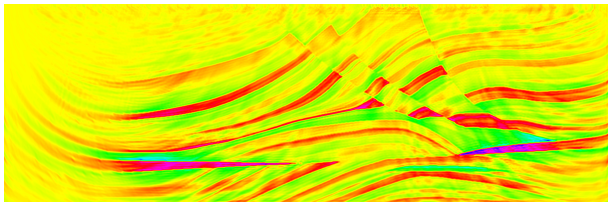

Figure 8: Sum of the Gabor functions influencing the seismograms collected from all shots.

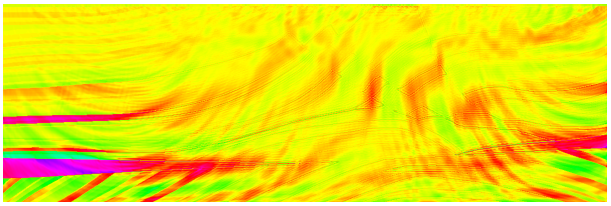

Figure 9: Part of the velocity difference from Figure 4 influencing no recorded seismogram.

information on the corresponding Gabor function. The sums of the Gabor functions influencing the seismograms recorded for shots 70 and 220 are displayed in Figures 6 and 7. The velocity difference from Figure 4 can be decomposed into the part to which the recorded seismograms are not sensitive and into the part to which the recorded seismograms are sensitive. The sum of the Gabor functions influencing the seismograms collected from all shots is displayed in Figure 8. This is the part of the velocity difference to which the recorded seismograms are sensitive. The remaining part of the velocity difference, influencing no recorded seismogram within the first–order Born approximation, is displayed in Figure 9. This part of the velocity difference cannot be recovered from the Marmousi seismograms.

The sensitivity Gaussian packets can enable migrations to be replaced by true linearized inversions of seismic reflection data. For the algorithm of the linearized inversion of the complete set of seismograms recorded for all shots, refer to [3].

Acknowledgements

The research has been supported by the Grant Agency of the Czech Republic under contract P210/10/0736, by the Ministry of Education of the Czech Republic within research project MSM0021620860, and by the members of the consortium "Seismic Waves in Complex 3–D Structures" (see "http://sw3d.cz").

References

[1] L. Klimeš. Sensitivity of seismic waves to the structure. *Stud. geophys. geod.*, **56**, No. 2, in press, 2012.

[2] L. Klimeš. Optimization of the structural Gabor functions in a homogeneous velocity model for a zero–offset surface seismic reflection survey. In: *Seismic Waves in Complex 3–D Structures, Report 18*, pp. 115–127, Dep. Geophys., Charles Univ., Prague, 2008, online at "http://sw3d.cz".

[3] L. Klimeš. Stochastic wavefield inversion using the sensitivity Gaussian packets. In: *Seismic Waves in Complex 3–D Structures, Report 18*, pp. 71–85, Dep. Geophys., Charles Univ., Prague, 2008, online at "http://sw3d.cz".

NUMERICAL SOLUTION OF ELASTIC WAVE PROPAGATION BY ISOGEOMETRIC ANALYSIS

R. Kolman, J. Plešek, M. Okrouhlík, D. Gabriel, J. Kopačka

Institute of Thermomechanics AS CR, v.v.i., Prague, Czech Republic;
e-mail: {kolman;plesek;ok;gabriel;kopacka}@it.cas.cz

Keywords: elastic wave propagation, isogeometric analysis, B-spline and NURBS shape functions

Introduction

A modern approach in the finite element analysis is the *isogeometric analysis* (IGA) [1], where shape functions are based on varied types of splines. For example, B-spline (basis spline), NURBS, T-spline and others are used for spatial discretization. This approach has an advantage that the geometry and approximation of the field of unknown quantities is prescribed by the same technique as in CAD commercial software. Another benefit is that the approximation is smooth. For one-dimensional or multi-dimension problems on the domains with straight boundaries, the B-spline basis functions could be used for spatial discretization.

The spatial discretization of elastic continuum by *finite element method* (FEM) [2] introduces dispersion errors to numerical solutions of stress wave propagation. When these propagating phenomena are modelled by FEM the speed of a single harmonic wave depends on its frequency and thus a wave packet is distorted. Moreover, the oscillations near the sharp wavefront in FE solution (called Gibb's effect) appears [3]. For higher order Lagrangian finite elements, the optical modes with the amplitude elongation in the spectrum exist. Furthermore, the high mode behaviour of classical finite elements is divergent with order of approximation of a field of displacements.

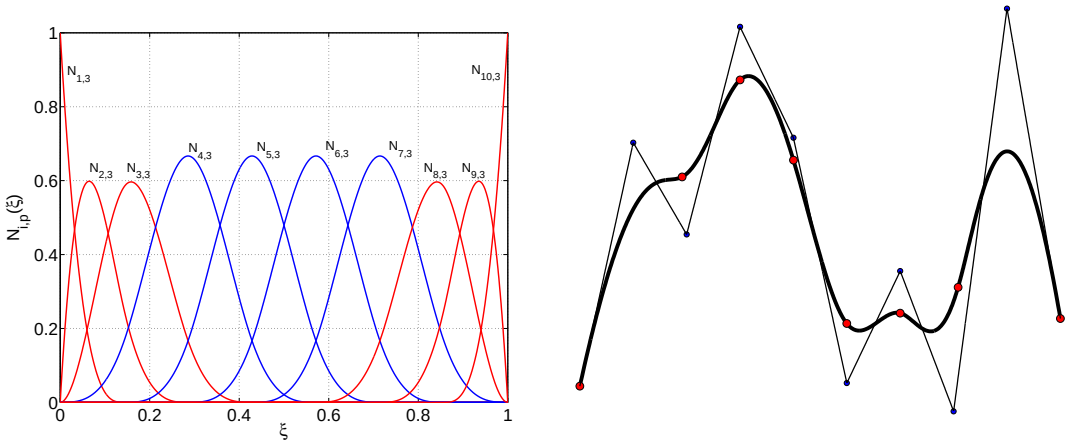

Figure 1: Example of cubic B-spline basis functions (on the left) for ten control points and the uniform knot vector. An open cubic B-spline curve interpolating end points (on the right).

It was shown for unbounded domains in [4], that the optical modes for isogeometric approach did not exist against higher order Lagrangian finite elements. This is an outcome of uniform continuous piecewise higher order polynomial shape functions, (blue functions in Figure 1). Further, dispersion and frequency errors for isogeometric analysis were reported to decrease with increasing order of spline [4]. Isogeometric analysis, where continuous piecewise higher order polynomials are used as shape functions, improves the dispersion errors and frequency spectrum. The spline based FEM with small dispersion errors and the variation diminishing property [1] could eliminate spurious oscillations, which are the outcome of the Gibb's effect and the dispersion behaviour of FEM.

Numerical tests

In this initial work, the B-spline FEM is tested in numerical modelling in elastic wave propagation problems. The first crucial test is a problem of axial elastic waves propagation in a free-fixed "thin" bar under the shock loading [5], see Fig. 2(on the left). The second test is a symmetrical impact of thick elastic plates [6], see Fig. 2(on the right), modelled as a three-dimensional problem with respect to symmetrical conditions. Both tests serve for the determination of accuracy and stability of IGA in wave propagation of sharp wave fronts. The special attention is devoted to the monitoring of approximation of theoretical wave-fronts, numerical dispersion and the existence of spurious oscillations near wave-fronts. The continuous Galerkin's approximation method is employed [1] and for the time integration, the Newmark method, the central difference method and the generalized-α method, respectively are compared [4].

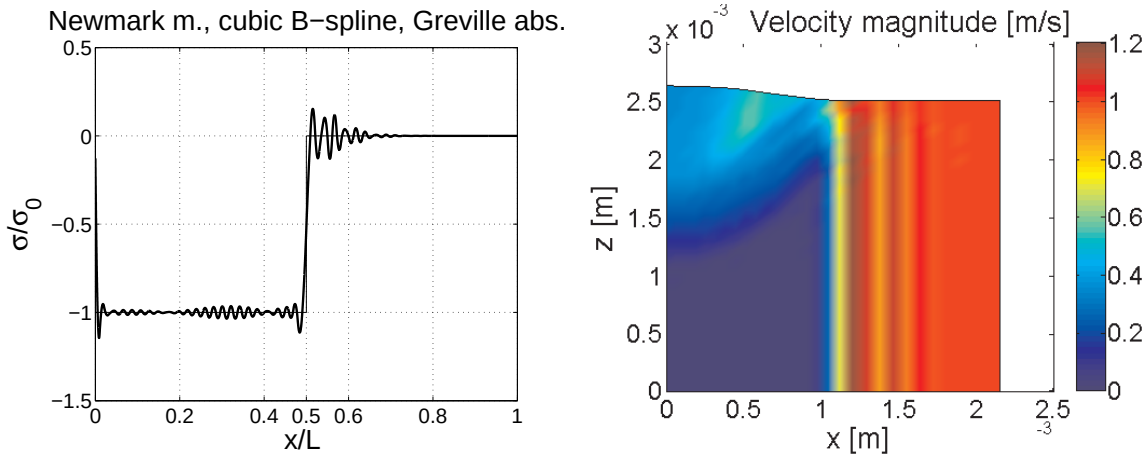

Figure 2: Dimensionless stress in an elastic free-fixed bar under the shock loading at time $t = 0.5L/c_0$ computed by the Newmark method with the consistent mass matrix for cubic B-spline FEM (on the left). Distribution of velocity amplitude for symmetrical impact problem of thick elastic plates (on the right), the half of deformed configuration is depicted at time $t = 0.56d/c_1$.

Details of the IGA in elastic wave propagation, its accuracy and performance will be presented at the Colloquium.

Acknowledgement

This work was supported by the grant projects GA ČR GPP101/10/P376, GA101/09/1630, GAP101/11/0288 and GAP101/12/2315 under AV0Z20760514.

References

[1] J.A. Cottrell, T.J.R. Hughes, Y.'Bazilevs. *Isogeometric Analysis: Toward Integration of CAD and FEA*. John Wiley & Sons, New York, 2009.

[2] T.J.R. Hughes. *The Finite Element Method: Linear and Dynamic Finite Element Analysis*. New York: Prentice-Hall, Englewood Cliffs, 1983.

[3] L. Jiang, R.J. Rogers. Effects of spatial discretization on dispersion and spurious oscillations in elastic wave propagation. *Int. J. Numer. Methods. Eng.*, **29**: 1205–1218, 1990.

[4] T.J.R Hughes, A. Reali, G. Sangalli. Duality and unified analysis of discrete approximations in structural dynamics and wave propagation: Comparison of p-method finite Elements with k-method NURBS. *Comput. Methods Appl. Mech. Engrg.*, **197**: 4104–4124, 2008.

[5] J.D. Achenbach. *Wave Propagation in Elastic Solids*. North Holland, Amsterdam, 1973.

[6] R. Brepta, F. Valeš. Longitudinal impact of bodies. *Acta Technica ČSAV*, **32**: 575–602, 1987.

STRUCTURES WITH TIME-DEPENDENT MOMENT OF INERTIA AND THEIR IMPLEMENTATION IN SENSORS, ACTUATORS AND DYNAMIC MATERIALS

Slava Krylov[1], Konstantin Lurie[2], Assaf Ya'akobovitz[1]

[1]School of Mechanical Engineering, Tel Aviv University, Tel Aviv, Israel; email: vadis@eng.tau.ac.il
[2]Department of Mathematical Sciences, Worcester Polytechnic Institute, Worcester, MA

Keywords: time-dependent moment of inertia, compliant structure, micro gyro, parametric excitation, dynamic materials

We introduce and analyze a new class of fully compliant dynamic structures with time-dependent inertia performing vibratory motion and characterized by non-zero averaged momentum. Note that while the tuning of structure's stiffness can be achieved, for example, by application of an electrostatic force [1-3], the tuning of inertial properties is more challenging since controllable attachment and detachment of the mass is problematic. Instead, in this work we propose to change the moment of inertia of the structure rather than its mass. The moment of inertia of the structures performing tilting vibrations is controlled, by means of an external force, in such a way that the angular momentum averaged during the period is not zero. It should be noted that in microstructures, an implementation of unidirectional, non-vibratory motion is difficult due to low reliability of parts performing relative motion accompanied by contact, friction and stiction. As a result, most of microdevices are realized as compliant structures performing vibratory motion with zero momentum averaged over period. For this reason, the operational principle of most of micromachined sensors and specifically of angular rate sensors differs from that governing the performance of their macro scale counterparts [4] and relies on the coupling between two vibratory modes arising due to Coriolis force [5].

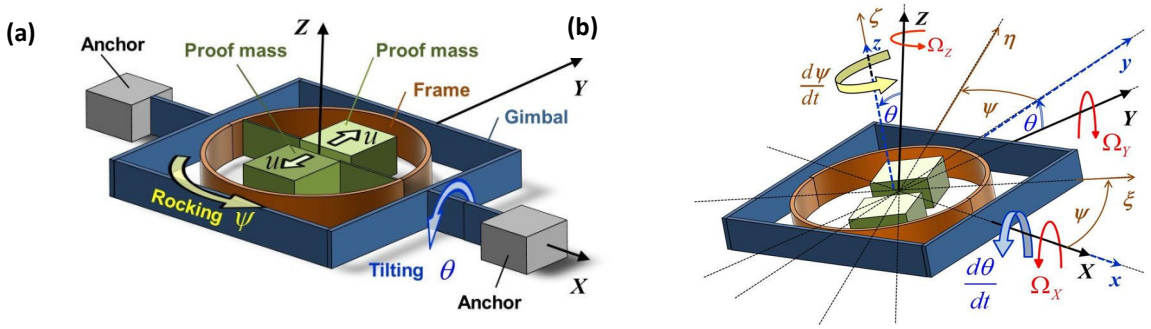

Figure 1. Geometry of the structure (a) and coordinate systems in the deformed configuration (b).

The structure analyzed in the present work incorporates a sensing element (a gimbal) attached to the substrate (rotating with a prescribed angular velocity) by torsion axes and performing a tilting motion, Fig.1. A frame is attached to the gimbal and is forced to perform a rocking motion (drive mode) around the axis perpendicular to the gimbal; one or several proof masses are attached to the frame. By moving the masses in the radial (with respect to the frame's rocking motion axis) direction, the moment of inertia of the frame can be changed. Note that the ability to provide a time-dependent inertial properties opens new possibilities for realization of a novel concept of dynamic materials (DM) [6] - the substances with material properties that may change in space and time - by using micromachined elements.

Equations of motion of the device were developed by using a variational principle. The detailed feasibility studies were carried out for the configuration corresponding to an infinite number of proof masses - a

massive expandable ring. We show that, similarly to the spinning disk gyro, the fully compliant device is distinguished by a non-zero average angular momentum and by an ability to extract the angular rate from the static tilting angle of the gimbal, Fig. 2. Simple asymptotic expressions relating the angular rate and the averaged tilting angle of the sensing element are obtained and verified numerically, Fig. 2. Several operational scenarios, based on the open and close loop control of the masses' motion, are investigated along with the influence of various parameters - the modulation depth of the moment of inertia, the ratio of the frequencies of the drive and sense modes and the phase of modulation. The operational principle can be efficiently implemented in angular rate sensors with increased sensitivity and lower structural coupling between the drive and sense modes as well as in the parametrically excited devices [7] and tunable inertial sensors [8,9].

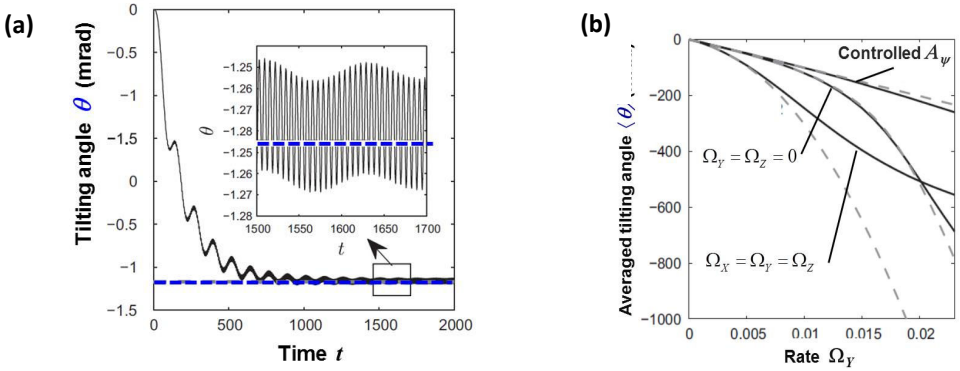

Figure 2. (a) Time history of the device with a ring-shaped proof mass and time-dependent moment of inertia: the sense mode -the gimbal tilting angle. (b) Averaged tilting angle (in mrad) of the gimbal (sense mode) as a function of an angular rate Ω_Y. The dashed lines correspond to the approximation of the static value.

References

[1] S. Krylov, I. Harari, Y. Cohen. Stabilization of Electrostatically Actuated Microstructures using Parametric Excitation. *J. Micromech. Microeng.,* **15**: 1188–1204, 2005.

[2] S. Krylov, Y. Gerson, T. Nachmias, U. Keren. Excitation of large amplitude parametric resonance by the mechanical stiffness modulation of a microstructure. *J. Micromech. Microeng.* 20:015041, 2010.

[3] J. Rhoads, S.W. Shaw, K.L. Turner. Nonlinear dynamics and its applications in micro- and nanoresonators Proc. DSCC2008 2008 ASME Dynamic Systems and Control Conference (2022 October, Ann Arbor, MI, USA) DSCC2008-2406, 2008.

[4] H. Baruch. *Analytical Dynamics*. WCB/McGraw Hill, 1999.

[5] C. Acar, A. Shkel. *MEMS Vibratory Gyroscopes: Structural Approaches to Improve Robustness*. Springer, New York, 2009.

[6] K.A. Lurie. *An Introduction to the Mathematical Theory of Dynamic Materials*. Springer Science + Business Media, LLC, New York, 2007.

[7] L.A. Oropeza-Ramos, C.B. Burgner, K.L. Turner. Robust micro-rate sensor actuated by parametric resonance *Sens. Act. A,* **152**:80–87, 2009.

[8] D. Schwartz, D.J. Kim, R.T. MCloskey. Frequency tuning of a disk resonator gyro via mass matrix perturbation, *J. Dyn. Syst. Control* 131:061004, 2009.

[9] S. Krylov., K.A. Lurie, A. Ya'akobovitz. Compliant structures with time-varying moment of inertia and non-zero averaged momentum and their application in angular rate microsensors, *J. of Sound Vib.*, **330**: 4875–4895, 2011.

THE LIÉNARD-WIECHERT POTENTIALS AND RETARDED FIELDS IN ELASTODYNAMICS

Markus Lazar

Heisenberg Research Group, Department of Physics, Darmstadt University of Technology, D-64289 Darmstadt, Germany; e-mail: lazar@fkp.tu-darmstadt.de

Keywords: non-uniform motion, radiation, retardation, elastic waves

The purpose of this presentation is to investigate the fundamental problem of the non-uniform motion of a point force in an unbounded, homogeneous, isotropic medium in analogy to the electromagnetic field theory [3]. The exact closed-form solutions of the displacement and elastic fields produced by a non-uniformly moving point force are calculated. The displacement field can be identified with the elastodynamic Liénard-Wiechert potential. We decompose the elastic fields into a radiation part (acceleration field) and a non-radiation part (velocity-dependent field) for a non-uniformly moving point force. We show that the solution of a non-uniformly moving point force is the generalization of the Stokes solution to the non-uniform motion. Elastodynamic fields propagate with finite velocities. There always is a time delay before a change in elastodynamic conditions initiated at a point of space can produce an effect at any other point of space. This time delay is called elastodynamic retardation.

We discuss the analogy between the non-uniform motion in elastodynamics [1] and in electrodynamics [2]. In electrodynamics, radiation is caused by the non-uniform motion of an electric point charge. The electric and magnetic potentials of such a non-uniformly moving point charge are called the Liénard-Wiechert potentials. The corresponding electric and magnetic field strengths consist of velocity-depending fields and acceleration-depending fields. The last ones are the fields of radiation. This is a standard topic in electromagnetic field theory and is covered in many books on electrodynamics (e.g. [2]). Using the electrodynamical analogy, we investigate the elastodynamical radiation caused by force distributions.

Acknowledgement

This work was supported by the grant project of the Deutsche Forschungsgemeinschaft (Grant Nos. La1974/2-1, La1974/3-1).

References

[1] J.D. Achenbach. *Wave Propagation in Elastic Solids*. North Holland, Amsterdam, 1973.

[2] J.D. Jackson. *Classical Electrodynamics*. 3rd ed., Wiley, New York, 1999.

[3] M. Lazar. The elastodynamic Liénard-Wiechert potentials and elastic fields of non-uniformly moving point and line forces. Submitted, 2012.

DYNAMICS OF BEAM TRUSSES UNDER IMPULSE LOADS

Yves Le Guennec[1], Éric Savin[1], Didier Clouteau[2]

[1]ONERA–The French Aerospace Lab, Châtillon, France; e-mail: yves.le_guennec@onera.fr, eric.savin@onera.fr
[2]École Centrale Paris, MSSMat Laboratory, Châtenay-Malabry, France; e-mail: didier.clouteau@ecp.fr

Keywords: high frequency, transport equation, discontinuous Galerkin method

Spatial structures are often subjected to impulse loads which induce high-frequency wave propagation. Despite some recent researches, the characterization of the transient response to such loads remains an open problem. These loads can damage the integrity of the structures or equipments attached to them. For example, the solar panels unfolding is set off by a pyrotechnic shock leading to high-frequency wave propagation in the panels. Another example is the pyrotechnic cut for the space launcher/satellite separation. Thus it is necessary to improve the prediction of the high-frequency structural responses with efficient theoretical and numerical models.

In this research, we are interested in high-frequency wave propagation within three-dimensional beam trusses. In the high-frequency range, classical global vibrational methods are not applicable on account of the small wavelength and the high modal density. Therefore two kinds of strategies have been developed by engineers: either global approaches like the Statistical Energy Analysis (SEA) [1] or local approaches like the vibrational conductivity analogy [2]. The main issue of the global approaches is the estimation of some core parameters like the coupling loss factors or the injected powers, whereas the extension of the existing local approaches to built-up systems seems to be difficult. The method adopted here is local and based on the microlocal analysis of classical wave systems. In this framework, it can be proved that the energy density associated with high-frequency elastic waves in a Timoshenko beam satisfy a Liouville-type transport equation [3]:

$$\partial_t w_\alpha + \{\lambda_\alpha, w_\alpha\} = 0, \tag{1}$$

where $w_\alpha(x,k,t)$ is the phase-space energy density of the energy mode α of which eigenfrequency is λ_α, $x \in \mathcal{S}$ is the curvilinear abscissa in the neutral fiber $\mathcal{S} \subset \mathbb{R}$ of the beam, $k \in \mathbb{R}$ is the wave number, and $\{f,g\} = \partial_k f \cdot \partial_x g - \partial_x f \cdot \partial_k g$ is the usual Poisson bracket. This equation highlights the conservation of the vibrational energy in an undamped beam. It is shown in [4] that the energetic modes are separated into two different families: the longitudinal modes that gather the compressional mode and bending modes, and the transverse modes that gather the shear modes and the torsional mode. The longitudinal modes have an eigenfrequency $\lambda_P = |k|\sqrt{E/\rho}$, where E is the Young modulus and ρ is the material density, and the transverse ones have an eigenfrequency $\lambda_T = |k|\sqrt{\kappa\mu/\rho}$, with $\kappa\mu$ the reduced shear modulus. It is remarkable to notice that there is no coupling between modes in the waveguide, an observation that could be somewhat counter-intuitive with an expected diffusive state. In fact all the coupling will occur at the junction.

Indeed, the energy flow is partly reflected and partly transmitted at the interface between substructures. The corresponding reflection/transmission coefficients are derived along the same lines as it is done in [5] for assemblies of two-dimensional beams or plates. The approach is to consider the boundary conditions of the classical wave equation and to derive power flow transmission/reflection coefficients consistent with quadratic observables (wave fluxes). Our results show that the rotational modes (*i.e.* bending and torsion) are totally uncoupled from the translational modes (*i.e.* compression and shear); a mode of one family impinging the junction can not be converted into a mode of the other family. This fact is a remarkable property of the high-frequency dynamics of slender structures.

The objective of this research is to extend the existing model to assemblies of three-dimensional curved beams and develop a reliable model of the high-frequency energy evolution within beam trusses in order to predict, for example, their steady-state behavior at late times or the energy paths. At first, Timoshenko beam theory has been used to describe wave propagation in the truss. The main issue of the proposed derivation is the choise of these kinematics for the beam. Timoshenko hypotheses are indeed not relevant anymore in the high-frequency limit, when the wavelength gets smaller than the cross-section dimensions. This model may be improved by the consideration of Pochhammer-Chree modes in one-dimensional waveguides [7].

As for the numerical resolution of the transport equation (1), classical (continuous) finite element methods can

not be used on account of the discontinuities of the energy density field at the junctions. Thus a Discontinuous Galerkin (DG) finite element method [8] is implemented. The key issue of this method is to introduce numerical fluxes depending on the traces of the physical fluxes at each side of the junction. The spatial discretization is achieved by Legendre polynomials and the direct time integration is performed with a Strong Stability-Preserving Runge-Kutta method [9]. DG methods have the advantages to be weakly dissipative and weakly dispersive depending on their order of interpolation. Thus they are well suited for long times simulation in order to exhibit a potential steady-state behavior. Numerical simulations using the DG method are presented for the example of a three-dimensional beam truss. The numerical implementation and the low-dissipation and low-dispersion properties of our schemes are validated by reversed-time computations. The analysis of these results shows that the steady-state behavior of the truss at late times corresponds to a diffusive behavior as assumed by SEA, for example.

References

[1] R. H. Lyon, R. G. DeJong, *Theory and Application of Statistical Energy Analysis*. Butterworth-Heineman, Boston MA, 2nd edition ,1995.

[2] D. J. Nefske, S. H. Sung. Power flow finite element analysis of dynamic systems: basic theory and application to beams. *ASME J. Vib. Acoust. Stress Reliab. Des.*, **111**: 94–100, 1989.

[3] G. C. Papanicolaou, L. V. Ryzhik, J. B. Keller. Transport equations for elastic and other waves in random media. *Wave Motion*, **24**: 327–370, 1996.

[4] Y. Le Guennec, É. Savin. A transport model and numerical simulation of the high-frequency dynamics of three-dimensional beam trusses. *J. Acoust. Soc. Am.*, **130**: 3706–3722, 2011.

[5] É. Savin. A transport model for high-frequency vibrational power flows in coupled heterogeneous structures. *Interaction Multiscale Mech.*, **1**: 53–81, 2007.

[6] B. Lapeyre, É. Pardoux, R. Sentis. *Introduction to Monte-Carlo Methods for Transport and Diffusion Equations*. Oxford University Press, Oxford, 2003.

[7] J. D. Achenbach. *Wave Propagation in Elastic Solids*. North-Holland, Amsterdam, 1973.

[8] J. S. Hesthaven, T. Warburton. *Nodal Discontinuous Galerkin Methods*. Springer, New York NY, 2008.

[9] S. Gottlieb, C.-W. Shu, E. Tadmor. Strong Stability-Preserving High-Order Time Discretization Methods. *SIAM Review*, **43**: 89–112, 2001.

ANALYSIS OF ELASTIC WAVE PROPAGATION BY AN IMPROVED FINITE ELEMENT METHOD

Mario Leindl[1], Eduard R. Oberaigner[2]

[1]Institute of Mechanics at University of Leoben, Leoben, Austria; e-mail: mario.leindl@unileoben.ac.at
[2]Institute of Mechanics at University of Leoben, Leoben, Austria; e-mail: ero@unileoben.ac.at

Keywords: elastic wave propagation, finite element method, Green's function, trigonometric shape functions

Introduction

The analysis of elastic wave propagation is of crucial importance in several areas of engineering, e.g., design of spacecraft and aeroplanes, exploration geophysics, design of civil structures. Since the middle of the last century technical innovations in the latter mentioned areas have increased the importance of understanding of dynamic phenomena. The first decades in studying dynamic aspects were marked by analytical methods [1, 4, 5, 6], e.g., integral transformation techniques like Laplace and Fourier transform or appropriate modifications of them, the Green's function method, etc. In the last decades of the 20th century digital computers became available for most scientists and numerical solution techniques, e.g., finite difference, boundary element, finite volume method [9], or finite element [2] method were used effectively, additionally nonlinear problems were analysed by numerical methods [3].
This work deals with analytical and numerical solution methods for elastic wave propagation phenomena in different structural elements like strings, rods and beams. As numerical technique the finite element method will be used and as analytical technique, to check numerical results, the Green's function method. It is known that the solution representing travelling or standing waves can be represented as a trigonometric series. Therefore it is a natural consideration to use trigonometric functions as trial functions in the Galerkin approximation or as shape functions in the finite element technique. For the analysis of free vibrations this approach is used in [7, 8]. Beside the discretization of structures in space via finite elements a time integration algorithm is necessary to solve the governing equations of wave propagation. In classical finite element texts the central difference approach is often used for this task [2] while in this work a Runge-Kutta method is presented. To show the power of the demonstrated approach some benchmark calculations with the finite element method are performed and compared with results obtained by the Green's function method. Furthermore, parameter studies are presented in which the thermophysical material properties as well as the discretization parameters, e.g., element size, time step, are considered. Finally it is discussed how the presented method can be applied to thermo-mechanically coupled wave propagation problems.

References

[1] J.D. Achenbach. *Wave Propagation in Elastic Solids*. North Holland, Amsterdam, 1973.

[2] K.J. Bathe. *Finite Element Procedures in Engineering Analysis*. Prentice Hall, Englewood Cliffs NJ, 1982.

[3] A. Berezovski, J. Engelbrecht and G.A. Maugin. *Numerical Simulation Of Waves And Fronts In Inhomogeneous Solids*. World Scientific Publishing Co. Pte. Ltd., Singapore, 2008.

[4] A.C. Eringen, E.S. Suhubi. *Elastodynamics: Finite Motions Vol. I*. Academic Press Inc., New York, 1974.

[5] A.C. Eringen, E.S. Suhubi. *Elastodynamics: Linear Theory Vol. II*. Academic Press Inc., New York, 1975.

[6] K.F. Graff. *Wave Motion in Elastic Solids*. Oxford University Press, Oxford, 1975.

[7] A. Houmat. An alternative hierarchical finite element formulation applied to plate vibrations. *Journal of Sound and Vibration*, **206**: 201–215, 1997.

[8] A. Houmat. Free vibration analysis of arbitrarily shaped membranes using the trigonometric p-version of the finite-element method. *Thin-Walled Structures*, **44**: 943–951, 2006.

[9] R.J. LeVeque. *Finite Volume Methods for Hyperbolic Problems*. Cambridge University Press, Cambridge, 2002.

VARIATIONAL TIME INTEGRATORS FOR NONLINEAR THERMOELASTIC CONTINUA WITH HEAT CONDUCTION

Adrian J. Lew[1], Pablo Mata Almonacid[2]

[1]Department of Mechanical Engineering, Stanford University, USA, email:lewa@stanford.edu
[2]Centro de Investigación en Ecosistemas de la Patagonia (CIEP), Coyhaique, Chile, email:pmata@ciep.cl

Keywords: variational integrators, thermoelasticity, heat conduction.

Variational time integrators are time-discretization schemes for Hamiltonian systems that are obtained from a discrete version of Hamilton's principle. The basic idea is to construct a discrete action S_d that to each discrete trajectory of the system assigns a scalar, and that approximates the exact action of the system in a precise sense not specified here. The discrete trajectories are then obtained as the stationary points of S_d among a class of admissible trajectories, akin to those in Hamilton's principle. As a byproduct, the resulting integrators: (a) are (multi-)symplectic, and hence have outstanding long-term energy conservation properties, and (b) conserve momenta conjugate to symmetries of S_d, as stated by a discrete version of Noether's theorem. In this way, if the original system conserves linear and angular momentum, for example, it is simple to construct time integrators that will do so as well. Additionally, time-integration schemes of any order, implicit or explicit, with or without constraints, can be constructed.

In this presentation we will first briefly summarize the main results and ideas of the last fifteen years on variational time integrators, including the creation of multi-time-step integrators for nonlinear elastic media termed asynchronous variational integrators [3, 4].

We will then introduce recent ideas on the creation of variational time integrators for nonlinear thermoelastic continua, with and without heat conduction. There are two key ideas here. The first one is the realization that thermoelastic systems without heat conduction (adiabatic) are in fact Hamiltonian, by regarding the temperature as a generalized velocity associated to "fictitious" thermal displacements [5]. The action of the system is then invariant under rigid translations of the thermal displacements, and the conjugate conserved quantity is the conservation of the entropy of the system. This is exactly reflected by the resulting variational time integrators, which conserve the entropy of the system exactly, in addition to conserving the energy and the pertinent mechanical momenta, see Fig. 1. As concrete examples, we constructed a second-order explicit algorithm, which is a generalization of central differences to adiabatic thermoelastic systems, as well as a fourth-order implicit one.

We extended essentially the same integrators to thermoelastic systems with Green-Naghdi type II heat conduction, in which the heat flux is a linear function of the gradient of the thermal displacements [2]. These systems are Hamiltonian, and once again the entropy is exactly conserved.

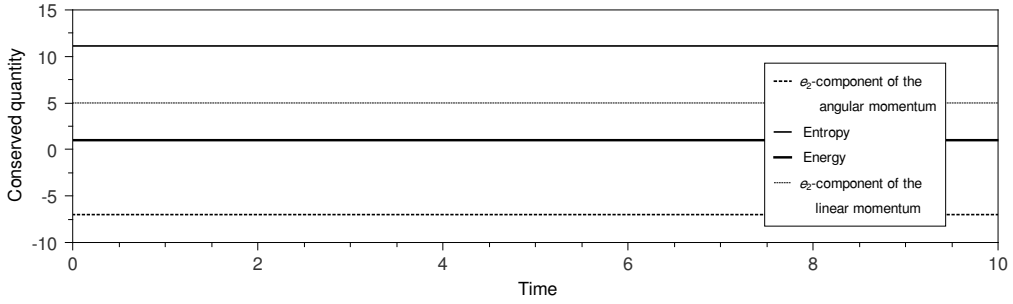

Figure 1: Conserved quantities in the long-time simulation of adiabatic thermoelastic mechanical systems, from [1].

The inclusion of Fourier heat conduction, in which the heat flux is a linear function of the gradient of the temperature is far less trivial. In this case, the system is no longer Hamiltonian, but for an isolated mechanical system the energy and mechanical momenta are still conserved, and the entropy does not decrease.

We will then describe recent progress in this direction, in which we first consider an integrable Hamiltonian mechanical system, and regard Fourier heat flow as non-Hamiltonian perturbation. Integrators for this type of systems can be constructed by adding these perturbations to the original algorithms, also regarded as a discrete version of Lagrange-d'Alembert variational principle. For *small enough perturbations*, we will show numerical evidence and some analytical results that suggest that the resulting algorithms effectively conserve the energy of isolated system for very long times, while guaranteeing that the entropy does not decrease, as the second-law requires. This is the second key idea.

References

[1] P. Mata, A.J. Lew. Variational time integrators for finite dimensional thermo-elasto-dynamics without heat conduction. *International Journal for Numerical Methods in Engineering*, **88**(1): 1–30, 2011.

[2] P. Mata, A.J. Lew. Variational integrators for the dynamics of thermo-elastic solids with finite speed thermal waves. *In preparation.*

[3] A. Lew, J.E. Marsden, M. Ortiz, M. West. Asynchronous Variational Integrators, *Archive for Rational Mechanics and Analysis*, **167**: 85–146, 2003.

[4] A. Lew, J.E. Marsden, M. Ortiz, M. West. Variational time integrators, *International Journal for Numerical Methods in Engineering*, **60**: 153–212, 2004.

[5] Dascalu C, Maugin GA. The thermoelastic material-momentum equation. *Journal of Elasticity*, **39**: 201-212, 1995.

EFFICIENT FINITE ELEMENT IMPLEMENTATION OF CONTINUUM THEORIES WITH MICRO-INERTIA

Mariateresa Lombardo[1], Harm Askes[2]

[1]School of Civil and Building Engineering, Loughborough University
Loughborough LE11 3TU, United Kingdom; e-mail: m.lombardo@lboro.ac.uk
[2]Department of Civil and Structural Engineering, University of Sheffield
Sheffield S1 3JD, United Kingdom; e-mail: h.askes@sheffield.ac.uk

Keywords: micro-inertia, finite element, wave dispersion, explicit time integration

Gradient enrichment is a powerful tool to equip continuum mechanics theories with additional terms that can be used to capture microstructural effects. Additional spatial derivatives, operating on relevant state variables (such as total strain or plastic strain) and accompanied with constitutive length scale parameters, can be used to set the width of shear bands, describe the size-dependent response of geometrically proportional structures, simulate stress and strain fields around sharp crack tips without singularities, and predict dispersive wave propagation — see [3] for a recent overview.

Of particular interest for the present study are continuum theories that are equipped with additional spatial gradients of the accelerations, i.e. so-called micro-inertia modifications of the classical equations of elasticity. Such theories can be used to simulate the dispersion of waves that propagate through heterogeneous media without the need to model the microstructure explicitly [9]— instead, the additional length scale parameters that accompany the acceleration gradients can often be linked straightforwardly to the microstructural geometry and/or material properties [11, 6, 12, 10, 7, 1, 8], thus greatly facilitating parameter identification. Furthermore, the use of acceleration gradients has an advantage over the use of strain gradients in that the need for additional boundary conditions is avoided [3]. Finally, the use of micro-inertia can also lead to an increase of the critical time step in conditionally stable time integration algorithms for time-domain computational dynamics [2, 4]. The latter aspect shows great promise for practical applications as this can lead to significant reductions in simulation times, however implementation of continuum theories with micro-inertia into finite element codes for explicit dynamics is, unfortunately, not straightforward. The reason can be seen from analysis of the semi-discretised equations of motion of an undamped elastic structure

$$[\mathbf{M} + \mathbf{M_m}]\,\ddot{\mathbf{u}} + \mathbf{K}\mathbf{u} = \mathbf{f} \tag{1}$$

where $\mathbf{M}$, $\mathbf{K}$ and $\mathbf{f}$ are the usual version of the mass matrix, stiffness matrix and external force vector, respectively. The micro-inertia modifications of the mass matrix $\mathbf{M_m}$ cannot be lumped, so that the system matrix is not diagonal and neither can it be made diagonal without losing the micro-inertia properties of the material model (see also the discussion in [5]). The equations of motion are coupled and consequently the explicit integration of the equations in the current form would require a non-trivial matrix inversion.

Main motivation of this study is the need to simulate wave phenomena in contina with micro-inertia by using numerical explicit integration scheme combined with finite element discretisation in space.

In this contribution, we suggest a solution algorithm based on formal modification of the equations of motion (1) that can be used to enable explicit dynamics simulations with micro-inertia. The system matrix is the usual lumped mass matrix and all the advantages of explicit integration are maintained. Numerical stability issues are addressed and it is shown how the increasing of the critical time step is preserved. The effects of the modification on the dispersive properties have been investigated and numerical examples are used to illustrate the various aspects of the newly proposed algorithm.

References

[1] I. Andrianov, J. Awrejcewicz, D. Weichert. Improved continuous models for discrete media. *Journal of Sound and Vibration*, **986242**, 2010.

[2] H. Askes, B. Wang, T. Bennett. Element size and time step selection procedures for the numerical analysis of elasticity with higher-order inertia. *Journal of Sound and Vibration*, **314**: 650–656, 2008.

[3] H. Askes, E.C. Aifantis. Gradient elasticity in statics and dynamics: An overview of formulations, length scale identification procedures, finite element implementations and new results. *International Journal of Solids and Structures*, **48**: 1962–1990, 2011.

[4] H. Askes, D. C. D. Ngyen, A. Tyas. Increasing the critical time step: micro-inertia, inertia penalties and mass scaling. *Computational Mechanics*, **47**: 657–662, 2011.

[5] T. Bennett, H. Askes. Finite element modelling of wave dispersion with dynamically consistent gradient elasticity. *Computational Mechanics*, **43**: 815–825, 2009.

[6] W. Chen, J. Fish. A dispersive model for wave propagation in periodic heterogeneous media based on homogenization with multiple spatial and temporal scales. *ASCE Journal of Applied Mechanics*, **68**: 153–161, 2001.

[7] M. Lombardo, H. Askes. Elastic wave dispersion in microstructured membranes. *Proceedings of the Royal Society A*, **466**: 1789–1807, 2010.

[8] M. Lombardo, H. Askes. Higher-order gradient continuum modelling of periodic lattice materials. *Computational Materials Science*, **52**: 204–208, 2012.

[9] A. V. Metrikine, H. Askes. One-dimensional dynamically consitent gradient elasticity models derived from a discrete microstructure Part 1: Generic formulation. *European Journal of Mechanics - A/Solids*, **21**: 555–572, 2002.

[10] A. V. Pichugin, H. Askes, A. Tyas. Asymptotic equivalence of homogenization procedures and fine-tuning of continuum-theories. *Journal of Sound and Vibration*, **313**: 858–874, 2008.

[11] M. B. Rubin, P. Rosenau, O. Gottlieb. Continuum model of dispersion caused by an inherent material characteristic length. *Journal of Applied Physics*, **77**: 4054–1063, 1995.

[12] Z. P. Wang, C. T. Sun. Modeling micro-inertia in heterogeneous materials under dynamic loading. *Wave Motion*, **36**: 473–485, 2002.

MATERIAL OPTIMIZATION IN DYNAMICS VIA MATERIAL STRUCTURES DISTRIBUTED IN SPACE-TIME

Konstantin Lurie

Worcester Polytechnic Institute, Worcester, MA, U.S.A.; e-mail: klurie@wpi.edu

Keywords: dynamic materials, regular (irregular, intermediate) scenarios

A typical optimization problem requires minimization of certain functional (cost) of a solution of a system of differential equation that include unknown functions or parameters termed *controls*. These functions belong to some *admissible sets* (available resources), and the goal is to determine controls minimizing the cost functional dependent on solutions.

This formulation particularly applies to a *material* design, i.e., to problems with controls in the coefficients of the original equations (these coefficients may be assumed to take just two values, corresponding to two admissible materials). The key principle of material optimization comes from the idea of *focusing* the physical fields implemented and maintained by special material layouts. This principle universally works in both statics and dynamics. However, because of fundamental differences between these two concepts, the phenomenon of focusing manifests itself in them through different scenarios.

In *statics*, the focusing is achieved by creation of material anisotropy aimed to control appropriate orientation of the physical fields at each point. This effect is produced through a build up of material composites assembled in *space* from the original constituents. This scenario is the only one applicable in statics, where the physical fields are commonly governed by the variational principle of minimal stored energy. Formally, the composites appear as the means aimed to compensate the lack of quasiconvexity in the original elliptic problem with controls in coefficients.

Over the years, this approach developed through the study of Pontryagin's maximum principle that received generalization to the coefficient control problems for PDEs. It also worked through the analysis of the s.c. G-*closures* – the sets of parameters of *all* mixtures assembled on a microscale from the original constituents. Eventually, it was implemented in the s.c. *direct method* capable of finding the layout specifically adjusted to a particular optimization problem.

In *dynamics*, the situation is in many aspects different. Focusing of physical fields remains to be a leading and universal mechanism of optimization maintained by material layouts, but this principle now displays itself through various scenarios. To be able to timely respond to temporally changing environment, the material constituents should be distributed in *space and time*, i.e., they become dynamic materials (DM). DM are thermodynamically open systems; their existence is supported due to a non-stop exchange of mass, momentum, and energy with the environment. Only the union of a DM and the environment may be thermodynamically closed. DM appear to be very effective controllers of dynamic processes; however, the study of an *optimal design and control* via such materials requires understanding of the specifics of said exchange.

This specifics is formally due to the principle of *stationary* action that now replaces the principle of *minimum* stored energy. DM are classified into *activated* (ADM) and *kinetic* (KDM), though a general DM need not be a pure case. ADM are maintained through the changes in material parameters produced by an external agent (e.g., by switching the inductances and capacitances along the transmission lines, or by attaching or release of masses along an elastic bar, or by operating the traffic lights on the road, etc.) KDM are produced due to a relative mechanical motion of material fragments that constitute a heterogeneous medium (c.f. Minkowski's material relations in electrodynamics of moving media). In the presence of dynamic disturbances, activation and kinetization both maintain a mass-momentum-energy flow. Because of the work produced by the environment against the dynamic disturbances (waves), this flow may be accompanied by accumulation of said quantities in a travelling disturbance. Alternatively, these quantities are released if the waves work against the environment.
In *statics*, materials are distributed in space, and practically every material geometry is consistent with standard compatibility conditions on material interfaces. Contrary to that, in *dynamics*, disturbances travelling through the DM structures may or may not comply with the compatibility conditions, depending on the material geometry. For example, a spatial-temporal laminate allows the incident wave to travel through it if the slope of the laminate is smaller (larger) than either of the phase velocities of the material constituents within layers. This case was termed regular; it introduces the *regular* optimization scenario similar to the one in statics. Otherwise, there will be a collision of characteristics, and unobscured transmission of disturbances across the material interfaces will no longer be possible. For this case, termed irregular, additional information is needed to specify the system's performance after collision of characteristics; this performance may include singularities, e.g., the strong discontinuities in solutions. We arrive at the second *(irregular*) scenario of focusing; this scenario requires additional physics and for this reason has no analogue in statics. Particularly, a relatively arbitrary layout of DM is possible for a regular case, and generally impossible for irregular. We also introduce the third, *intermediate* scenario, in which the characteristics do not collide, but are asymptotically attracted to some selected wave routes that represent limit cycles. This performance is demonstrated by the wave motion through a rectangular checkerboard material structure in 1D space + time, within certain ranges of the structural parameters.

In the absence of a general existence theorem, all three scenarios of optimization may participate in the optimal material assembly.

Interestingly, they demonstrate substantial differences in the energy performance. In the regular case, the wave energy is preserved in average, with no energy exchange with environment. In irregular case, energy is irreversibly lost in a DM as result of dynamic collisions. An intermediate range allows for an intensive energy exchange with the environment, particularly, the energy accumulation in the travelling waves.

All these scenarios of optimization will be illustrated by examples.

A DIFFERENT LOOK AT SAWs: QUASI-PARTICLE RE-INTERPRETATION

Gérard A. Maugin, Martine Rousseau

Université Pierre et Marie Curie – CNRS UMR 7190,
Institut Jean le Rond d'Alembert, Paris France;
e-mail: gerard.maugin@upmc.fr; martine.rousseau@upmc.fr

Keywords: surface acoustic waves, quasi-particle, duality, Noether's theorem

In recent years, inspired by the notions of phonons in solid-state science and solitons in mathematical physics, the authors have advocated a new approach to the formulation and interpretation of dynamical solutions of the surface acoustic wave type (so-called SAWs) of which Rayleigh waves are the most celebrated case. This approach can be schematically summarized thus. On one side we have the common wavelike view of the phenomenon: a guided propagation essentially parallel to the upper limiting plane, a polarization in the sagittal plane Π_S or orthogonally to it (so-called shear horizontal or SH waves), an exponential decrease of amplitude with depth in the substrate, and a typical wave length λ. On the other side we have a quasi-particle moving essentially along the wave propagation direction and characterized by a "mass", a velocity or linear momentum, and an energy , these three entities forming a "point mechanics". Familiar systems of point mechanics are those of Newton and Lorentz-Poincaré-Einstein but other systems may be constructed that defy usual understanding (see Maugin and Christov, [1]). The main question is how these three entities are defined from the wavelike motion if we know the analytical wave solution? This contribution answers this question and provides a sufficient number of treated examples of SAW modes and application to the transmission-reflection problem with potential application to NDE techniques. In a few words: both visions serve to describe a propagating information via their well founded duality. The wave modelling favours a description of the propagation of information in terms of wave number and frequency. As to the particle model, it pertains to a diffusion of information through certain interactions in terms of momentum and energy.

The main idea supporting the present exploration in a rather unknown landscape is the due exploitation of so-called *conservation laws* that are canonically associated with field equations by the mediation of the celebrated Noether's theorem (1918) – probably the most powerful theorem of mathematical physics established in the 20th century. It is salient to recall that in a well constructed field theory one distinguishes between "field equations" (in the present case, the propagation equation in physical space complemented by boundary conditions on the limiting surface and radiation conditions at infinity) and "conservation laws" that result from a group-theoretic argument, here invariance under time and material-space translations (time and space parametrizations) according to Noethers's theorem ([2], Chapter 4). This symmetry argument here provides local statements of the conservation of energy and so-called canonical momentum. This strictly applies to a variational formulation of the theory. But we know how to obtain these laws in the presence of dissipation and/or material inhomogeneities by mimicking the so-called Noether's identity, once we have at hand the local balance laws ([2], Chapter 5). Field equations and conservation laws do not serve the same purpose. The former provides the looked for solution – here SAWs – analytically or numerically. The latter are currently used, just like in a post-processing strategy, to formulate a criterion of progress (e.g., in fracture or in the progress of phase transformation fronts [2]). Here they are exploited to formulate the relevant point-mechanics of the associated quasi-particle. The procedure consists in substituting for the known SAW solution in the local conservation laws and integrating the latter over an element of volume that is most

representative of the studied wave motion – usually one wavelength in propagation space – and effecting the required identification. This procedure is more or less simple depending on the type of SAW considered.

More precisely, the general strategy first is presented in the framework of pure homogenous elasticity. Then the results of a series of worked out examples are given which concern surface waves both of the Rayleigh type (polarization in the sagittal plane) and SH type, the latter when the chosen configuration allows for its existence (case of Bleustein-Gulyaev surface waves in piezoelectrics or surface waves in the Murdoch-Gurtin theory of a substrate covered with a material surface endowed with both energy and inertia). This series of examples is sufficient to exhibit a large and rich variety of behaviours of associated quasi-particles. For instance, in the standard Rayleigh case – which is a rather complicated one – the obtained quasi-particle motion is Newtonian and conservative but with a "mass" of which the definition involves all parameters of the analytical wave solution [3]. Perturbation by a surface energy causes perturbation in both "mass" and velocity of the associated quasi-particle but its motion remains well defined and Newtonian. In the case of so-called "leaky" Rayleigh waves (occurring when an inviscid fluid is superimposed on top of the substrate) a direct approach yields a pathological situation with a complex "mass" corresponding to the unphysical re-emission in the fluid. For a piezoelectric coupling that guarantees the existence of SH Bleustein-Gulyaev waves the situation is much simpler with a strict Newtonian-Leibnizian behaviour of the quasi-particle [4]. Perturbation of the last case by a quartic nonlinear elasticity of the substrate – thus causing the appearance of the third harmonic in the wavelike solution – yields a perturbed "mass" but still a strict Newtonian-Leibnizian mechanical behaviour of the quasi-particle [5]. But a perturbation by a weak viscosity granted to the elastic substrate yields a two-dimensional particle motion (with a small component in the depth direction) while the "mass" evolves in time due to the present dissipation [6]. The case of dispersive Murdoch surface waves – much simpler than the case of Love waves – is particularly enlightening as it shows well the relative influence of substrate and material-surface properties. In all studied cases the "mass" is always proportional to the square of the amplitude of the wavelike solution.

Finally, the presented formalism is exploited in the exemplary problem of transmission-reflection. This is examined for an interface (discontinuity) of vanishing thickness – including the possibility of delamination – , a sandwiched slab of a different elasticity, and a layered slab made of a series of piled up elastic layers of various properties. The quasi-particle properties are related to the energy conservation of the wavelike picture expressed in terms of reflection and transmission coefficients.

References

[1] G.A. Maugin, C.I. Christov. Nonlinear duality between elastic waves and quasi-particles. In *Selected Topics in Nonlinear Wave Mechanics*, C.I. Christov, A. Guran (eds), Birkhäuser, Boston, 117–160, 2002.
[2] G.A. Maugin. *Configurational forces: Thermomechanics, Physics, Mathematics, and Numerisc*. CRC/Chapman & Hall/Taylor and Francis, Boca Raton, London, New York, 2011.
[3] M. Rousseau, G.A. Maugin. Rayleigh surface waves and their canonically associated quasi-particles. *Proc. Royal Soc. Lond*. **A467**: 495–507, 2011.
[4] G.A.Maugin, M. Rousseau. Bleustein-Gulyaev SAW and its associated quasi-particle. *Int. J. Engn. Sci* (Special issue honouring K. Rajagopal), **48:** 1462–1469, 2010.
[5] M. Rousseau, G.A.Maugin. Quasi-particles associated with Bleustein-Gulyaev SAWs: perturbations by elastic nonlinearities. *Int. J . Non-linear Mechanics*, **47**: 67–71, 2012.
[6] M. Rousseau, G.A. Maugin. Influence of viscosity on the motion of quasi-particles associated with surface acoustic waves. *Int. J. Engng. Sci*., **50:** 10–21, 2012.

ANALYSIS OF A SELF-SIMILAR LAPLACIAN IN n DIMENSIONS AND SOME APPLICATIONS TO WAVES PROPAGATION PROBLEMS

Thomas M. Michelitsch[1], Gérard A. Maugin[1]
Andrzej F. Nowakowski[2], Franck C. G. A. Nicolleau[2]

[1] Université Pierre et Marie Curie, Paris 6
Institut Jean le Rond d'Alembert, CNRS UMR 7190, France; e-mail: michel@lmm.jussieu.fr

[2] Sheffield Fluid Mechanics Group, Department of Mechanical Engineering
University of Sheffield, United Kingdom; e-mail: f.nicolleau@sheffield.ac.uk

Keywords: Fractals, self-similarity, Laplacian, wave propagation, fractal mechanics, fractional calculus, generalized functions, distributions, Green's functions, self-similar continuum

Abstract: We analyze a Laplacian operator that is defined in an infinite spatially homogeneous body with self-similar harmonic interparticle interactions. Self-similarity implies that the interparticle interactions are scale invariant long-range non-local interactions. In this contribution we generalize our model for the one dimensional case [1, 2] to $n = 1, 2, 3, ..$ dimensions of the physical space. This Laplacian takes in its continuous representation the form of a nonlocal convolution with a power law kernel (fractional integral). In one dimension $n = 1$ the Laplacian takes the form of fractional integrals [2].

The point of departure for the approach is our recent one-dimensional linear chain model which gives rise to a fractal dispersion relation in the form of a Weierstrass-Mandelbrot function [1]. First of all let us give a definition of the notion "self-similar". We call a function $\Lambda(h)$ self-similar with respect to the variable h when the relation

$$\Lambda(Nh) = N^{\delta}\Lambda(h) \tag{1}$$

is fulfilled for a prescribed fixed scaling factor $N > 1$ and valid vor any $h > 0$. We assume real valued scaling exponents $\delta \in \mathbb{R}$. Generally a self-similar function which fulfills (1) for a prescribed N can be written in the form

$$\Lambda(h) = \sum_{s=-\infty}^{\infty} N^{-\delta s} f(N^s h) \tag{2}$$

which converges for suffficiently good functions f [1]. We define a continuum limit by putting $N = 1+\zeta$ $(0 < \zeta << 1)$. In the limiting case of infinitesimally small (positive) ζ, the quantity $\tau = hN^s$ becomes a continuous variable and we can write (2) assymptotically as an integral

$$\Lambda(h) = \sum_{s=-\infty}^{\infty} N^{-\delta s} f(N^s h) \approx \frac{h^{\delta}}{\zeta} \int_0^{\infty} \frac{f(\tau)}{\tau^{\delta+1}} \mathrm{d}\tau \tag{3}$$

taking the form of a continuous power function $\Lambda(h) = const\, h^{\delta}$ in h. A self-similar Laplacian operator can then be defined in the above sense by choosing as function f a second difference $f(h) = u(x+h) + u(x-h) - 2u(x)$ [1]

$$\Delta_{(N,\delta,h)} u(x) = \sum_{s=-\infty}^{\infty} N^{-\delta s} \left\{u(x+h) + u(x-h) - 2u(x)\right\} \tag{4}$$

This series converges in the range $0 < \delta < 2$ for "good" fields $u(x)$, (i.e. $\lim_{x\to\pm\infty} u(x) \to 0$) [1] and as a consequence of self-similarity (4) is necessarily a non-local and *self-adjoint* negative semi-definite operator (i.e. its eigenvalues are all ≤ 0). As a further symmetry property we observe that operator (4) is isotropic (i.e. in 1D an even function with respect to h). Performing the continuum limit defined by (3) a continuous representation of the self-similar Laplacian operator is obtained as

$$\Delta_{(\delta,h,\zeta)}u(x) = \frac{h^\delta}{\zeta}\int_0^\infty \frac{(u(x-\tau)+u(x+\tau)-2u(x))}{\tau^{1+\delta}}\,\mathrm{d}\tau\,, \qquad 0<\delta<2 \tag{5}$$

and in the interval of convergence of this integral is $0 < \delta < 2$. To generalize (5) we define a Laplacian of the n-dimensional-space acting on a scalar field variable $u(\mathbf{x})$ as

$$\Delta_{n,\delta}u(\mathbf{x}) = \frac{h^\delta}{\zeta}\int \frac{(u(\mathbf{x}+\mathbf{r})+u(\mathbf{x}-\mathbf{r})-2u(\mathbf{x}))}{r^{\delta+1}}\mathrm{d}^n\mathbf{r}\,, \qquad n-1<\delta<n+1 \tag{6}$$

where we integrate over the entire $n = 1, 2, 3$-dimensional infinite space. For $n = 1$ (6) coincides with (5). Integral (6) exists for sufficiently smooth, at infinity vanishing fields $u(\mathbf{x})$ in the interval $n - 1 < \delta < 2 + n - 1 = n + 1$ where $n = 1, 2, 3, .. \in \mathbb{N}$.

In this presentation we determine the dispersion relation and n-dimensional infinite-space Green's function of the Laplacian (6), i.e. the inverse of the self-similar Laplacian operator in explicit form. We further consider some examples of wave propagation in the linear elastic infinite n-dimensional medium where the material functions are of self-similar (scaling invariant) and of isotropic symmetry. This case is the simplest example for an *elastic self-similar medium* of $n = 1, 2, 3$ dimensions.

The present approach gives us the starting point to formulate any physical problem which is defined in terms of field equations such as for instance by Maxwell equations in electro-dynamics or by Lamé equations in elasticity for *self-similar symmetry of the medium*. When we say "self-similarity of the medium" we mean the material functions are self-similar in the above defined sense. The notion of the "self-similar medium" is here completely analogous as the notion of the "transversely isotropic medium" in linear elasticity, i.e. characterizing the symmetry of the material functions. A consequence of this notion of self-similarity is inevitably the non-locality of the constitutive relations in such a medium where the material functions appear as self-similar power function kernels. In a microscopic picture the self-similar constitutive behavior as defined here, can be regarded as self-similar interparticle interactions where the "particles" are the "material points" which build up the medium. As the physical nature of the fields is not important for the approach introduced, the presented model is completely general and has therefore the potential of general applicability to interdisciplinary "self-similar" field problems.

References

[1] T. M. Michelitsch, G. A. Maugin, F. C. G. A. Nicolleau, A. F. Nowakowski, S. Derogar. Dispersion relations and wave operators in self-similar quasicontinuous linear chains. *Phys. Rev. E*, **80**: 011135, 2009.

[2] T. M. Michelitsch, G. A. Maugin, F. C. G. A. Nicolleau, A. F. Nowakowski, S. Derogar. Submitted.

ANALYSIS OF WAVE PROPAGATION IN TOROIDAL SHELLS

Jonas Morsbøl[1], Sergey Sorokin[2]

Department of Mechanical and Manufacturing Engineering, Aalborg University,
Aalborg, Denmark; e-mail: [1]jm@m-tech.aau.dk, [2]svs@m-tech.aau.dk

Keywords: Perturbation methods, Galerkin method, toroidal shells, flexible pipes.

Risers used in the oil and gas industry, hydraulic hoses for power transmission, but also blood vessels are all examples of flexible piping systems. Common for these examples is that they are all subjected to time varying loading in their practical setting. Risers are suffering from self-induced vibrations especially when gas is flowing through, while the hydraulic hoses can act as structural components guiding waves between different parts of a hydraulic power transmission system [1]. In both cases vibrations can lead to fatigue failure of the pipes themselves or of the equipment to which they are attached. In the perhaps more controversial example of regarding blood vessels as flexible pipes studies indicate a correlation between different cardiovascular diseases and the interaction between the pulsating blood stream and blood vessels [2]. In all three examples a common factor is also that fluid-structure interaction plays a significant role. A complete model must therefore incorporate a model of the structure and the fluid and how they interact. Though, in what follows, the dynamical behaviour of the structural part is studied.

Flexible pipes, like those mentioned above, typically consist of a sequence of somewhat straight and curved sections. A straight section can be regarded as a cylinder while a section of relatively constant curvature can be regarded as parts of a torus. An immediate modelling strategy could then be to model each section as a beam by enforcing certain assumptions on the kinematic of the pipe cross section. But consequently the cross section would then only be able to deform due to poisson coupling. This might be too restrictive when modelling *flexible pipes*. In order to incorporate a higher order of flexibility each section could instead be modelled as a shell, and thereby only enforce kinematic assumptions to the pipe wall and not the whole cross section.

Each point in a cylindrical shell refers to an orthogonal coordinate system oriented in the principal directions, i.e. in the circumferential directions and the axial direction. Free waves will consist of standing waves in the circumference, having a period of 2π, while in the axial direction they can be either travelling or trapped. Expressed in wave numbers the circumferential waves will have purely imaginary integral wave numbers while the axial wave numbers can be either purely imaginary or complex valued. In this situation the relation between the frequency and the axial wave number can be studied independently for each individual circumferential wave number. This manifests itself through the very fundamental modes of the cylinder where bending, longitudinal, and torsional modes are completely uncoupled [3]. Now, if the cylinder shell is bend it turns into a section of a toroidal shell. In the toroidal shell the axial waves related to each circumferential wave number will interact as they propagate. This can be imagined by considering the fundamental vibrations modes of the torus where in-plane bending couples with the longitudinal mode and out-off-plane bending couples with torsion. Thus, the axial mode related to each circumferential mode cannot be studied independently as in the cylinder.

In this project, the complications of coupling modes have been evaded through different approaches. The wave propagation through the toroidal shell has been studied by means of, respectively, the Galerkin method and by perturbation methods. The results of these analytical approaches have been compared to classical curved beam theory. In both analytical methods the solution is found in the frequency domain and is assumed to be separable in the two directions of the shell coordinates. In the axial direction the solution is assumed to take the usual complex exponential form. By enforcing this the governing equations of the toroidal shell reduce to three coupled ordinary differential equations with periodic coefficients. In these differential equations the periodic coefficients appears as functions of the circumferential coordinate.

In the Galerkin method, a truncated Fourier series has been enforced as the circumferential mode and the corresponding axial response as function of the frequency has been determined. At one hand a Fourier series can simply be regarded as an arbitrary periodic function. On the other hand the Fourier series can be seen as a sum of the individual circumferential modes known from the cylinder shell. Now, in the toroidal shell where the individual modes from the cylinder are coupling, a natural *ansatz* is therefore to study the response to such sum of circumferential modes. As the number of terms in the truncated Fourier series is increased similarly the complexity and computation time also increases. Therefore, the Fourier series only includes the first few low-order terms and thus the solution obtained through this approach is only able to predict the very fundamental and low-frequency modes.

The governing equations of the toroidal shell have also been seized to an asymptotic analysis, but only with partial success. Due to the complexity of the governing equations of the toroidal shell a full asymptotic picture of the dispersion relations has still not been found. It has though been possible to obtain asymptotic estimates of cut-on frequencies which is valuable in it self, but also in validation of the Galerkin solution.

Future work includes validation of the analytic solutions by means of, respectively, wave finite element analysis and classical curved beam theory. Besides the purpose of validating the analytical shell models the validity range of the classical curved beam theory can then also be assessed. As long as the analytical shell solutions agree with the wave finite element model and with the beam theory within its range of certain validity it is expectable that the shell model will be valid even beyond the beam theory, because shell theory is a higher order theory.

Acknowledgement

The work is funded by The Danish Council for Independent Research, Technology and Production Sciences (grant number UK 95 OS 63822 PJ 830021).

References

[1] S.P.C. Belfroid, D.P. Shatto, R.M. Peters. *Flow Induced Pulsation Caused by Corrugated Tubes.* ASME Pressure Vessels and Piping Division Conference, 2007.

[2] D. Bessems, M. Rutten, F. van de Vosse. *A wave propagation model of blood flow in large vessels using an approximate velocity profile function.* Journal of Fluid Mechanics, 145-168, 2007.

[3] S.V. Sorokin, J.B. Nielsen, N. Olhoff. *Green's matrix and the boundary integral equation method for the analysis of vibration and energy flow in cylindrical shells with and without internal fluid loading.* Journal of Sound and Vibration, 815-847, 2004.

A GRADIENT ELASTICITY THEORY DERIVED FROM THE CONTINUALISATION OF A DISCRETE PERIODIC LATTICE STRUCTURE

Duc C.D. Nguyen[1], Mariateresa Lombardo[2], Harm Askes[1]

[1]Department of Civil and Structural Engineering, University of Sheffield, United Kingdom
[2]Department of Civil and Building Engineering, Loughborough University, United Kingdom
e-mails: cia07dn@sheffield.ac.uk, m.lombardo@lboro.ac.uk, h.askes@sheffield.ac.uk

Keywords: lattice, continualisation, dispersion, gradient elasticity, length scale

New manufacturing techniques have enabled the mass production of engineered materials whereby the microstructure consists of a sparse, periodic lattice. Such materials have an excellent mechanical performance compared to their weight, but their engineered microstructure also lends itself to optimised mechanical behaviour under dynamic loading conditions. For instance, the material's microstructure can be manipulated such that wave filters emerge, whereby certain frequencies can propagate through the material and certain other frequencies cannot.

For the modelling of such materials with lattice microstructures, various techniques can be used. For instance, detailed simulations can be carried out whereby every strut of the lattice structure is modelled with a separate beam element, using for instance Euler-Bernoulli or Timoshenko beam theory. However, a more efficient approach is to replace such a detailed microscopic material model with an enriched continuum model. In particular, the effects of the microstructure can be captured efficiently and effectively by equipping the continuum equations of elasticity with an appropriate set of higher-order spatial derivatives, so that a *gradient elasticity* formulation is obtained.

In order to link the additional constitutive coefficients of the gradient elasticity model to the geometric and mechanical properties of the lattice, in this paper we use continulatisation techniques whereby a discrete model of beams is translated into a homogeneous (though not necessarily isotropic) continuum formulation. With an appropriate mix of Taylor series expansions and Padé approximations, the higher-order coefficients of the gradient elasticity macroscale model can be typically linked to the length of the beams in the lattice.

We explore a range of modelling options. For the microscale modelling, we use Euler-Bernoulli beam theory. For the discretisation of the inertia contribution, either lumped mass or consistent mass is used. The use of Padé approximations is usually required to ensure stability of the gradient elasticity model. Stability requirements are formulated to help perform these operations. The resulting continuum formulation is equipped with a range of strain gradient and inertia gradient terms. The dispersive properties of the model are then tested to check for the occurrence of wave filters and how these can be controlled.

References

[1] I.V. Andrianov, J. Awrejcewicz, R.G. Barantsev. Asymptotic approaches in mechanics: new parameters and procedures. *ASME Appl. Mech. Rev.*, **56**: 87-110, 2003.

[2] A.V. Metrikine, H. Askes. An isotropic dynamically consistent gradient elasticity model derived from a 2D lattice. *Phil. Magaz.*, **86**: 3259–3286, 2006.

[3] M. Lombardo, H. Askes. Higher-order gradient continuum modelling of periodic lattice materials. *Comput. Mater. Sci.*, **52**: 204–208, 2012.

ULTRASONIC WAVE PROPAGATION IN INHOMOGENEOUS ANISOTROPIC POROUS BONE LAYER

Vu-Hieu Nguyen, Salah Naili

Université Paris-Est, Laboratoire Modélisation et Simulation Multi Echelle, MSME UMR 8208 CNRS, France;
e-mail: vu-hieu.nguyen@univ-paris-est.fr, salah.naili@univ-paris-est.fr

Keywords: anisotropic poroelastic, ultrasound, hybid analytical/spectral finite element.

Introduction. Mechanical modeling of experiments using the axial transmission technique deals with considering a model describing vibro-acoustic interactions of a solid waveguide (which represents the cortical bone) coupled with two fluid media (which represents soft tissues such as skin or marrow). Bone is a strongly heterogeneous material with complex structures whose the architecture displays an organization at different hierarchical levels: the macrostructure (bone), the microstructure (harvesian system, osteon, interstitial tissues) and the other structures at lower scales. It has been shown that the microstructure of the bone has strong influence on characteristics of ultrasonic wave propagation. However, for modeling the guided ultrasonic waves propagating in cortical long bones, most of works has considered cortical bone as an equivalent linear isotropic or anisotropic elastic medium.

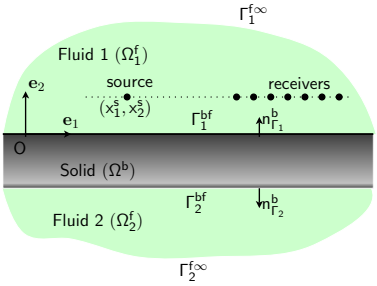

Figure 1: Poroelastic bone plate immersed in fluids

In this work, an anisotropic poroelastic model was employed to represent the cortical bone in order to be able to describe the link between the bone microstructure (bone matrix properties as well as porosity) and the time-domain response of ultrasonic wave propagation. For this purpose, we have developed a semi-analytical finite element method for simulating the transient ultrasonic waves propagating in cortical bones considered as an anisotropic poroelastic medium. The bone is assumed to be homogeneous in its axial direction but may be heterogeneous in the radial direction (Fig. 1)

Time-domain analysis using semi-analytical/spectral finite element approach. The problem presented deals with solving a system of linear partial differential equations in which the coefficients are homogeneous in the longitudinal direction given by x_1-axis. Here, a hybrid analytical/finite element has been developped as follows: (i) the system of equations is firstly transformed into frequency-wavenumber domain by using a Fourier transform with respect to x_1 combined with a Laplace transform with respect to t; as a consequence, a one-dimensional system of PDEs with respect to x_1 can be established; (ii) in the frequency-wavenumber domain, the wave equations in two fluid domains (Ω_f^1 and Ω_2^f) are analytically solved providing impedance boundary conditions for the solid domain; (iii) the weak and finite element formulations are then established in the domain (Ω^b) only; (iv) the space-time solution is finally obtained by performing the inverse Fourier transform (using FFT technique) and the inverse Laplace transform (using the CQM technique) [1]. The formulation has been validated by comparing with conventional FE method [2]

Results and discussions. Using the proposed approach, a parametric study has been carried out in order to consider the influence of the bone's porosity on the behavior of guided ultrasonic wave in long bones. We assume that the solid phase of the bone material is transversely isotropic elastic medium which has $c_{11}^m = 28.7$ GPa, $c_{12}^m = 9.1$ GPa, $c_{22}^m = 23.6$ GPa, $c_{66}^m = 7.25$ GPa. The elastic stiffness ($\mathbb{C}$) and Biot's coefficients ($\boldsymbol{\alpha}$, M) are then determined by using a homogenization procedure. The fluid phase in bone and both fluid domains are assumed to be water with the mass density $\rho_f = 1000$ kg.m^{-3} and the bulk modulus $K_f = 2.25$ GPa. The thickness of the bone plate is $h = 4\,mm$. An impulse with a central frequency $f_0 = 1$ MHz is emitted at $(x_1^s, x_2^s) = (0, 2)\,mm$.

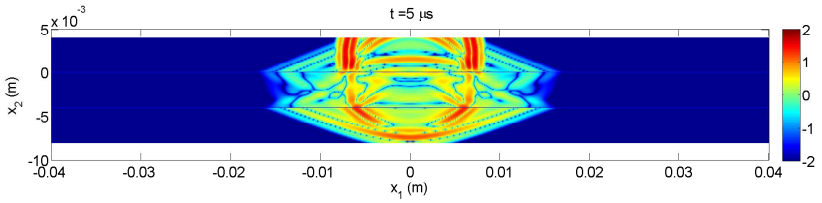

Figure 2: Snapshot of fluid pressures in the fluids and pore fluid pressure in the bone ($\phi = 5\%$)

The influence of the bone's porosity on the FAS velocity (denoted by V_F) has been studied. For this purpose, the material properties of bone matrix ($\rho^m, \mathbb{C}^m$) were fixed. The poroelastic properties were then determined by using the micromechanics analysis. In order to determine V_F, the p_1-signal is captured at 14 sensors located in the upper fluid domain (Ω_1^f) (Fig.1). Then V_F is evaluated by the slope of the linear regression of the first zero-crossing locations over 14 sensors (Fig. 3 (left)).

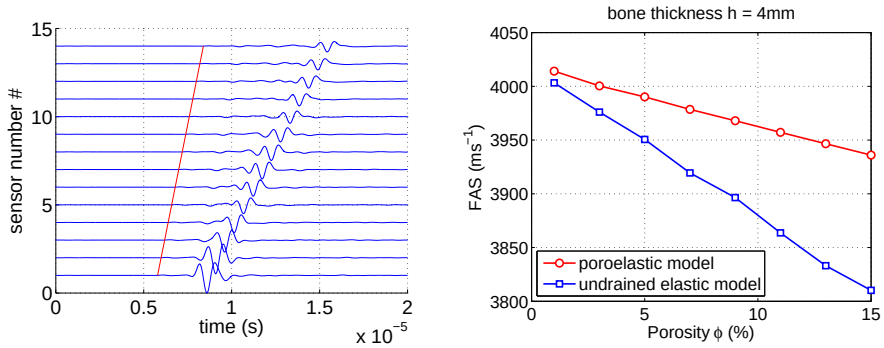

Figure 3: Pressure signals captured at sensors (left) and variation of V_F versus bone's porosity

Figure 3 (right) shows the variation of the FAS velocity with respect to ϕ when considering a bone plate with thickness $h = 4$ mm. One may observe that the V_F *versus* ϕ relation is practically linear and V_F decreases when the porosity ϕ is higher. The V_F *versus* ϕ relation obtained by using equivalent elastic media is also presented. For a given porosity ϕ, an equivalent elastic model, which has a mass density taken as the mixture density and an elasticity tensor taken as the undrained elasticity tensor, has also been analyzed. For lower porosities, the V_F obtained by using the poroelastic model are slightly different from the ones obtained using the elastic model. The difference becomes more significant for higher porosity because the fluid-solid movement is more important and would be not negligible.

References

[1] Nguyen VH, Naili S. Simulation of ultrasonic wave propagation in anisotropic poroelastic bone plate using hybrid spectral/FE method. *Int. J. Num. Meth. Biomed. Eng.*, 2012 (in press).

[2] Nguyen VH, Naili S, Sansalone V. Simulation of ultrasonic wave propagation in anisotropic cancellous bones immersed in fluid. *Wave Motion*, **47**(2):117–129, 2010.

THE WKB APPROXIMATION FOR WAVE PROPAGATION IN CORRUGATED AND SPATIALLY CURVED ELASTIC RODS

Rasmus Nielsen[1], Sergey V. Sorokin[2]

Department of Mechanical and Manufacturing Engineering, Aalborg University, Aalborg, Denmark;
[1]e-mail: rn@m-tech.aau.dk, [2] email: svs@m-tech.aau.dk

Keywords: Perturbation methods, WKB approximation, corrugated beams, curved rods, Green's matrix

Rods and beams are used in numerous applications, where they act as structural members carrying either static or dynamic loads. In cases of dynamic loads, the rod may act as a transmission path for vibration, which typically is regarded as a negative effect. It is therefore reasonable to pursue a better understanding of the dynamics of rods and to gain knowledge on how certain preferred properties can be achieved.

An approach to predict and assess the impact of irregularity on the dynamics of elastic rods is presented. Irregularity of rods can, for instance, take the form of corrugated cross sectional area or spatial curvature. In mathematical terms this, in general, results in sets of governing differential equations having varying coefficients, contrary to rods with constant cross section and curvature that is governed by differential equations with constant coefficients. Furthermore, a nonzero curvature introduces couplings between the governing equations which as well complicate matters. The challenges of corrugated cross section and varying curvature of rods can be handled using the finite element method to determine eigenfrequencies, eigenmodes and response to forced excitation. However, it does not immediately facilitate the understanding of the role of the system parameters in the final results. Meanwhile, the perturbation technique *The WKB approximation* is well known for providing simple structured approximations to solutions of differential equations having slowly varying coefficients. In essence, the WKB method typically results in a solution in the exponential form having a wave number and amplitude with a slow evolution. The WKB approximation has traditionally been developed and applied to problems in celestial and, in particular, quantum mechanics [1, 2]. Also the WKB approximation has been applied in fluid mechanics to problems of sound transmission through curved ducts with flow, [3]. The present study demonstrates how the WKB methodology can be applied to problems of wave propagation in rods. Furthermore, the competitiveness of the method is tested against the finite element method.

The study treats two distinct problems, namely, straight beams having corrugated cross section and curved beams. In the former case, the WKB approximation has been applied by [4] to determine the wave number and amplitude modulation of Bernoulli-Euler and Timoshenko beams. For a corrugated cantilever Bernoulli-Euler beam, formulae are derived for eigenfrequencies and eigenmodes in [4]. These results are subjected to a study of the robustness and accuracy of WKB solutions to beam problems, with improvements being suggested.

The use of the WKB method is carried on to wave propagation in rods with spatial curvature. Dynamics of rods with spatial curvature are in the most general case governed by six coupled differential equations with varying coefficients. Additionally, by looking into forcing problems the WKB method can be used to build Green's matrix for a spatial rod which constitute a fast and reliable way of predicting both forced and free vibrations. This can potentially be an efficient tool in the design phase of machines where curved rods provides structural functionality, but at the same time acts as a waveguide when isolation would have been preferred instead. It is expected that the use of the WKB approximation is beneficial in the sense that the role of system parameters will be better understood as opposed to an analysis conducted with the use of purely numerical tools.

Acknowledgement

The work is funded by *The Danish Council for Independent Research, Technology and Production Sciences*, grant number UK 95 OS63822 PO83004.

References

[1] N. Fröman, P.O. Fröman. *Physical Problems Solved by the Phase-Integral Method*. Cambridge University Press, Cambridge, 2004.

[2] C. Bender, S. Orszag. *Advanced Mathematical Methods for Scientists and Engineers*. McGraw-Hill, US, 1973.

[3] E. J. Brambley, N. Peake. Sound transmission in strongly curved slowly varying cylindrical ducts with flow. *Journal of Fluid Mechanics*, **596**: 387–412, 2008.

[4] A. D. Pierce. Physical Interpretation of the WKB or Eikonal Approximation for Waves and Vibrations in Inhomogeneous Beams and Plates. *Journal of the Acoustical Society of America*, **48**: 275–284, 1970.

DYNAMIC EFFECTIVE MEDIUM THEORY FOR PERIODIC ACOUSTIC MEDIA

A. N. Norris[1], A. L. Shuvalov[2], A. A. Kutsenko[2]

[1]Mechanical and Aerospace Engineering, Rutgers University, Piscataway, USA;
[2]Institut de Mécanique et d'Ingénierie de Bordeaux, Université de Bordeaux, Talence, France;
email: norris@rutgers.edu, a.shuvalov@i2m.u-bordeaux1.fr, kucenkoa@rambler.ru

Keywords: homogenization, dynamic effective medium

While methods exist for computing effective moduli of periodic composites under quasistatic conditions, the more challenging task is to define frequency-dependent dynamic effective constants capable of describing finite frequency effects such as phononic band gaps. A general effective medium theory for such systems has been developed by Willis [1, 2, 3], but the theory does not provide expressions for the effective moduli at finite frequency, or a direct algorithm for their evaluation. This paper provides an analytical resolution of this problem, illustrated for the particular case of a periodic acoustic medium. We show that the homogenized equations are of Willis form with semi-explicit finite frequency effective parameters expressed in terms of plane wave expansions (PWE) of the original acoustic parameters.

The equations governing waves in a fluid with density $\rho(\mathbf{x})$ and bulk modulus $K(\mathbf{x})$ ($\mathbf{x} \in \mathbb{R}^d$ d =1, 2 or 3), are normally phrased in terms of acoustic pressure $p(\mathbf{x}, t)$ and particle displacement $\mathbf{u}(\mathbf{x}, t)$ as

$$\rho \mathbf{u}_{,tt} = -\nabla p, \qquad p = -K \operatorname{div} \mathbf{u}. \tag{1}$$

It is more convenient to use different field variables: particle velocity $\mathbf{v}(\mathbf{x}, t) = \mathbf{u}_{,t}$, dilatation $d(\mathbf{x}, t) = \operatorname{div} \mathbf{u}$ and a potential $\phi(\mathbf{x}, t)$ defined such that $p = -\phi_{,t}$. Equations (1) are then replaced by the system

$$d_{,t} = \operatorname{div}\mathbf{v}, \qquad \begin{pmatrix} \mathbf{v} \\ d \end{pmatrix} = \begin{pmatrix} \mu & 0 \\ 0 & B \end{pmatrix} \begin{pmatrix} \nabla\phi \\ \phi_{,t} \end{pmatrix}, \tag{2}$$

the first of which can be considered as an equilibrium condition, and the second as constitutive relations defined by the alternate acoustic parameters $\mu \equiv \rho^{-1}$, $B \equiv K^{-1}$. Equations (2) are in a form suitable for homogenization using the general procedure of [4]. Here we summarize the application of the results derived for elasticity in [4] to the special but different case of acoustics.

We consider an acoustic medium with $\mathbf{T}$-periodic parameters: $h\big(\mathbf{x}+\sum_{j=1}^d n_j\mathbf{a}_j\big) = h(\mathbf{x})$, $n_j \in \mathbb{Z}$, for $h = \rho$, K, and vectors $\mathbf{a}_j \in \mathbb{R}^d$ define the unit cell $\mathbf{T}$. Fourier coefficients $\hat{h}(\mathbf{g})$ are defined by $h(\mathbf{x}) = \sum_{\mathbf{g}\in\Gamma} \hat{h}(\mathbf{g}) e^{i\mathbf{g}\cdot\mathbf{x}}$ where $\Gamma = \{\mathbf{g} : \mathbf{g} = \sum_{j=1}^d 2\pi n_j \mathbf{b}_j,\ n_j \in \mathbb{Z}\}$, is the set of reciprocal vectors and $\mathbf{a}_j \cdot \mathbf{b}_k = \delta_{jk}$ (hats indicate Fourier domain quantities). The governing equations, (1) or (2), admit Bloch wave solutions of the form $h(\mathbf{x}, t) = h(\mathbf{x})e^{i(\mathbf{k}\cdot\mathbf{x}-\omega t)}$ where $h(\mathbf{x})$ is the unique periodic part of $h(\mathbf{x}, t) = \mathbf{u}, \mathbf{v}, p, d, \phi$. We present equations for the *effective field variables*

$$h^{\text{eff}}(\mathbf{x}, t) = \langle h \rangle\, e^{i(\mathbf{k}\cdot\mathbf{x}-\omega t)} \quad \text{for } h = \mathbf{u}, \mathbf{v}, p, d, \phi, \tag{3}$$

where $\langle h \rangle$ ($= \hat{h}(0)$) denotes the average of $h(\mathbf{x})$ over the single cell. Our results can be summarized as follows. Introduce the infinite vectors $\hat{\boldsymbol{\mu}}$, $\hat{\mathbf{B}}$ and matrices $\hat{\mathbf{D}}$, $\hat{\mathbf{G}}$ in the Fourier domain with components

$$\left.\begin{aligned} \hat{\mu}[\mathbf{g}] = \hat{\mu}(\mathbf{g}), \quad \hat{B}[\mathbf{g}] = \hat{B}(\mathbf{g}), \quad \hat{D}_i[\mathbf{g}, \mathbf{g}'] = (g_i + k_i)\delta_{\mathbf{g}\mathbf{g}'}, \\ \hat{G}[\mathbf{g}, \mathbf{g}'] = \big((\mathbf{k}+\mathbf{g})\cdot(\mathbf{k}+\mathbf{g}')\,\hat{\mu}(\mathbf{g}-\mathbf{g}') - \omega^2\hat{B}(\mathbf{g}-\mathbf{g}')\big)^{-1}, \end{aligned}\right\} \quad \mathbf{g},\, \mathbf{g}' \in \Gamma\backslash\mathbf{0}, \tag{4}$$

and define the scalar $B^{\text{eff}}(\omega, \mathbf{k})$, the vector $\mathbf{S}^{\text{eff}}(\omega, \mathbf{k})$ and the tensor $\boldsymbol{\mu}^{\text{eff}}(\omega, \mathbf{k})$,

$$B^{\text{eff}} = \langle K^{-1} \rangle + \omega^2 \hat{\mathbf{B}}^+ \hat{\mathbf{G}} \hat{\mathbf{B}}, \quad S_i^{\text{eff}} = -\omega \hat{\boldsymbol{\mu}}^+ \hat{\mathbf{D}}_i \hat{\mathbf{G}} \hat{\mathbf{B}}, \quad \mu_{ij}^{\text{eff}} = \langle \rho^{-1} \rangle \delta_{ij} - \hat{\boldsymbol{\mu}}^+ \hat{\mathbf{D}}_i \hat{\mathbf{G}} \hat{\mathbf{D}}_j \hat{\boldsymbol{\mu}}. \tag{5}$$

The homogenized dynamic equations are then

$$q^{\text{eff}}_{,t} = \operatorname{div} \mathbf{v}^{\text{eff}}, \qquad \begin{pmatrix} \mathbf{v}^{\text{eff}} \\ q^{\text{eff}} \end{pmatrix} = \begin{pmatrix} \boldsymbol{\mu}^{\text{eff}} & \mathbf{S}^{\text{eff}} \\ -\mathbf{S}^{\text{eff}+} & B^{\text{eff}} \end{pmatrix} \begin{pmatrix} \nabla\phi^{\text{eff}} \\ \phi^{\text{eff}}_{,t} \end{pmatrix}. \tag{6}$$

Several comments are in order: Equations (6) allow us to define effective constants for any frequency-wavenumber combination, including, but not restricted to, values of $\{\omega, \mathbf{k}\}$ on the Bloch wave branches. For real-valued frequency ω and wave-vector $\mathbf{k}$ it can be shown that $\boldsymbol{\mu}^{\text{eff}}$ and B^{eff} are real. The effective equations (6) and the dispersion relation for solutions of the assumed form (3),

$$\mathbf{k} \cdot \boldsymbol{\mu}^{\text{eff}} \mathbf{k} - \omega \mathbf{k} \cdot (\mathbf{S}^{\text{eff}} + \mathbf{S}^{\text{eff}*}) - \omega^2 B^{\text{eff}} = 0. \tag{7}$$

are consistent with the Bloch wave dispersion relations, and yield the correct relations between the spatially averaged field variables, suitable for solving boundary value problems [4].

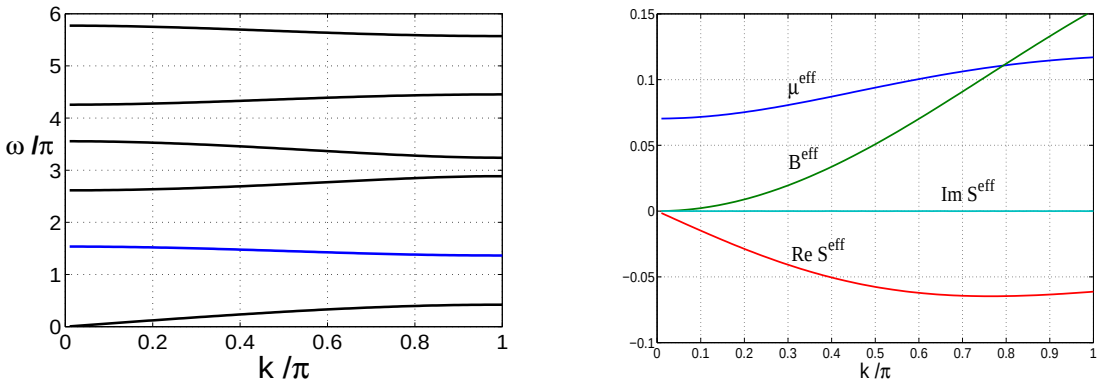

(a) ω vs. k for the first six branches

(b) Parameters for the second branch

Figure 1: (a) Bloch wave dispersion branches and (b) effective parameters on the second branch, for a 1D layered acoustic medium with $\mu_1 = B_1 = 1$, $\mu_2 = B_2 = 0.1$, of volume fractions $f_1 = 1 - f_2 = 0.3$

Apart from the appearance of tensorial quantities that are normally scalar, the concept of dynamic effective parameters is novel and requires a different frame of mind. General properties of the PWE effective parameters, derived in [4], include the possibility of singular values. One important example is the limiting case of a uniform medium. Consider, for instance the 1D case of ρ, K constant. Equation (7) with constant values of μ^{eff}, B^{eff} and $S^{\text{eff}} = 0$ gives us $\omega^2 = (K/\rho)k^2$, whereas the Floquet branches are $\omega_n^2 = (K/\rho)(k + 2\pi n)^2$ for $k \in [-\pi, \pi], n = 0, 1, ...$ The talk will elaborate on this aspect and on the dynamic acoustic properties using a variety of examples, such as the 1D case in Figure 1.

Acknowledgement

The work of ANN was supported by CNRS and by ONR.

References

[1] J.R. Willis. *Dynamics of composites*, volume 495 of *Continuum Micromechanics: CISM Lecture Notes*, chapter 1, 265–290. Springer, Wien/New York, 1997.

[2] J.R. Willis. Effective constitutive relations for waves in composites and metamaterials. *Proc. R. Soc. A*, 467: 1865–1879, 2011.

[3] A. Srivastava, S. Nemat-Nasser. Overall dynamic properties of 3-D periodic elastic composites. *Proc. R. Soc. A*, 468:269–287, 2012.

[4] A.N. Norris, A.L. Shuvalov, A.A. Kutsenko. Analytical formulation of three-dimensional dynamic homogenization for periodic elastic systems. *Proc. R. Soc. A*, doi:10.1098/rspa.2011.0698, 2012.

A METHOD FOR COMPUTATION OF WAVE PROPAGATION: BASIC ALGORITHM DESCRIPTION

K. C. Park[1,2], S. S. Cho[3], H. Huh[4]

[1]Department of Aerospace Engineering Sciences, University of Colorado at Boulder, CO 80309-0429, USA, and
[2]Department of Ocean Systems Engineering, KAIST, Daejeon 305-701, Republic of Korea, e-mail: kcpark@colorado.edu
[3]Korea Atomic Energy Research Institute, 989-111 Daedeok-daero, Yuseong-gu, Daejeon 305-353, Korea
[4]Department of Mechanical Engineering, KAIST, Daejeon 305-701, Republic of Korea

Keywords: explicit time integrator, wave propagation, spurious oscillations

The essence of the present method consists of a combination of two wave capturing characteristics: a new pushfoward-pullback integration formula that is designed to filter post-shock oscillations and the central difference method that is known to intrinsically filter out front-shock oscillations. A judicious combination of these two wave capturing characteristics is shown to reduce substantially both spurious front-shock and post-shock oscillations.

Suppose that the integration step size is Δt whereas the critical step sizes for two heterogeneous domains are Δt_{c1} and Δt_{c2}, respectively. In order to minimize spurious oscillations as $\Delta t < \Delta t_{c1}$ and $\Delta t < \Delta t_{c2}$, we advance initially to Δt_{c1} and Δt_{c2} by a suitable pushforward explicit integrators. The states at time $t = (n+1)\Delta t$ is then obtained by pullback interpolations.

It turns out that the preceding pushforward-pullback combination integrations mainly filter pre-shock front oscillations. As it is well known that typical tracing of waves by an explicit integrators triggers post-wave front oscillations, we construct an average filter by combining the pushforward-pullback combination integrator and the conventional explicit integrator. Thus, the present algorithm employs three steps: a) explicit integration by a suitable explicit integration; b) a pushforward-pullback integration; and, c) an averaging of the two integration outcome.

An example of the performance of the present algorithm is illustrated in Figure 1 as compared with the central difference method and the Runge-Kutta method. Observe that both the central difference method and the Runge-Kutta method trigger unwanted spurious oscillations as shown in the center of Figure 1. It should be mentioned that all existing explicit time integration method this deleterious spurious oscillations. In contrast the the same problem is integrated with the same step size, as shown on the right in Figure 1, the present method as shown on the right side eliminate all but small cusps on the corners of the discontinuities.

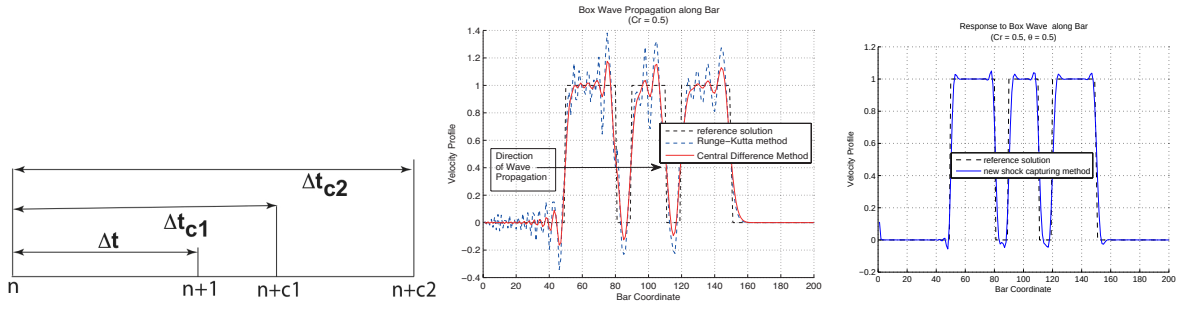

Figure 1: One-dimensional multi-box wave wave propagation problem. *Left figure:* extrapolation of the displacements $(w_1(x,t), w_2(x,t))$ at steps $((n+c1),(n+c2))$ followed by interpolations at the next step (n+1) for heterogeneous problems. *Center figure:* post-shock spurious oscillations by the Runge-Kutta fourth-order method and the central difference method when integrated with $\Delta t = 0.5\Delta x/c$; *Right figure:* Responses to box waves by the new method with $\Delta t = 0.5\Delta x/c$ and $\theta = 0.5$.

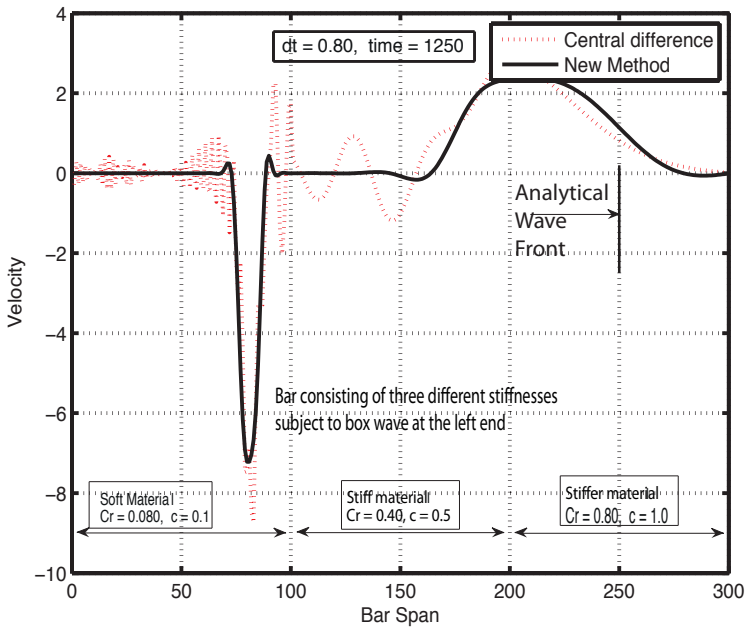

Figure 2: Response to box wave for a bar consisting of three heterogeneous materials.

The second example is a consisting of three material properties as shown in Figure 2, for which a box wave is applied at the left end with the right end fixed. A significantly better response by the new method is clearly seen as compared with the central difference method.

For details of the present algorithm and its performance, the reader is referred to [1] and will be presented at the Colloquium.

Acknowledgement

The present study has been partially supported by WCU (World Class University) Program through the Korea Science and Engineering Foundation funded by the Ministry of Education, Science and Technology, Republic of Korea (Grant Number R31-2008-000-10045-0). The third author has been partially supported by the Brain Korea 21 Program (KAIST Valufacture Institute of Mechanical Engineering), Ministry of Education, Science and Technology.

References

[1] K. C. Park, S. J. Lim, H. Huh. A method for computation of discontinuous wave propagation in heterogeneous solids: basic algorithm description and application to one-dimensional problems. International Journal for Numerical Methods in Engineering, Published online: 8 FEB 2012. DOI: 10.1002/nme.4285

HYPERELASTIC CLOAKING THEORY

William J. Parnell[1], Andrew N. Norris[2]

[1] School of Mathematics, Alan Turing Building, University of Manchester, Manchester, UK;
e-mail: William.Parnell@manchester.ac.uk
[2] Mechanical and Aerospace Engineering, Rutgers University, Piscataway, NJ 08854-8058, USA;
e-mail: norris@rutgers.edu

Keywords: Hyperelastic, cloaking, pre-stress, elastodynamics

The principle underlying cloaking theory is the transformation method whereby the material properties of the cloak are defined by a (singular) spatial transformation. For elastodynamics, Milton et al. [1] concluded that the transformed materials are described by the Willis model, involving coupling between stress and velocity, in addition to anisotropic inertia. For a restricted transformation, Brun et al. [2] found transformed material properties with isotropic inertia and elastic behavior of Cosserat type, i.e. with properties that are the same as those of "standard" linear elasticity except that the moduli do not satisfy the minor symmetry, i.e. $C^*_{jikl} \neq C^*_{ijkl}$.

The transformed elastodynamic constitutive parameters may be characterized through their dependence on (i) the transformation (mapping function) and (ii) on the relation between the displacement fields in the two descriptions, represented by matrices: $\mathbf{F}$, the deformation gradient matrix, and $\mathbf{A}$, respectively. It was shown [3] that requiring stress to be symmetric implies $\mathbf{A} = \mathbf{F}$ and that the material must be of Willis form, as in [1]. Setting $\mathbf{A} = \mathbf{I}$, on the other hand, results in Cosserat materials with non-symmetric stress but isotropic density, as found by Brun et al. [2]. In this paper we consider a class of materials displaying non-symmetric stress of the type necessary to achieve elastodynamic cloaking by taking advantage of the similarities between transformation elasticity and small-on-large motion in the presence of finite pre-strain [4]. Such an approach has already been shown to be successful; by using an incompressible neo-Hookean material with a radially symmetric cylindrical pre-strain, Parnell [5] showed that the resulting small-on-large equations are identically those required for cloaking of the horizontally polarized shear (SH) wave motion. Here we consider the more general elastic transformation problem, including but not limited to SH motion.

It is useful to define the Navier-Lamé operator for linear elasticity and time-harmonic waves of angular frequency ω as

$$\mathcal{L}(\mathbf{a}, \mathbf{C}, \rho, \omega)\mathbf{v} = \frac{\partial}{\partial a_i}\left(C_{ijk\ell}\frac{\partial v_\ell}{\partial a_k}\right) + \rho\omega^2 v_j$$

where $C_{ijk\ell}$ and ρ refer to the elastic modulus tensor and density respectively. Thus transformation elasticity takes the Navier-Lamé equations $\mathcal{L}(\mathbf{X}, \mathbf{C}^0, \rho_0, \omega)\mathbf{u}^0 = \mathbf{0}$ for some homogeneous material properties $C^0_{ijk\ell}$ and ρ_0 and applies the mapping $\mathbf{x} = \boldsymbol{\chi}_0(\mathbf{X})$ so that the governing equations become $\mathcal{L}(\mathbf{x}, \mathbf{C}^*, \rho_*, \omega)\mathbf{u}^* = \mathbf{0}$ where $\mathbf{u}^*(\mathbf{x}) = \mathbf{u}^0(\mathbf{X}(\mathbf{x}))$, $\rho_* = \rho_0/J_0, C^*_{ijk\ell} = F^0_{im}F^0_{kn}C^0_{mjn\ell}/J_0$ and $\mathbf{F}^0 = \mathrm{Grad}\boldsymbol{\chi}_0, J_0 = \mathrm{Det}\mathbf{F}^0$. Thus for cloaking, a singular mapping $\boldsymbol{\chi}_0$ can be chosen such that the origin is mapped to a finite radius say a whilst some radius further out, say B remains fixed. Thus the cloak is the region $a \leq r \leq B$. However we see that in general $C^*_{ijk\ell} \neq C^*_{ij\ell k}$. Thus the "cloak" is required to be an inhomogeneous Cosserat material.

Whereas the above refers to an "imaginary" transformation that allows the determination of the cloak properties, let us now consider an actual *physical* deformation (pre-stress) of a hyperelastic material with initial density ρ_r and constitutive behaviour governed by strain energy function (SEF) $\mathcal{W}$. As in [5] this is taken to be a pre-stress such that an initially small cavity with radius A is inflated to a cavity with radius $a > A$. The outer cloak radius is B. The deformation gradient is $\mathbf{F} = \mathrm{Grad}\boldsymbol{\chi}$ where $\mathbf{x} = \boldsymbol{\chi}(\mathbf{X})$ and the small-on-large equations governing wave propagation through this pre-stress material are $\mathcal{L}(\mathbf{x}, \mathbf{M}, \rho, \omega)\mathbf{u} = 0$, where $\rho = \rho_r/J$ and $M_{ijk\ell} = (1/J)F_{im}F_{kn}\partial^2\mathcal{W}/\partial F_{jm}\partial F_{\ell n}$ with $J = \mathrm{Det}\mathbf{F}$. Ensuring the transformed and small-on-large equations are equivalent requires $\mathbf{u} = \mathbf{u}^*$, $\rho = \rho_*$ and $M_{ijk\ell} = C^*_{ijk\ell}$. It transpires that this gives a restriction on the SEF which for isotropic

materials is required to be the so-called semi-linear SEF: $\mathcal{W} = (\lambda_r/2)(\mathrm{tr}(\mathbf{U}-\mathbf{I}))^2 + \mu_r \mathrm{tr}(\mathbf{U}-\mathbf{I})^2$ where $\mathbf{U}^2 = \mathbf{F}^T\mathbf{F}$ and λ_r, μ_r are the isotropic elastic moduli of the hyperelastic material. The deformation $r = r(R)$ can be determined explicitly but the invariance places the restriction that $r_1/R_1 < 2$.

Defining the shear wavenumber via $K_s^2 = \omega^2\rho_r/\mu_r$, in Figure 1 we illustrate reduction in SH wave scattering from a cylindrical region by using a cloak generated by pre-stress, where a source is located at $K_sR_0 = 8\pi, \Theta_0 = 0$. Top left image shows the scattered field from a cavity of (scaled) radius $K_sa = 2\pi$ whereas the top right is with the presence of the cloak. In particular note that the scattered field is far more isotropic than without the cloak. The plots underneath show the scattering cross-section (SCS) without (solid) and with (dashed) a cloak (left) and percentage reduction in SCS (right). Although the effectiveness of the cloak is reduced by the restriction $r_1 < 2R_1$, we see a significant reduction in scattering by employing the cloak. Similar effects are seen in the in-plane compressional-shear (P/SV) elastodynamic problem.

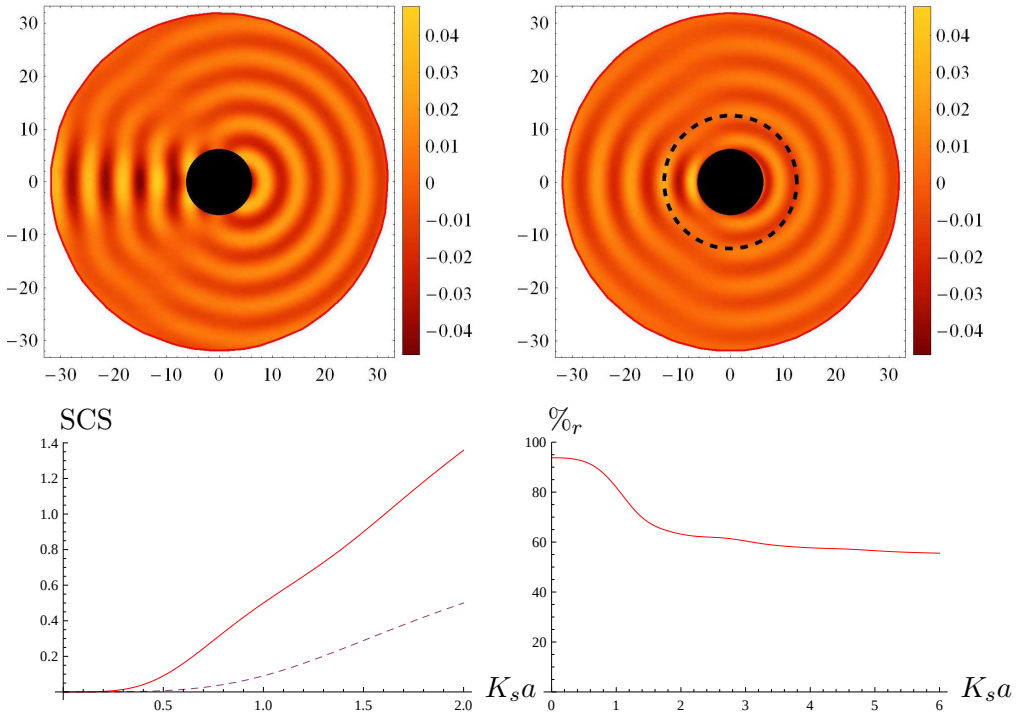

Figure 1: Top: Illustrating the scattered SH wave field of a cavity without (left) and with (right) a cloak. Bottom: Scattering cross-section (left) without (solid) and with (dashed) a cloak and percentage reduction in SCS (right) plotted against scaled cavity radius K_sa where K_s is the shear wavenumber.

References

[1] G. W. Milton, M. Briane, J. R. Willis. On cloaking for elasticity and physical equations with a transformation invariant form. *New J. Phys.*, **8**: 248–267, 2006.

[2] M. Brun, S. Guenneau, A. B. Movchan. Achieving control of in-plane elastic waves. *Appl. Phys. Lett.*, **94**: 061903, 2009.

[3] A. N. Norris, A. L. Shuvalov. Elastic cloaking theory. *Wave Motion*, **49**: 525–538, 2011.

[4] R. W. Ogden. Incremental statics and dynamics of pre-stressed elastic materials. In *Waves in Nonlinear Pre-Stressed Materials: CISM International Centre for Mechanical Sciences*, M. Destrade and G. Saccomandi (eds). Springer, 1–26, 2007.

[5] W. J. Parnell. Nonlinear pre-stress for cloaking from antiplane elastic waves. *Proc. R. Soc. A*, **468**: 563–580, 2012.

NONLINEAR STRAIN WAVES IN BI-ATOMIC CRYSTALS

Alexey V. Porubov, B.R. Andrievsky

Institute of Problems in Mechanical Engineering of the RAS, Saint-Petersburg, Russia;
e-mail: alexey.porubov@gmail.com

Keywords: Solitary wave, kink, moving defects, coupled nonlinear equations, numerical solution

Recently [1] a one-dimensional model has been developed to account for structural re-arrangement in bi-atomic lattices. Mathematically the model is described by the coupled nonlinear equations,

$$\rho U_{tt} - E\ U_{xx} \ = \ S(\cos(u) - 1)_x, \tag{1}$$

$$\mu u_{tt} - \kappa u_{xx} \ = \ (SU_x - p)\sin(u). \tag{2}$$

written for the macro-displacement U and relative micro-displacement u for the pair of atoms with masses m_1, m_2,

$$U \ = \ \frac{m_1\ U_1 + m_2 U_2}{m_1 + m_2},\ u \ = \ \frac{U_1 - U_2}{a}$$

Nonlinearity is introduced via the trigonometric functions that ensures description of translational symmetry in the crystalline lattice.

Further study of the solutions of Eq. (1), (2) revealed an important and decisive role of the phase velocity V for the existence of one or another kind of moving localized defect accounted for the solution for u [2]. Namely, either bell-shaped

$$u \ = \ \pm \arccos\left(\frac{(\rho V^2 - E)U_x}{S} + 1\right),$$

or kink-shaped wave u

$$u \ = \ \pm 2\pi \mp \arccos\left(\frac{(\rho V^2 - E)U_x}{S} + 1\right),\ \text{for}\ \theta \ \leq \ 0,$$

$$u \ = \ \pm \arccos\left(\frac{(\rho V^2 - E)U_x}{S} + 1\right),\ \text{for}\ \theta \ > \ 0,$$

may accompany the bell-shaped wave U_x,

$$U_x \ = \ \frac{A}{Q\ \cosh(k\ \theta) + 1}, \text{or}\ U_x \ = \ -\frac{A}{Q\ \cosh(k\ \theta) - 1}.$$

where $\theta \ = \ x - V\ t - x_{11}$, x_{11} is a constant phase shift, other coefficients may be found in [2]. This is not typical for celebrated nonlinear wave equations whose shapes of solution are defined by the structure of equation. In particular, presence of nonlinear and dispersion terms is needed for a bell-shaped wave, however, these term do nor support a kink.

A natural question arises will we achieve suitable velocity in a more general solution than a single traveling wave one? The control of the phase velocity may be studied numerically but using particular exact solutions to confirm numerical results. An influence of the amplitude and velocity of the initial conditions for U_x and u will be considered first. It will be found that those of the input for v are

the most important when a bell-shaped wave u is generated, while the initial position and velocity of u affects the waves evolution stronger when the kink evolution is studied. Simultaneous existence of the bell-shaped and kink-shaped waves u will be found as a result of suitable choice of initial conditions. Our results show that this bell-shaped wave may arise or decay in a crystalline lattice due to propagation of a macro-strain bell-shaped wave U_x. Variations in the amplitude of U_x, in its initial velocity or in its initial position relatively to the input of u provide appearance or absence of the bell-shaped wave u before the kink wave u. One can note that resulting velocities of the bell-shaped and kink-shaped waves in numerical solutions agree well with those of the exact single traveling wave solutions.

A stability of these nonlinear wave solutions will be also studied.

Some preliminary results were obtained in Refs.[3, 4].

References

[1] E.L. Aero, A.N. Bulygin. Strongly Nonlinear Theory of Nanostructure Formation Owing to Elastic and Nonelastic Strains in Crystalline Solids. *Mechanics of Solids*, **42**: 807–822, 2007.

[2] A.V. Porubov, E.L. Aero, G.A. Maugin, Two approaches to study essentially nonlinear and dispersive properties of the internal structure of materials. *Phys. Rev. E*, **79**: 046608, 2009.

[3] A.V. Porubov, B.R. Andrievsky. Influence of coupling on nonlinear waves localization. *Commun. Nonlinear Sci. Numer. Simulat.*, **16**: 3964–3970, 2011.

[4] A.V. Porubov, G.A. Maugin, B.R. Andrievsky. Solitary wave interactions and reshaping in coupled systems. *Wave Motion*, **48**: 773–781, 2011.

TWO-POINT PARAXIAL TRAVEL TIME APPROXIMATION

Ivan Pšenčík[1], Umair bin Waheed[2] and Vlastislav Červený[3]

[1]Institute of Geophysics, AS CR, Prague, Czech Republic; e-mail: ip@ig.cas.cz
[2]Physical Sciences and Engineering Division, KAUST, Saudi Arabia; e-mail: umairbin.waheed@kaust.edu.sa
[3]Charles University, Fac. Math. and Phys., Prague, Czech Republic; e-mail: vcerveny@seis.karlov.mff.cuni.cz

Keywords: two-point paraxial travel time, geodesic deviations, inhomogeneous isotropic or anisotropic media

We study efficiency and accuracy of the two-point paraxial travel time $T(R', S')$, see formula [1]. The formula was designed for the approximate determination of travel time between two points, S' and R', arbitrarily chosen in a paraxial vicinity of two points, S and R, on a reference ray Ω, between which the travel time $T(R, S)$ is known. The reference ray can be traced in an arbitrary, laterally varying, layered medium of arbitrary anisotropy. The formula offers an efficient, although approximate, replacement of more time consuming procedures (like, e.g., two-point ray tracing) to determine travel time between S' and R' from knowledge of quantities obtained by ray tracing and dynamic ray tracing between points S and R on the reference ray Ω.

The interest in the two-point travel time computations has a long history. It has been studied already by Hamilton in the early nineteenth century [2]. Hamilton derived equations for geodesics, which correspond to ray equations. He then also studied the travel time between two points, and called it *the characteristic function*. For more details see the contribution of Klimeš [3]. Klimeš extended Hamilton's treatment of the characteristic function by providing equations of geodesic deviations (in seismic literature known as dynamic ray tracing equations). He derived relations between the 6×6 ray propagator matrix of dynamic ray tracing in Cartesian coordinates and the second-order spatial derivatives of the Hamilton's characteristic function. These derivatives play a basic role in the computation of the two-point paraxial travel time $T(R', S')$. In [1], instead of the 6×6 ray propagator matrix of dynamic ray tracing in Cartesian coordinates, the 4×4 ray propagator matrix in ray-centered coordinates was used for the evaluation of the two-point paraxial travel time $T(R', S')$.

The two-point paraxial travel time formula, see [1], has the following form:

$$\begin{aligned} T(R',S') &= T(R,S) + [x_i(R') - x_i(R)]p_i(R) - [x_i(S') - x_i(S)]p_i(S) \\ &+ \tfrac{1}{2}[x_i(R') - x_i(R)][f^R_{Mi}(\mathbf{P}_2^{(q)}\mathbf{Q}_2^{(q)-1})_{MN} f^R_{Nj} + (p_i\eta_j + p_j\eta_i - p_i p_j \mathcal{U}_k \eta_k)_R][x_j(R') - x_j(R)] \\ &+ \tfrac{1}{2}[x_i(S') - x_i(S)][f^S_{Mi}(\mathbf{Q}_2^{(q)-1}\mathbf{Q}_1^{(q)})_{MN} f^S_{Nj} - (p_i\eta_j + p_j\eta_i - p_i p_j \mathcal{U}_k \eta_k)_S][x_j(S') - x_j(S)] \\ &- [x_i(S') - x_i(S)] f^S_{Mi}(\mathbf{Q}_2^{(q)-1})_{MN} f^R_{Nj}[x_j(R') - x_j(R)] \ . \end{aligned} \tag{1}$$

The uppercase indices M, N take values 1 and 2, and the lowercase indices i, j take values 1,2 and 3. The Einstein summation convention is used. In (1), $x_i(S)$ and $x_i(R)$ are Cartesian coordinates of two points, S and R, on the reference ray Ω; $x_i(S')$ and $x_i(R')$ are Cartesian coordinates of points S' and R' situated in close vicinities of S and R, respectively. The symbols $\mathbf{Q}_1^{(q)} = \mathbf{Q}_1^{(q)}(R, S)$, $\mathbf{Q}_2^{(q)} = \mathbf{Q}_2^{(q)}(R, S)$, and $\mathbf{P}_2^{(q)} = \mathbf{P}_2^{(q)}(R, S)$ denote 2×2 submatrices of the 4×4 ray propagator matrix in ray-centred coordinates calculated along Ω from S to R by dynamic ray tracing. The symbols f^S_{Mi} and f^R_{Mi} denote Cartesian components of vectors perpendicular to Ω at S and R, respectively. For their determination, a vectorial, ordinary differential equation must be solved along Ω. The symbols p_i, $\mathcal{U}_i$ and η_i denote Cartesian components of slowness vector, ray-velocity vector and the vector $\mathrm{d}\mathbf{p}(\tau)/\mathrm{d}\tau$, respectively, determined during tracing the reference ray Ω. The symbol τ denotes travel time along Ω. The indices S and R indicate if the corresponding quantities are considered at point S or R. For more details see [1].

Once the reference ray and the above-mentioned quantities calculated along it are available, two-point paraxial traveltimes can be evaluated easily. Let us note that the formula cannot work properly if

model parameters variation is too strong or if the matrix $\mathbf{Q}_2^{(q)}$ is singular at point R. The latter problem occurs when there is a caustic at the point R.

As an illustration of the accuracy of the two-point paraxial traveltime formula, we present the result of a test performed in a 2D model of a vertically inhomogeneous isotropic medium, with P-wave velocity of 2 km/s at $z = 0$ km and constant vertical gradient of 0.7 s^{-1}. The model is covered by a rectangular grid with 0.1 km spacing in both x and z directions. Point S' coincides in this test with S, and both have coordinates (0,0), see Figure 1. Point R on the reference ray Ω (white curve) has coordinate (1,1). Points R' are distributed at grid points covering the whole model. Figure 1 shows differences of paraxial and exact travel times. We can see that highly accurate results are obtained around the ray Ω between S and R and behind R, and around the wavefront passing through the point R.

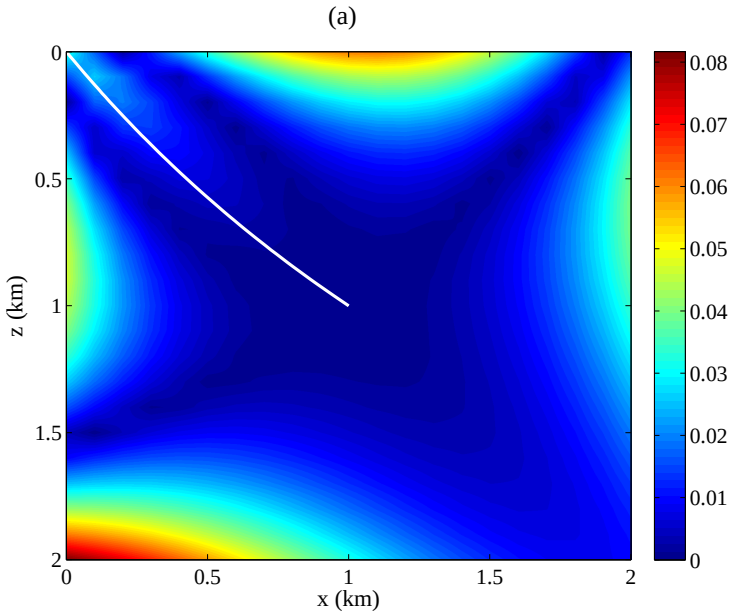

Figure 1: Differences of two-point P-wave paraxial and exact travel times computed from S (0,0) to grid points of the grid covering an isotropic model with velocity 2 km/s at $z = 0$ km and linear vertical gradient of 0.7 s^{-1}. The two-point paraxial travel times are computed from $T(R, S)$ and dynamic ray tracing quantities obtained along the reference ray (white curve) between S and R (1,1).

More details about the two-point paraxial travel time formula and tests of its efficiency on more general models will be given at the presentation.

Acknowledgement

We are grateful to project "Seismic waves in complex 3-D structures" (SW3D) and Research Projects 210/11/0117 and 210/10/0736 of the Grant Agency of the Czech Republic for support and to KAUST.

References

[1] V. Červený, E. Iversen, I. Pšenčík. Two-point paraxial travel times in an inhomogeneous anisotropic medium. *Geophysical J. Int.*, in print, 2012.

[2] W.R. Hamilton. Third supplement to an essay on the theory of systems of rays. *Trans. Roy. Irish Acad.*, **17**: 1–144, 1837.

[3] L. Klimeš. Relation between the propagator matrix of geodesic deviation and second-order derivation of characteristic function. In *Seismic Waves in Complex 3-D Structures, Report 19*, Charles Univ., Faculty of Mathematics and Physics, Dept. of Geophysics, Prague, 103–114, 2009.

WAVE BEHAVIOUR OF TRUSS-CORED STRUCTURES USING THE WAVE AND FINITE ELEMENT METHOD

Jamil M. Renno[1], Brian R. Mace[1,2]

[1]Institute of Sound and Vibration Research, University of Southampton, Southampton SO17 1BJ, United Kingdom;
e-mail: renno@isvr.soton.ac.uk, brm@isvr.soton.ac.uk
[2]Department of Mechanical Engineering, University of Auckland, 20 Symonds Street, Auckland, New Zealand;
e-mail: b.mace@aucklanduni.ac.nz

Keywords: wave propagation, finite element, truss-cored structures, mid-frequency.

The propagation of waves in structures is of interest for many applications. Examples include the transmission of structure-borne sound, shock response, damage detection, statistical energy analysis, acoustic radiation and non-destructive testing. Understanding wave propagation also provides the background necessary for the utilisation and a better implementation of many techniques, e.g. knowledge of high frequency wave propagation is fundamental in ultrasonic and acoustic emission techniques. Wave approaches are particularly useful at higher frequencies, when the size and computational cost of finite element (FE) analysis of the structure as a whole becomes impractically large. In this paper, the WFE method [1] is used to examine the wave behaviour of a truss-cored structure. The method is based on post-processing the conventional FE model of a small segment of the structure using periodic structure theory. This leads to an eigenproblem whose solution yields the full details of the wave characteristics of the whole structure.

The method is applied to examine the wave behaviour of truss-cored panels, typically used in train constructions. An example of such a structure is shown in Figure 1. Kohrs and Petersson [2, 3] investigated free wave propagation in these structures, using a two dimensional discrete Fourier transform to extract the wavenumber characteristics of train floor panels. They also considered a train floor panel with finite width, and analysed the behaviour of the waveguide in the *y*-direction using the WFE method [3]. Below, the same structure is considered but using a two-dimensional formulation of the WFE method [4].

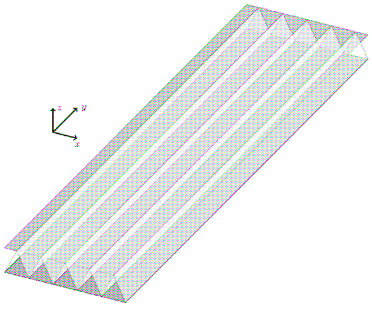

Figure 1: Schematic of a train floor panel with 45° core truss-elements.

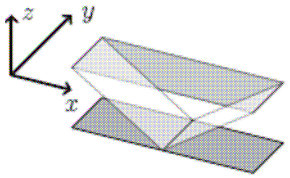

Figure 2: Cell of the train floor panel shown in Figure 1.

A cell, Figure 2., can be meshed using any finite element package. Here, the cell is meshed using SHELL63 elements of ANSYS. The dimensions and material properties of the structure are all given in [2]. The length of the cell in the *y*-direction is somewhat arbitrary, but must be neither too short to avoid numerical round-off errors nor too large to avoid substantial FE discretisation errors [5]. The upper and lower panels are meshed using 10 elements each. The diagonal panels are meshed using 7 elements each. Hence, the cell has 68 nodes with 408 DOFs.

Figure 3 and Figure 4 show the wavenumber in the *x*- and the *y*-directions as functions of frequency. Only real-valued solutions are shown. Propagation in the *x*-direction is clearly influenced by the geometric periodicity of the floor panels (Figure 3). At very low frequency there are 3 wavemodes, which correspond broadly to global bending, shear and axial waves in the panel, analogous to waves in an orthotropic plate. At higher frequencies the situation becomes much more complicated, other wavemodes cut-on and periodic structure effects are apparent, such as stop- and pass-bands for the various wave modes.

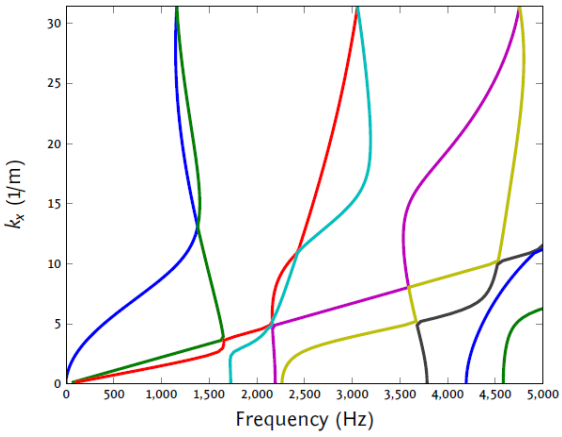

Figure 3: Dispersion characteristics of train floor panels in the *x*-direction.

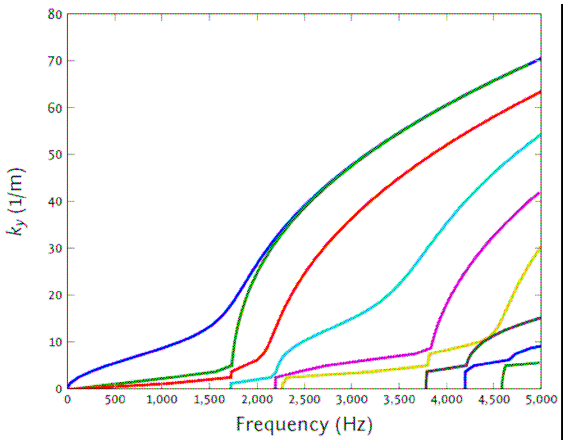

Figure 4: Dispersion characteristics of train floor panels in the *y*-direction.

On the other hand, wave propagation in the *y*-direction, Figure 4, shows no periodic structure effects. This is due to the homogeneity of the structure in the *y*-direction. At low frequencies, three types of wavemodes are distinct and these are global vibrations of the whole floor panel. The three waves correspond to axial, flexural and shear vibration of the whole floor panel. At higher frequencies, more complicated wavemodes cut-on and complicated dispersion phenomena are evident, especially veering.

Acknowledgement

The authors gratefully acknowledge the financial support provided by the Engineering and Physical Sciences Research Council under grant number EP/F069391/1, the European Commission in the context of the collaborative project “Mid-Mod: mid-frequency vibro-acoustic modelling tools – innovative CAE methodologies to strengthen European competitiveness” under grant agreement number 218508.

References

[1] B.R. Mace, J.M. Renno, E. Manconi. Waves and Finite Element Method. In *NOVEM -- Noise and Vibration: Emerging Methods*. Sorrento, Italy, 2012.
[2] T. Kohrs, B.A.T. Petersson. Wave propagation in light weight profiles with truss-like cores: Wavenumber content, forced response and influence of periodicity perturbations. *Journal of Sound and Vibration*, **304**(3-5): 691–721, 2007.
[3] T. Kohrs, B.A.T. Petersson. Wave beaming and wave propagation in light weight plates with truss-like cores. *Journal of Sound and Vibration*, **321**(1-2): 137–165, 2009.
[4] B.R. Mace, E. Manconi. Modelling wave propagation in two-dimensional structures using finite element analysis. *Journal of Sound and Vibration*, **318**(4-5): 884–902, 2008.
[5] Y. Waki, B.R. Mace, M.J. Brennan. Numerical issues concerning the wave and finite element method for free and forced vibrations of waveguides. *Journal of Sound and Vibration*, **327**(1-2): 92–108, 2009.

WAVE DISPERSION IN HOMOGENIZED PERIODIC DOUBLE POROUS FLUID SATURATED SOLIDS

Eduard Rohan[1], Alexander Mielke[2]

[1]Faculty of Applied Sciences, University of West Bohemia, Pilsen, Czech Republic; e-mail: rohan@kme.zcu.cz
[2]WIAS & Humboldt University, Berlin, Germany; e-mail: mielke@wias-berlin.de

Keywords: fluid-saturated porous solids, Biot model, homogenization, double porosity

Wave propagation in fluid-saturated porous media presents a classical but still extremely challenging area of research due the complexity of the problem studied and its obvious applicability in geosciences and material engineering. In the paper we apply the homogenization approach which is based on asymptotic analysis of periodic structure w.r.t. the scale of heterogeneities. We consider the Biot compressible model relevant to the mesoscale characterized by the *periodic representative cell* $Y \in \mathbb{R}^n$, $n = 2, 3$. The dynamic problem formulation involving displacements $\boldsymbol{u}$, seepage velocity $\boldsymbol{w}$ and pressure p is constituted by the momentum equation $(1)_1$, by the Darcy law $(1)_2$, relating the total fluid pressure to the seepage velocity, and by the fluid volume conservation $(1)_3$,

$$\begin{aligned} -\nabla\cdot(\mathbb{D}\boldsymbol{\epsilon}(\boldsymbol{u})) + \nabla(\boldsymbol{\alpha}p) + \bar{\rho}\ddot{\boldsymbol{u}} + \rho^f\dot{\boldsymbol{w}} &= \boldsymbol{f}\ , \\ \rho^f\ddot{\boldsymbol{u}} + \rho^w\dot{\boldsymbol{w}} + \boldsymbol{K}^{-1}\boldsymbol{w} + \nabla p &= 0 \\ \boldsymbol{\alpha}:\boldsymbol{\epsilon}(\dot{\boldsymbol{u}}) + \mathrm{div}\boldsymbol{w} + \frac{1}{\mu}\dot{p} &= 0\ . \end{aligned} \tag{1}$$

where $\boldsymbol{\epsilon}(\boldsymbol{u})$ is the strain, $\rho^f, \rho^w, \overline{rho}$ are densities, $\boldsymbol{K}$ is the permeability and coefficients $\mathbb{D}, \boldsymbol{\alpha}, \mu$ determine the poroelasticity properties. In [4] we developed the homogenized model and derived analytical formulae for dispersion curves for laminated structures. In the present work we study influence of the microstructure geometry and material anisotropy on the dispersion properties (polarization, attenuation). For this we use finite element method employed to compute *characteristic responses* of the microstructure and to evaluate the homogenized coefficients listed in (2), right.

Polarizations $(\bar{\boldsymbol{u}}, \bar{p})$ of plane waves with a given frequency ω propagating in the direction $\boldsymbol{n}$ satisfy

$$\begin{pmatrix} \mathbf{T}(\gamma^2) & \frac{\gamma}{\omega}\mathbf{b} \\ \gamma\omega\mathbf{b}^T & a(\gamma^2) \end{pmatrix}\cdot\begin{pmatrix} \bar{\boldsymbol{u}} \\ \bar{p} \end{pmatrix} = \begin{pmatrix} \boldsymbol{0} \\ 0 \end{pmatrix}\ , \quad \text{where} \quad \begin{aligned} \mathbf{T}(\gamma^2) &:= \boldsymbol{\mathcal{M}}(\mathrm{i}\omega) + \gamma^2\mathbb{D}:\boldsymbol{n}\otimes\boldsymbol{n}\ , \\ \mathbf{b} &:= (\boldsymbol{\mathcal{A}} - \rho^f\mathrm{i}\omega\boldsymbol{\mathcal{K}}(\mathrm{i}\omega))\cdot\boldsymbol{n}\ , \\ a(\gamma^2) &:= \mathcal{Q} + \gamma^2\mathrm{i}\omega\boldsymbol{\mathcal{K}}(\mathrm{i}\omega):\boldsymbol{n}\otimes\boldsymbol{n}\ , \end{aligned} \tag{2}$$

where $1/\gamma$ is the *phase velocity*, $\boldsymbol{\mathcal{K}}(\mathrm{i}\omega)$ is the dynamic permeability and $\boldsymbol{\mathcal{M}}(\mathrm{i}\omega) = \bar{\rho}_Y I - \mathrm{i}\omega(\rho^f)^2\boldsymbol{\mathcal{K}}(\mathrm{i}\omega)$ represents the homogenized mass tensor. For any $\omega > 0$ there are just two pressure (dilatation) waves and $n-1$ shear waves with "**b**-orthogonal" (complex) polarizations in $\mathbb{C}^n$, $n = 2, 3$.

Double porous medium. Many important materials like rocks, soils, bone tissue, etc. are characterized by porosities at several scales, see [1, 2]. It is classical to treat them using homogenization with the double porosity ansatz consisting in scaling the permeability, as explained below, cf. [5]. We consider periodic microstructures generated by the unit representative cell $Y =]0,1[^3$ which involves two compartments, the matrix Y_m and channels Y_c, so that $Y_m \subset Y$ and $Y_c = Y \setminus \overline{Y_m}$ is such that $(\overline{Y_c} + \boldsymbol{e}^i) \cup \overline{Y_c}$ is simply connected for any $i = 1, \ldots, n$ ($\boldsymbol{e}^i$ is the directional unit vector aligned with the i-th axis). All material parameters involved in (1) are defined piecewise in the dual porosity (matrix) Y_m and in the primary porosity Y_c. There are strong fluctuations in permeability: $\boldsymbol{K}^\varepsilon := \boldsymbol{K}_c(y)$ for $y \in Y_c$, however, $\boldsymbol{K}^\varepsilon := \varepsilon^2\boldsymbol{K}_m(y)$ for $y \in Y_m$ for a given scale parameter ε. Although the wave dispersion is studied using the homogenized model ultimately obtained by asymptotic analysis $\varepsilon \to 0$ of (1), i.e. the wave response is described by displacements and pressure like in (2), for the sake of simplicity we can consider a rigid skeleton, reducing (1) to the 2nd and the 3rd equations: $\rho^w\dot{\boldsymbol{w}} + \boldsymbol{K}^{-1}\boldsymbol{w} + \nabla p = 0$ and $\mathrm{div}\boldsymbol{w} + \frac{1}{\mu}\dot{p} = 0$. Recall that for a homogeneous isotropic medium ($\boldsymbol{K} = \varkappa\boldsymbol{I}$), a harmonic plane

wave $p(x) = \bar{p}\exp\{\mathrm{i}k\boldsymbol{n}\cdot\boldsymbol{x}\}$ satisfies $-\nabla\cdot(\mathrm{i}\omega\varkappa^{-1} - \omega^2\rho^w)\nabla p + \mu^{-1}p = 0$. For the double-porous periodic structure, the pressure waves in the *homogenized medium* satisfy the *macroscopic equation*

$$-\nabla\cdot\boldsymbol{\mathcal{C}}(\mathrm{i}\omega)\nabla p + [Q + \omega^2\mathcal{N}(\mathrm{i}\omega)]p = 0\ , \tag{3}$$

where $Q = \int_Y 1/\mu$ and coefficients $\boldsymbol{\mathcal{C}}$ and $\mathcal{N}$ are computed in terms of *microstructural responses* $\boldsymbol{\psi}^i, \hat{\boldsymbol{\psi}}$ and $\hat{\pi}$ given in (5), as follows

$$\begin{aligned}
&\boldsymbol{\mathcal{C}} = (\mathcal{C}_{ij}),\quad \mathcal{C}_{ij}(\mathrm{i}\omega) = \int_{Y_m}[(\mathrm{i}\omega\boldsymbol{K}_c^{-1} - \omega^2\rho^w\boldsymbol{I})\boldsymbol{\psi}^i]\cdot\boldsymbol{\psi}^j\\
&\mathcal{N}(\mathrm{i}\omega) = \int_{Y_m}[\boldsymbol{K}_m^{-1}\hat{\boldsymbol{\psi}}]\cdot\hat{\boldsymbol{\psi}} + \mathrm{i}\omega\int_{Y_m}\mu^{-1}|\hat{\pi}|^2\ .
\end{aligned} \tag{4}$$

Two microscopic problems imposed in Y_c and Y_m must be solved; their solutions are defined in a weak sense in Sobolev spaces of Y-periodic functions, as indicated by $_\#$ (notation: $H_{0\#}(\mathrm{div}, Y_c) = \{\boldsymbol{v}\in H_\#(\mathrm{div}, Y_c)|\boldsymbol{v}\cdot\boldsymbol{n} = 0 \text{ on } \partial Y_c\setminus\partial Y\}$, $\tilde{H}_\#(\mathrm{div}, Y_m) = \{\boldsymbol{v}\in H_\#(\mathrm{div}, Y_m)|\int_{Y_m}\mathrm{div}\boldsymbol{v} = 0\}$, $H^1_{0\#}(Y_m) = \{v\in H^1_\#(Y_m)|v = 0 \text{ on } \partial Y_m\setminus\partial Y\}$). The couples $(\boldsymbol{\psi}^i, \pi^i)\in H_{0\#}(\mathrm{div}, Y_c)\times H^1_\#(Y_c)$ and $(\hat{\boldsymbol{\psi}}, \hat{\pi})\in \tilde{H}_\#(\mathrm{div}, Y_m)\times H^1_{0\#}(Y_m)$ satisfy

$$\begin{aligned}
&\int_{Y_c}\left[(\boldsymbol{K}_c^{-1} + \mathrm{i}\omega\rho^w\boldsymbol{I})\boldsymbol{\psi}^j + \nabla_y\pi^j\right]\cdot\boldsymbol{v} = \frac{\mathrm{i}}{\omega}\int_{Y_c}\boldsymbol{e}^j\cdot\boldsymbol{v}\ ,\quad \int_{Y_c}\nabla_y\cdot\boldsymbol{\psi}^j q = 0\ ,\quad i = 1,\dots,n\ ,\\
&\int_{Y_m}\left(\boldsymbol{K}_m^{-1}\hat{\boldsymbol{\psi}} + \nabla_y\hat{\pi}\right)\cdot\hat{\boldsymbol{v}} = 0\ ,\quad \int_{Y_m}\left(\nabla_y\cdot\hat{\boldsymbol{\psi}} + \frac{\mathrm{i}\omega}{\mu}\hat{\pi}\right)\hat{q} = \frac{\mathrm{i}}{\omega}\int_{Y_m}\frac{1}{\mu}\hat{q}
\end{aligned} \tag{5}$$

for all $(\boldsymbol{v}, q)\in\mathbf{L}^2(Y_c)\times L^2(Y_c)$ and $(\hat{\boldsymbol{v}}, \hat{q})\in\mathbf{L}^2(Y_m)\times L^2(Y_m)$, respectively.

In the paper we present classification of the wave propagation modes for the model (3)-(5) *extended by deformation of the elastic skeleton*, see [5] for the quasistatic case. Using a numerical model based on the mixed finite elements, cf. [3], we explore sensitivity of the dispersion properties w.r.t. the microstructure geometry and topology.

Acknowledgement

The research is supported by the European Regional Development Fund (ERDF), project "NTIS – New Technologies for Information Society", European Centre of Excellence, CZ.1.05/1.1.00/02.0090, and in part by the Czech Scientific Foundation project GACR P101/12/2315.

References

[1] J. Berryman, H. Wang. Elastic wave propagation and attenuation in a double-porosity dual-permeability medium. *Rock Mechanics and Mining Sciences*, **37**: 63–78, 2000.

[2] M. Brajanovski, B. Gurevich, M. Schoenberg. A model of p-wave attenuation and dispersion in a porous medium permeated by aligned fractures. *Geophysics J. Int.*, **163**: 372–384, 2005.

[3] F. Brezzi, M. Fortin. *Mixed and hybrid finite element methods.* Springer, 1991.

[4] A. Mielke, E. Rohan. Homogenization of elastic waves in fluid-saturated porous media using the Biot model, *Submitted* (2012).

[5] E. Rohan, S. Naili, R. Cimrman, T. Lemaire. Multiscale modelling of a fluid saturated medium with double porosity: relevance to the compact bone. *Jour. Mech. Phys. Solids*, doi:10.1016/j.jmps.2012.01.013:In Press, 2012.

NUMERICAL MODELLING OF DYNAMIC TESTING OF MATERIALS USING THE SPLIT HOPKINSON PRESSURE BAR DEVICE

Timo Saksala

Department of Mechanics and Design, Tampere University of Technology, Tampere, Finland;
e-mail: timo.saksala@tut.fi

Keywords: split Hopkinson pressure bar, FEM, material model, wave shaping

This paper considers numerical modelling of dynamic materials testing using the Split Hopkinson Pressure Bar (SHPB) device. A simulation method with predictive modelling capabilities of the SHPB response can be a valuable tool in designing the particular material tests. Moreover, it can be used in calibration of a specific material model under dynamic loading. As an example of such, Saksala et al. [1] calibrated a viscoplastic-damage model for rock via simulation of the dynamic Brazilian disc test using the SHPB. This same test is chosen in this paper as an example of a particular test to be modelled.

The method developed herein includes a two-phase simulation model for the SHPB device, as illustrated in Figure 1. In Phase 1, the generation of the incident wave, $\sigma_i(t)$, due to the impact of the striker bar to the incident bar is simulated using explicit dynamics based FEM. Different wave shaping techniques, such as the external pulse shaper made of copper or rubber placed between the impacting bars or a striker with variable impedance, i.e. varying cross section [2], can be simulated. The main purpose of these techniques is to control the loading rate of the incident pulse in order to prevent the failure of the specimen until the stress equilibrium has been reached. In Phase 2, the incident stress pulse simulated in Phase 1 is applied on the incident node of the simplified model consisting only of two nodes representing the bars of the SHPB device and the FE mesh of the specimen (see Figure 1). Viscous dashpots are attached to the nodes so as to simulate long bars. The contact interaction between these nodes and the discretised disc is modelled by imposing impenetrability constraints between the incident and transmitted nodes and disc mesh nodes. The equations of motion of the nodes representing the SHPB device are added to the discretised equations of motion of the specimen mesh. The equations of motion for the whole system coupled with the contact constraints are solved by explicit time stepping.

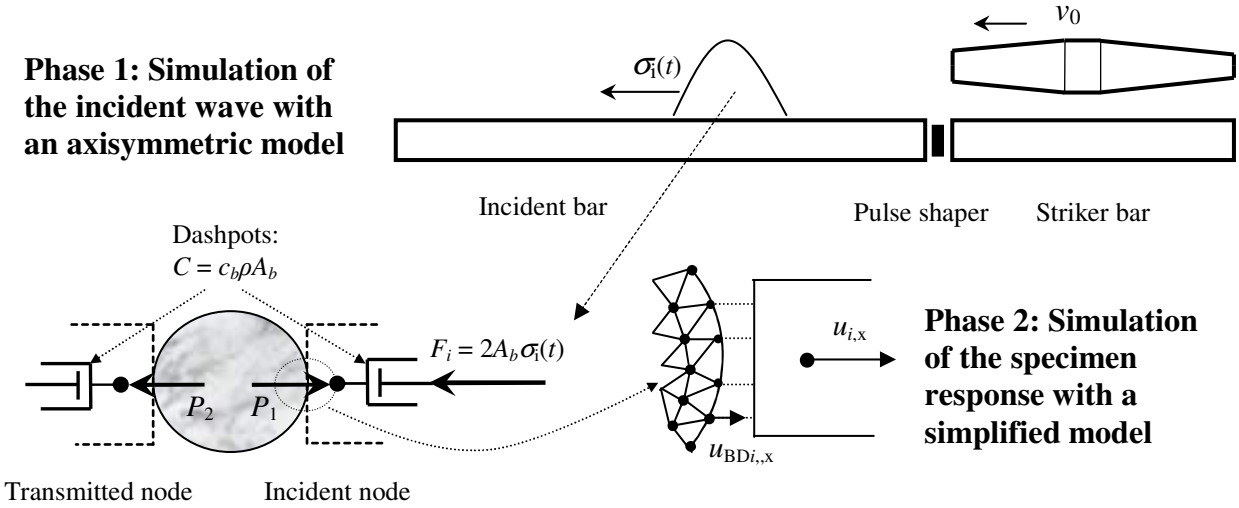

Figure 1: Two-phase numerical modelling of material testing with the SHPB device.

The material of the specimen is described as an elastic-viscoplastic damaging continuum, see [1] for further details. Thereby, the rate effects are naturally accommodated. A simulation example using the present method is shown in Figure 2.

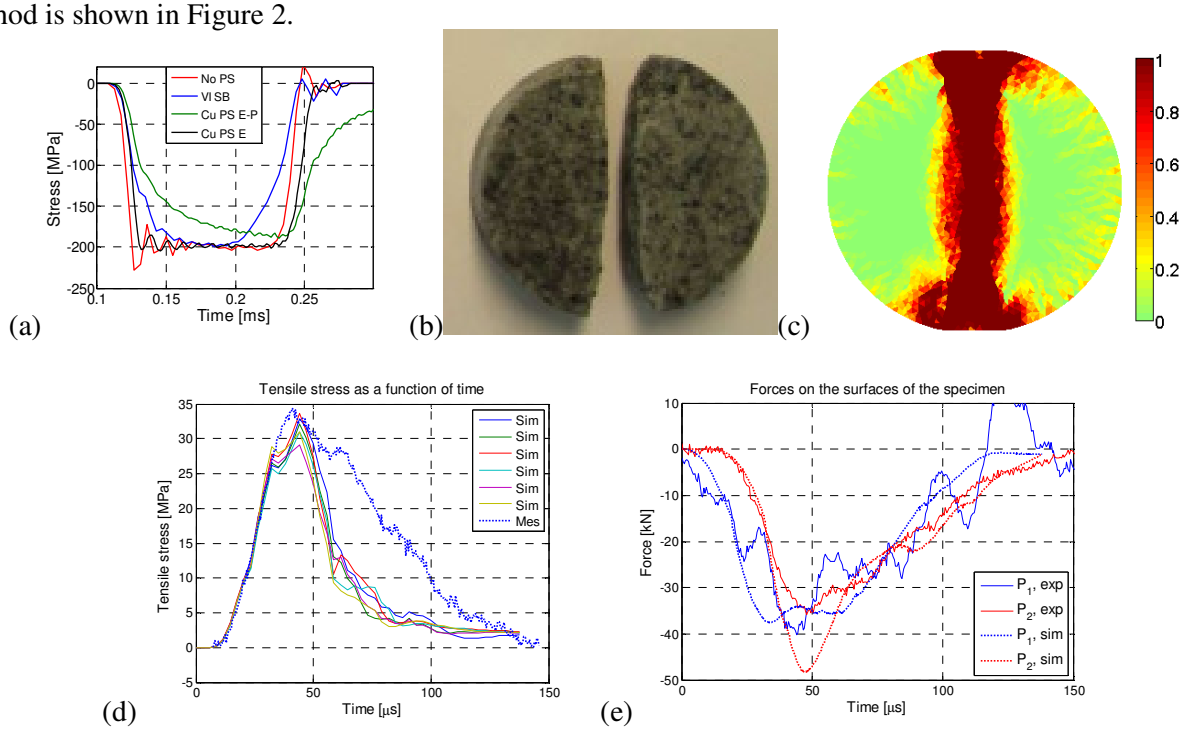

Figure 2: Simulation results: Incident waves with different pulse shaping techniques (a), experimental (b) and simulated (c) axial splitting failure mode of a Brazilian disc made of Kuru granite, measured and simulated tensile stresses of the disc (d), and forces P_1 and P_2 at contact surfaces of the disc and bar ends.

The effect of different pulse shaping techniques (PS = pulse shaper, SB = striker bar, VI = variable impedance, E-P = elasto-plastic, E = elastic) with v_0 = 10 m/s are illustrated in Figure 2a. Figures 2b-e show experimental and simulated results for a dynamic Brazilian disc test on Kuru granite. The experimental axial splitting failure mode (illustrated via tensile damage pattern) in Figure 2b is correctly predicted in Figure 2c. The striker velocity was 11.5 m/s in this test and a rubber pulse shaper was used. The experimental tensile stresses in Figure 2d are based on the elasticity solution of a diametrically loaded disc and, therefore, they are valid only up to the failure of the disc. The tensile stress is calculated according to: $\sigma_T = 2P_1 / \pi LD$ where L and D are the thickness and diameter (16 and 40.5 mm) of the disc, respectively. The discrepancy in the postpeak region of the results in Figure 2d is due to the fact that the diametrical splitting mode releases the tensile stresses much faster than the compressive stresses (the simulated stresses are recorded in a patch of six CST elements at the center of the disc). The simulated and experimental contact forces P_1 and P_2, shown in Figure 2e, are in fairly good agreement. Finally, it is noted that strong strain rate hardening effect is attested for Kuru granite in the experiments as the dynamic indirect tensile stress is about 34 MPa while the quasistatic tensile stress for Kuru granite is about 13 MPa.

Acknowledgement. This work was financed by Finnish Academy (grant no. 251626).

References

[1] T. Saksala, M. Hokka M, V.-T. Kuokkala J.M. Mäkinen. Numerical Simulation of Dynamic Brazilian Disc Test on Rock. In: *Proceedings of the 24th Nordic Seminar on Computational Mechanics*, J. Freund, R. Kouhia (eds.). 3-4 November 2011, Helsinki, Finland.

[2] D.S. Liu, Y.D. Peng, X.B. Li. Inverse design and experimental study of impact piston. *Chinese Journal of Mechanical Engineering*, **34**: 78–84, 1998.

ON THE INFLUENCE OF MATERIAL PROPERTIES ON THE WAVE PROPAGATION IN MINDLIN-TYPE MICROSTRUCTURED SOLIDS

Andrus Salupere, Kert Tamm

CENS, Institute of Cybernetics at Tallinn University of Technology, Tallinn, Estonia
e-mails: salupere@ioc.ee; kert@cens.ioc.ee

Keywords: microstructure, nonlinearity, dispersion, wave propagation

A Mindlin-type mathematical model of microstructured solids with nonlinearities in the macro- and microscale is used to study propagation of 1D solitary waves in such media (see [1] and references therein). The results can be applied for the stress analysis as well as for the nondestructive testing of materials. The model is derived by starting from the Lagrangian

$$L = K - W, \quad K = \frac{1}{2}\rho u_t^2 + \frac{1}{2} I \varphi_t^2, \quad W = W(u_x, \varphi, \varphi_x). \tag{1}$$

Here K is the kinetic energy, W – potential energy, φ – microdeformation, u – displacement, ρ – density and I – microinertia, subindex denotes partial derivative with respect to space coordinate x or time t. The Euler-Lagrange equations are used for deriving governing equations based on the free energy

$$W = \frac{A}{2}u_x^2 + \frac{B}{2}\varphi^2 + \frac{C}{2}\varphi_x^2 + D\varphi u_x + \frac{N}{6}u_x^3 + \frac{M}{6}\varphi_x^3. \tag{2}$$

Here A, B, C, D are material parameters responsible for the linear part of the model and N, M are responsible for the nonlinearity in the macro- and microscale, respectively [1, 2]. Equations of motion based on free energy (2) can be written as

$$\begin{aligned} \rho u_{tt} &= D\varphi_x + Au_{xx} + Nu_x u_{xx}, \\ I\varphi_{tt} &= C\varphi_{xx} + M\varphi_x\varphi_{xx} - B\varphi - Du_x. \end{aligned} \tag{3}$$

For further analysis dimensionless variables U, X and T and parameters $b, \mu, \delta, \beta, \gamma$ and λ are introduced (see [2] for details). By making use of the slaving principle (see [1] for details) it is possible to derive a single equation in terms of displacement U from the (3):

$$U_{TT} - bU_{XX} - \frac{\mu}{2}\left(U_X^2\right)_X = \delta\left(\beta U_{TT} - \gamma U_{XX} + \frac{\lambda\sqrt{\delta}}{2}U_{XX}^2\right)_{XX}. \tag{4}$$

Equation (4) can be considered as an approximation of the full system of equations (3) and its wave operator at the right hand side demonstrates explicitly the influence of the microstructure on the wave propagation.

The main goals of the study are:
(i) to simulate the propagation of solitary waves in Mindlin-type microstructured solids over a wide range of material parameters involved in free energy expression (2);
(ii) to analyse the influence of nonlinear and microstructural properties of the media on the character of the solution, i.e., on the character of the wave propagation.

Equations (3) and (4) are solved numerically under localised initial and periodic boundary conditions

$$U(X,0) = U_0 \mathrm{sech}^2 B_0 X, \quad U(X,T) = U(X + 2km\pi, T), \quad 0 \le X < 2k\pi, \quad m = 1, 2, \ldots. \tag{5}$$

Here $2k\pi$ is the length of the space period. For the numerical integration the pseudospectral method and for the analysis of the time-space behaviour of numerical solutions the discrete spectral analysis

are applied (see [3, 4] and references therein for details). In most cases the speed c of the initial pulse $U(X,0)$ is taken to be zero, which results in $U_T(X,0) = 0$ and can be interpreted as starting from the peak of the interaction of two waves propagating in opposite directions. For the full system of equations (3) two more initial conditions are needed for the microdeformation. We assume that at $T = 0$ the microdeformation and the corresponding velocity are zero, i.e., $\varphi(X,0) = 0$ and $\varphi_T(X,0) = 0$.

A typical solution of the full system of equations (3) is presented in Fig. 1. One can see that besides two solitary waves a certain radiation is formed from the initial localised pulse. Our analysis has demonstrated that in many cases these two solitary waves can travel at nearly constant speeds and amplitudes over relatively long time intervals notwithstanding to the influence of the emerged radiation [4]. In other words, in a certain domain of material parameters the behaviour of the solution is very close to that of solitons.

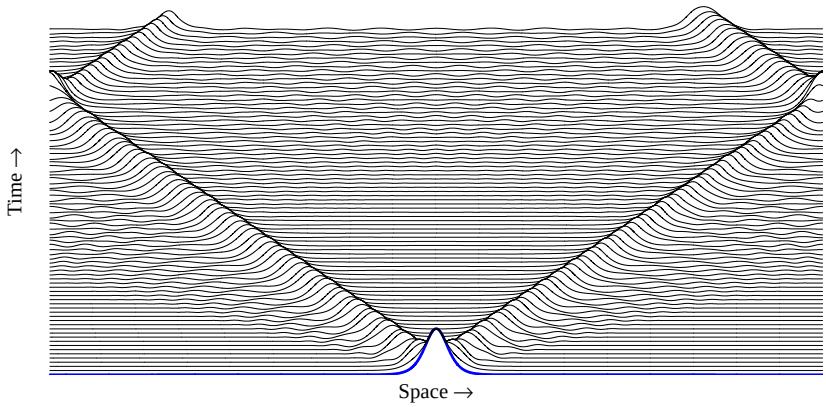

Figure 1: Formation, propagation and interaction of two solitary waves from a localised initial pulse in case of the the full system of equations (3).

During the presentation we will demonstrate how do the values of (i) (linear) parameters B and C, purely related to the properties of the microstructure (see eq. (2)); (ii) (linear) parameter D, related to the interaction between macro - and microstructural properties; and (iii) parameters M and N, related to nonlinear properties of the micro - as well as macrostructure, influence the wave propagation.

Acknowledgement

The research is supported by the Estonian Science Foundation Grant No 8658, the Estonian Ministry of Education and Research (block grant SF0140077s08) and by the European Union through the Regional Development Fund. Authors thank Prof. J. Engelbrecht and Dr. T. Peets for helpful discussions and suggestions.

References

[1] J. Engelbrecht, A. Berezovski, F. Pastrone, M. Braun. Waves in microstructured materials and dispersion. *Philosophical Magazine*, **85**: 4127–4141, 2005.

[2] J. Janno, J. Engelbrecht. Solitary waves in nonlinear microstructured materials. *Journal of Physics A: Mathematical and General*, **38**: 5159–5172, 2005.

[3] A. Salupere. The pseudospectral method and discrete spectral analysis. In *Applied Wave Mathematics,* E. Quak and T. Soomere, (eds). Springer, 301–334, 2009.

[4] K. Tamm. *Wave Propagation and Interaction in Mindlin-Type Microstructured Solids: Numerical Simulation.* PhD thesis, Tallinn University of Technology, 2011.

LASER-BASED RESONANT ULTRASOUND SPECTROSCOPY FOR QUANTITATIVE EVALUATION OF ADVANCED MATERIALS

Hanuš Seiner, Petr Sedlák, Michaela Janovská, Lucie Bodnárová, Jan Zídek, Michal Landa

Institute of Thermomechanics AS CR, v.v.i., Prague, Czech Republic;
e-mail: ML@it.cas.cz

Keywords: laser ultrasound, resonant ultrasound spectroscopy, elasticity, internal friction

Resonant ultrasound spectroscopy (RUS) is a technique for investigation of elastic properties of solids based on the inversion of natural frequencies of free elastic vibrations of a small simply shaped specimen. The method can, in principle, provide the full elastic tensor of the sample from a single measurement, which is considerable advantage e.g. in the characterization of low symmetry single crystals.

Authors have modified the standard RUS experimental setup replacing the piezo-crystal transducers by pulse-laser as the source of ultrasonic vibration and scanning laser interferometer as the receiver, which brought the following improvements:

1) There is not any mechanical coupling between the specimen and transducers, which improves resonance quality and measurement reproducibility.
2) The measurement is more appropriate to carry out in temperature and vacuum chambers.
3) The scanning laser interferometer provides information about eigenmode shapes, which enable mode identification and thus considerably improve the inversion calculation.
4) We can observe the temperature evolution of one individual mode, which allows evaluation of elastic constants and their temperature derivatives with the same relative accuracy.
5) Reliable measurement of quality of resonances, attenuations, and evaluation of internal friction coefficients

Above improvements of the RUS method ([1-3] in details) enable to evaluate elasticity and internal friction of layered materials, thin films on substrates, FGM (functionally graded material), and polycrystalline materials, e.g. [4-6]. An overview of the use of RUS methods for the problems of material research is presented.

Acknowledgement

This work was supported by the CSF the grant project 101/09/0702

References

[1] M. Landa, H. Seiner, at al. Resonant Ultrasound Spectroscopy Close to Its Applicability Limits. In: *Horizons in World Physics, Vol 268.* Eds: M. Everett and L. Pedroza, Nova Science Publishers, 2009.
[2] M. Landa, P. Sedlák, at al. Modal resonant ultrasound spectroscopy for ferroelastics. *Applied Physics A - Materials Science & Processing*, **96**(3), 557–567, 2009.
[3] P. Sedlák, M. Landa at al, Non-contact resonant ultrasound spectroscopy for elastic constants measurement. In: Abstract, proc. of the 1st internat. symposium on laser ultrasonics, *The e-Journal of NDT and Ultrasonics*, 2008.
[4] H. Seiner, L Bodnarová, at al. Application of ultrasonic methods to determine elastic anisotropy of polycrystalline copper processed by equal-channel angular pressing, *Acta Materialia*, **58**, 235–247, 2010.

[5] H. Seiner, P. Sedlák, at al. Sensitivity of the resonant ultrasound spectroscopy to weak gradients of elastic properties. *J.Acoust.Soc.Am.*, **131**, 3775–3785, 2012.
[6] M. Růžek, P. Sedlák, at al. Linearized forward and inverse problems of the resonant ultrasound spectroscopy for the evaluation of thin surface layers. *J. Acoust. Soc. Am.,* **128,** 3426–3437, 2010.

PRECISE EVALUATION OF ELASTICITY FROM ULTRASONIC MEASUREMENTS

Pavla Stoklasová, Petr Sedlák, Hanuš Seiner, Jan Zídek, Michal Landa

Institute of Thermomechanics AS CR, v.v.i., Prague, Czech Republic;
e-mail: Pavla.Stoklasova@it.cas.cz

Keywords: elasticity, inverse problem, resonant ultrasound spectroscopy, surface acoustic waves

For characterization of novel materials such as ferroics, FGMs and other functional materials, a variety of ultrasonic methods have been developed during the past decades, covering the all possible sample geometries: bulks, layered structures and thin films. A great effort is usually devoted to experimental arrangements and the instrumentation, including various modifications of the acoustic microscopy, resonant ultrasound spectroscopy, laser-based ultrasound, etc. Nevertheless, the precise evaluation of elastic properties of studied solids from experimentally obtained acoustic data sets (phase velocities, resonant frequencies, etc.) is still a substantial problem. Each experimental arrangement itself enables the evaluation of all independent elastic coefficients, but the sensitivity to the individual sought parameters differs from method to method. Thus, it seems to be a good idea to combine data from different measurements (e.g. pulse-echo and resonant ultrasound spectroscopy). On this purpose, we need a tool for sensitivity analysis of each method as well as for their combinations.

In this contribution, we describe the evaluation of elastic coefficients from resonant ultrasound spectroscopy (RUS) measurements. RUS method consists in the measurement of dynamical response of a free-standing sample, and an inverse procedure used for the determination of material parameters (elastic components or their combinations) from an optimal fit of corresponding computed and measured resonant frequencies.
The frequency spectra are computed by the Ritz method with properly chosen functional basis (e.g. Legendre polynomials). The procedure is a multivariable nonlinear inverse problem, the solution of which represents the keystone problem of the RUS methods [1,2]. It was shown, that incorporation of modal analysis, i.e. identification and following association of computed and measured resonance modes (based on experimentally obtained resonant modal shapes) significantly improves the minimization of the error function. The efficiency of the determination of the elastic coefficients by acoustic data inversion is improved by deriving the analytical expression of the gradient and the Hessian of the error function. This modified RUS method was applied for quantitative analysis of strongly anisotropic crystals of intermetallics, layered (fine twinned) solids, weak elastic anisotropy of textured materials, functionally graded materials and thin films [3,4,5,6].

This procedure may be adopted for other approaches based on wave propagation (bulk waves, surface acoustic waves (SAW), and guided waves, generally). The direct problem in all mentioned cases can be also solved by the Ritz method with suitable constrains (free surfaces of the sample for RUS, infinite homogeneous medium for bulk waves, one infinite free surface for SAW). This approach enables a unified representation of all acoustic methods via the resonant frequencies, and, consequently, a formulation of a joint objective function for a combination of two or more of them.

As an example, we will show results from application of RUS and SAW for evaluation of carbon layers deposited on Si wafers. Nanocrystalline diamond coatings (NCD) prepared under different conditions (FAST and SLOW growing) and diamond like carbon coating (DLC) were analyzed. The obtained SAW dispersion curves (Figure 1) enable the determination of both the elastic moduli and the thickness of the layer.

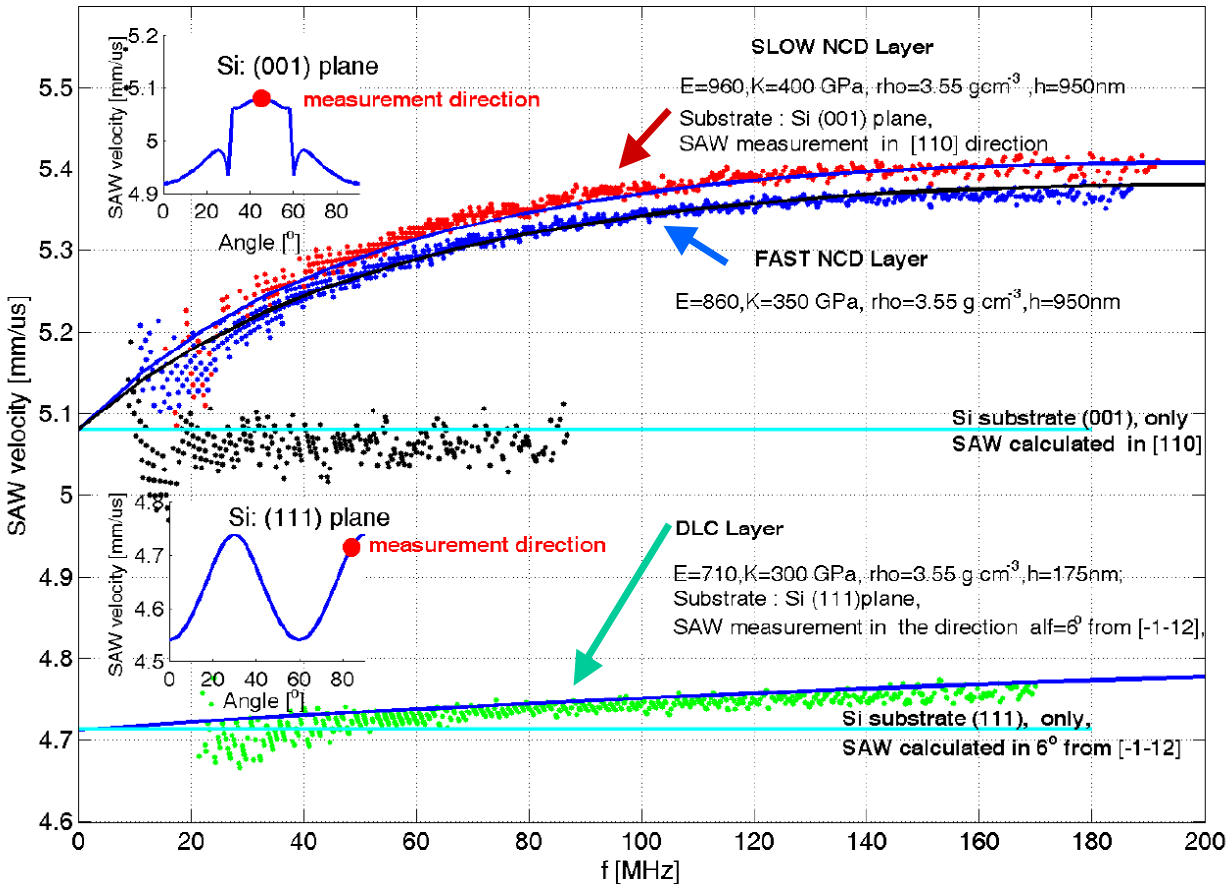

Figure 1 : Dispersive curves of SAW, propagating in carbon surface layer on Si substrate and evaluation of material properties of the layers (points - experimental values, solid lines- best-fit calculation).

Acknowledgement

This work was supported by the Czech Science Foundation, the grant project 101/09/0702 and 101/12/P428.

References

[1] M. Landa, H. Seiner, at al. Resonant Ultrasound Spectroscopy Close to Its Applicability Limits. In: *Horizons in World Physics, Vol 268.* Eds: M. Everett and L. Pedroza, Nova Science Publishers, 2009.
[2] M. Landa, P. Sedlák, at al. Modal resonant ultrasound spectroscopy for ferroelastics. *Applied Physics A - Materials Science & Processing*, **96**(3): 557–567, 2009.
[3] H. Seiner, L. Bodnarová, at al. Application of ultrasonic methods to determine elastic anisotropy of polycrystalline copper processed by equal-channel angular pressing. *Acta Materialia*, **58**: 235–247, 2010.
[4] H. Seiner, P. Sedlák, at al. Sensitivity of the resonant ultrasound spectroscopy to weak gradients of elastic properties. *J.Acoust.Soc.Am.*, in press.
[5] M. Růžek, P. Sedlák, at al. Linearized forward and inverse problems of the resonant ultrasound spectroscopy for the evaluation of thin surface layers. *J. Acoust. Soc. Am.,* **128**: 3426–3437, 2010.
[6] T. Kocourek, M. Růžek, at al. Evaluation of elastic properties of DLC layers using resonant ultrasound spectroscopy and AFM nanoindentation. *SURFACE & COATINGS TECHNOLOGY,* **205**: 67–70, 2011.

NUMERICAL SIMULATION OF WAVE DISPERSION CURVES IN CYLINDRICAL RODS BY EUROPLEXUS

G. Valsamos, F. Casadei, G. Solomos

Joint Research Centre, European Laboratory for Structural Assessment (IPSC/ELSA), T.P. 480, I-21027 Ispra (VA), Italy
e-mail: {georgios.valsamos; folco.casadei; george.solomos}@jrc.ec.europa.eu

Keywords: dispersion curves, Pochhammer-Chree equation, wave propagation, finite element calculation

The phenomenon of dispersion is the reason why waves with different wavelengths travel at different speeds in the same material. This phenomenon appears in cylindrical rods when the radius of the rod is a lot larger than the wavelength of the wave propagated in the rod. The magnitude of the effect depends on the Poisson's ratio value of the material. This effect needs to be taken into account in several cases, for example, in the high strain-rate testing with a Hopkinson bar apparatus. The strain pulses travelling in the incident and transmitter bars suffer this type of dispersion, and results of better quality are obtained if a correction, based on dispersion theory (e.g the classical Pochhammer-Chree analytical solution), is performed.

A study has been conducted on the ability of the EUROPLEXUS code to capture wave dispersion in cylindrical rods with circular cross-section. EUROPLEXUS is a fast transient dynamics explicit Finite Element code suitable for simulating wave propagation in continuous media. A new tool has been developed to calculate the dispersion curves for "longitudinal" wave propagation modes from a numerical simulation. These curves relate phase-velocities and the corresponding wavelengths for each mode. Two different methodologies are implemented for the extraction of the desired data from a numerical solution and for the construction of the Pochhammer-Chree dispersion curves.

In both cases dynamic excitation in the axial direction is applied at the near end of a semi-infinite rod. The history of the load is different for each methodology. In the first methodology a set of numerical simulations is performed where the applied load is a harmonic excitation for each desired frequency. In the second methodology a single simulation is performed with a step function load. Although the second methodology needs a much more complicated post treatment procedure, the total time for the dispersion curves extraction is reduced significantly since with just one simulation the whole data set for all the frequencies under investigation is calculated. The identification of the contributing modes is based on Fourier transform techniques of the calculated rod response both in the time and in the space domains. The various steps and the whole procedure have been automated in the code in order to optimise the efficiency of each methodology.

The dispersion curves resulting from a numerical simulation are compared with the analytical ones obtained by solving the corresponding Pochhammer-Chree equation. The two results are found to be in excellent agreement. The performance of the methodologies for various models, with respect to the type of finite elements employed (e.g. linear, parabolic etc.) and to the density of the mesh, is discussed and assessed. An investigation of the influence of Poisson's ratio on the dispersion curves of a cylindrical rod with circular cross-section has also been carried out.

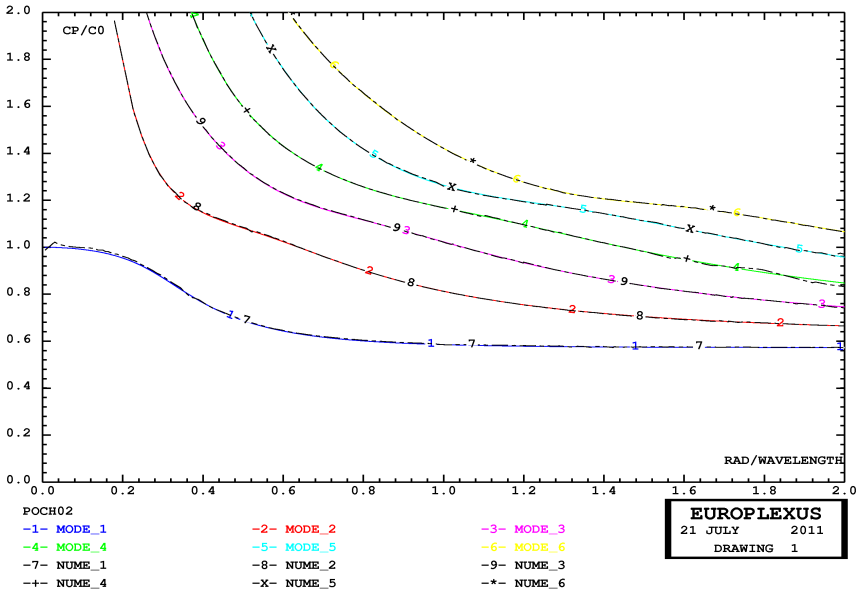

Figure 1: Dispersion curves (Analytical-Numerical) for a cylindrical rod.

References

[1] M. Redwood. *Mechanical waveguides.* Pergamon Press, New York, 1960.
[2] A.E.H. Love. *A treatise in the mathematical theory of elasticity, fourth edition.* Dover Publications, New York, 1944.
[3] Karl F. Graff. *Wave motion in elastic solids.* Dover Publications, New York, 1975.
[4] H. Kolsky. *Stress wave in solids.* Dover Publications, New York, 1963.
[5] A.D. Puckett. Fidelity of a finite element model for longitudinal wave propagation in thick cylindrical wave guides. Thesis, Los Alamos National Laboratories , New Mexico, 2000.
[6] S.T. Marais, R.B. Tait, T.J. Cloete, G.N. Nurick. Material testing at high strain rate using the split Hopkinson pressure bar. *Latin American Journal of Solids and Structures*, **1**: 319–339, 2004.
[7] F. Casadei, E. Gabellini. Implementation od a 3D coupled spectral element/ finite element solver for wave propagation and soil-structure interaction simulation. *JRC EUR* . Report N. 18051 EN, 1998.
[8] J.E. Cooley, J.W. Tukey. An algorithm for machine calculation of complex Fourier series. *Math. Comput.*, **19**(2): 297–301, 1998.
[9] C. Chree: "The Equations of an Isotropic Elastic Solid in Polar and Cylindrical Coordinates their Solutions and Applications", *Trans. Philos. Soc.*, **14**: 250–369, 1889.

THERMODYNAMICS OF GENERALIZED MECHANICS – WAVE PROPAGATION AND GENERIC STABILITY

Peter Ván

Wigner Research Centre for Physics, Department of Theoretical Physics, Budapest, Hungary,
Department of Energy Engineering, Budapest University of Technology and Economics, Hungary,
Montavid Thermodynamic Research Group; e-mail: van.peter@wigner.mta.hu

Keywords: generalized mechanics, generic stability

Traditionally the evolution equations of generalized continuum mechanics (e.g. microdeformation or Cosserat continua) are obtained by the analogy of elasticity and continuum mechanics. However, evolution equations of internal variables are routinely generated by the Second Law of thermodynamics. The long recognized problem is that the evolution equations of internal variables are ordinary differential equations and on the other hand their character is dissipative and cannot model inertial effects.

Recently it was recognized, that dual internal variables with a weakly nonlocal constitutive state space can overcome the above mentioned problematic aspects [1]. Moreover, one can get a general structure that incorporates generalized continua, like the theory of Mindlin [2] and gives an insight to other phenomena, too [3, 4].

However, the evolution equations of dual internal variables in [1] were introduced without considering the basic balances of continuum mechanics, and this fact was not considered in [2]. In this presentation we will investigate the continuum mechanics on the material manifold with two weakly nonlocal internal variables. The thermodynamic constraints are analysed with the help of Liu's procedure. The basic equations of dissipative, generalized Mindlin theory are derived and in the case of zero entropy production the evolution equations of the usual Mindlin theory are recovered.

The basic balances of the continuum in a Piola-Kirchhoff framework are introduced as constraints of the Second Law inequality. Those are the balances of momentum and energy:

$$\begin{aligned} \varrho_0 \dot{v}^i - \partial_j T^{ij} &= 0, \\ \varrho_0 \dot{e} + \partial_i q^i &= 0, \end{aligned}$$

where ρ_0 is the density, T^{ij} is the first Piola-Kirchhoff stress, e is the total energy and q^i is its flux. The Einstein summation rule for the repeated indices is applied. The relation of the deformation gradient and the velocity field is fixed by the following constraint:

$$\dot{F}^i{}_j - \partial_j v^i = 0. \tag{1}$$

The evolution equations of the internal variables Ψ^{ij} and β^{ij} are

$$\dot{\Psi}^{ij} = f^{ij}, \qquad \dot{\beta}^{ij} = g^{ij}. \tag{2}$$

Here the constitutive functions

$$T^{ij}, q^i, f^{ij}, g^{ij}, s, J^i \tag{3}$$

are defined on the weakly nonlocal constitutive state space spanned by the following variables:

$$\partial_j v^i, F^i{}_j, \partial_k F^i{}_j, e, \partial_i e, \Psi^{ij}, \partial_k \Psi^{ij}, \partial_{kl} \Psi^{ij}, \beta^{ij}, \partial_k \beta^{ij}, \partial_{kl} \beta^{ij}. \tag{4}$$

After some calculations ne can give a complete solution of all the Liu equations and obtain the entropy production in the following form:

$$\partial_i\left(\frac{1}{T}\right)\underbrace{\left(q^i+v_iT^{ij}\right)}_{\hat{q}^i}+\frac{1}{T}\underbrace{\left(T^{ij}+\varrho T\partial_{F_{ij}}s\right)}_{\hat{T}^{ij}}\partial_i v_j-\underbrace{\left(\partial_{\Psi^{ij}}s-\partial_k\partial_{\partial_k\Psi^{ij}}s\right)}_{-A_{ij}}\varrho f^{ij}-$$
$$\underbrace{\left(\partial_{\beta^{ij}}s-\partial_k\partial_{\partial_k\beta^{ij}}s\right)}_{-B_{ij}}\varrho g^{ij}\geq 0$$

One can derive the evolution equations of the dissipative, heat conducting generalized continua by introducing linear relationships between the constitutive thermodynamic fluxes $\hat{q}^i, \hat{T}^{ij}, f^{ij}, g^{ij}$ and their multipliers, the thermodynamic forces. The requirement of nonnegative entropy production gives several restrictions on the coefficients. The different special cases, e.g. Mindlin theory, arise in a straightforward manner.

Thermodynamics is long ago thought to be connected to stability of continua. The simplest possible expectation is *generic stability*, the stability of homogeneous equilibrium. This requirement can be investigated by dispersion relations [5]. In the presentation an analysis of generic stability and the corresponding dispersion relations of the thermodynamic theory of generalized continua is shown. Some examples to demonstrate the characteristic features of the generalization beyond Mindlin are also given.

Acknowledgement.

The work as supported by the Hungarian National Research Fund (OTKA), grant No. K81161.

References

[1] P. Ván, A. Berezovski, J. Engelbrecht. Internal variables and dynamic degrees of freedom. *Journal of Non-Equilibrium Thermodynamics*, **33**: 235-254, 2008.

[2] A. Berezovski, J. Engelbrecht, G.A. Maugin. Generalized thermomechanics with dual internal variables. *Arch. Appl. Mech*, **81**: 229-240, 2011.

[3] A. Berezovski, J. Engelbrecht, G.A. Maugin. Thermoelasticity with dual internal variables. *Journal of Thermal Stresses*, **34**: 413-430, 2011.

[4] A. Berezovski, J. Engelbrecht, M. Berezovski. Waves in microstructured solids: a unified viewpoint of modeling, *Acta Mechanica*, **220**: 349-363, 2011.

[5] P. Ván. Generic stability of dissipative non-relativistic and relativistic fluids. *Journal of Statistical Mechanics: Theory and Experiment*, P02054, 2009.

FORMULATIONS OF NON-REFLECTING RADIATION CONDITIONS FOR THE TRANSVERESELY ISOTROPIC LAYERED STRIPS, CYLINDERS AND PLATES USING 3-D ORTHOGONALITY OF WAVES

Dmitrii D. Zakharov

Dept. of Math. Analysis, Moscow State University of Railway Engineering, Moscow, Russia;
e-mail: dd_zakh@mail.ru

Keywords: non-reflecting boundary conditions, eigenwaves, plates, strips, rods, orthogonality

Introduction

The problem of possible replacement of an infinite solid by a solid of finite size with artificial boundary conditions, transparent for outgoing waves, is discussed. In contrast to other different analytical or semi-analytical approaches, or to the implementation of perfectly matched layers [1], the non-reflecting boundary conditions in the frequency domain are suggested in the nonlocal modal formulations. The infinite part Ω of solid or structure considered is assumed in the form of layered cylinder or layered slab (or layered strip for the case of 2-D geometry) as shown in Fig.1 (a). The layer materials can be elastic with transversal isotropy. The finite inner part of solid may have more complicated geometry and include inelastic processes. Omitting the cumbersome details let us describe the main steps below.

Foundations

The derivation is based on such fundamental property of 2-D and 3-D eigenwaves in elastic waveguide as their generalized orthogonality. These properties for waves in strips and cylinders with homogeneous boundary conditions (stress free, rigidly clamped, etc.) have been intensively studied since 70th [2–4]. In the longitudinal direction these waves propagate as $e^{i(kz-\omega t)}$ and the "wavefront" in this direction is plane. Nevertheless, for the case of 3-D "wavefront" as for the eigenwaves in a slab with the propagation law $e^{-i\omega t}H_n^{(1,2)}(kr)$, the orthogonality can be also proved [5, 6]. Physically, the orthogonality is based on symmetry of the respective energy functional and reciprocity [7, 8]. Mathematically, the orthogonality relations are expressed in the form of integral over the waveguide cross section – plane or in the form of cylindrical surface – for waves with any wavenumbers $k_m^2 \neq k_s^2$ from the spectrum. For our purpose one corollary is very important: while representing the field as the series of eigenwaves with direct and opposite directions of propagation, the orthogonality relations permit one to obtain each magnitude as such integrals using the total field and the particular eigenwave.
Thus, the idea is the following: to represent the field in the infinite part of solid in the form of series of outgoing and ingoing waves, and to require that the magnitude of parasitic waves must equal zero.

Main results

(1) A formulation of the non-reflecting boundary conditions as the set of integral relations including the unknown displacements and stresses on the cross section – a common boundary between the finite inner part and the infinite outer part of solid – and including the same field values for each particular wave with positive direction of propagation. The latter means the correct sign of group velocity for real wavenumber k_m and the correct sign of $\mathrm{Im}\, k_m$ providing wave decay for complex k_m. This demand is equivalent to the absence of magnitude for the opposite wave $A(-k_m)=0$. Note, that for each frequency we have a finite number of real k_m and the infinite set of complex k_m. In the case of 3-D slab there is an additional

dependence $A(n,-k_m)=0$ of the order of angular harmonic $\cos n\theta \leftrightarrow \sin n\theta$. In the case of cylinder the spectrum itself also depends on n: $k_m = k_m(n)$.

More details can be found in [9]. The dependence (or double dependence) on the infinite set is not very convenient for numerical implementation. In order to avoid this disadvantage the obtained integrals can be combined and transformed to special sums.

(2) Another formulation of non-reflecting boundary conditions contains only three types of integrals. Instead of particular waves for each k_m we use Green's functions. Two of them represent the response to the concentrated forces applied in the tangential directions with respect to the cross section. The third Green function is a response to the center of extension in the longitudinal direction. For the case of strip or cylinder this is just a dipole (double forces) solution. Each concentrated is applied in the point of the cross section considered or of the parallel cross section situated at the arbitrary small distance. The illustration for 3-D slab is shown in Fig. 1 (b, c) for the cross section of virtual cylinder, complementary to the region Ω.

It can be proved that the formulations (1) and (2) are equivalent. In the numerical procedure the formulation (2) can be used for each node of the grid dicretizing the cross section boundary.

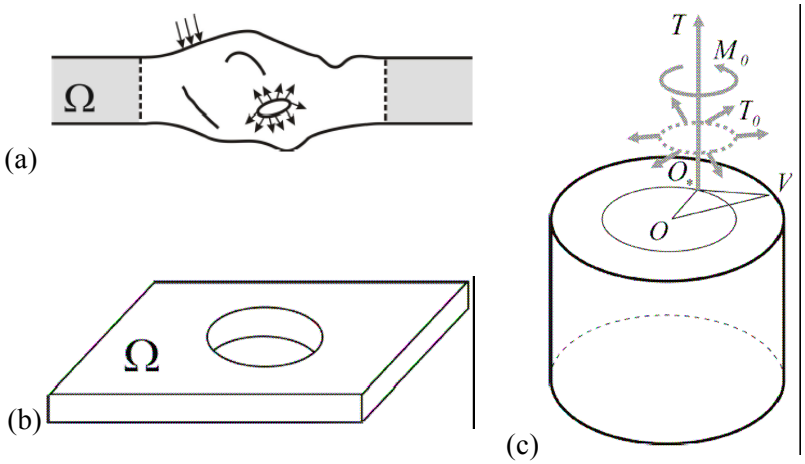

Figure 1: Geometry of solid and example of concentrated loads.

Acknowledgement: This work was supported by the grant project RFBR 12/08/01150.

References

[1] E.A. Skelton, S.D.M. Adams, R.V. Craster. Guided elastic waves and perfectly matched layers. *Wave motion*, **144** : 573–592, 2007.

[2] Y.I. Bobrovnitskii. Orthogonality relations for Lamb waves. *Soviet Acoustical Physics*, **18**: 432–433, 1973.

[3] W.B. Fraser. Orthogonality relations for Rayleigh-Lamb modes of vibration of a plate. *Journal of the Acoustical Society of America,* **59**: 215–216, 1976.

[4] B.G. Prakash. Generalized orthogonality relations for rectangular strips in elastodynamics. *Mechanical Research Communications,* **15**: 251–255, 1978.

[5] D.D. Zakharov. Generalized orthogonality relations for eigenfunctions in three dimensional dynamic problem for an elastic layer. *Mechanics of Solids,* **6**: 62–68, 1988.

[6] D.D. Zakharov. Orthogonality of 3D guided waves in viscoelastic laminates and far field evaluation to a local acoustic source. *International Journal of Solids and Structures,* **45**: 1788–1803, 2008.

[7] A.S. Zilbergleit, B.M. Nuller. Generalized orthogonality of the homogeneous solutions to the dynamic problems of elasticity. *Doklady–Physics,* **234**: 333–335, 1977.

[8] L.I. Slepyan. Betti theorem and orthogonality relations for eigenfunctions. *Mechanics of Solids,* **1**: 83–87, 1979.

[9] D.D. Zakharov. Dirichlet–Neumann conditions and the orthogonality of three-dimensional guided waves in layered solids. *Computational Mathematics and Mathematical Physics,* **50**: 1522–1535, 2010.

DECAY OF ELASTIC PRECURSOR WAVES IN PURE ALUMINUM OVER 300 - 932 K TEMPERATURE RANGE

E. Zaretsky[1], G. Kanel[2]

[1]Dept. of Mechanical Eng., Ben-Gurion University, P.O.B. 653, Beer Sheva 84105, Israel; e-mail: zheka@bgu.ac.il
[2]Joint Institute for High Temperatures RAS, Izhorskaja 13/19, Moscow 127412, Russia; e-mail: kanel@ficp.ac.ru

Keywords: aluminium, elastic precursor wave decay, high strain rate

Experiments with plane shock waves in condensed matter present a way to study the properties of materials at extremely high strain rates with well-controllable loading conditions [1]. Information about the strain-rate and the temperature dependences of the yield stress of metals at high strain rates of shock-wave compression constitutes a basis for developing the models and governing relationships describing mechanical response of materials. In this paper, we present results of investigations of the response of pure (99.99%) polycrystalline aluminum to shock-wave loading over wide range of temperatures and strain rates.

In experiments, plane samples of different thickness were impacted by 0.5 mm thick copper flyer plates. The sample thickness was varied from 0.1 mm to 2 mm, the initial temperature was varied from 300 K up to 932 K that is about 1 K below the aluminum melting point. The free surface velocity histories of the shocked samples were recorded with a VISAR [2] at nanosecond time resolution. Results of the measurements at 300 K and 932 K are shown in Fig. 1. The waveforms demonstrate formation of distinct elastic precursor waves the stress at front of which (the Hugoniot elastic limit – HEL) decreases with the propagation distance and anomalously grows with temperature. Measurements of decay of the elastic precursor wave give us estimation of initial plastic strain rate as a function of stress [3, 4] which in turn may be treated in terms of the dislocation dynamics.

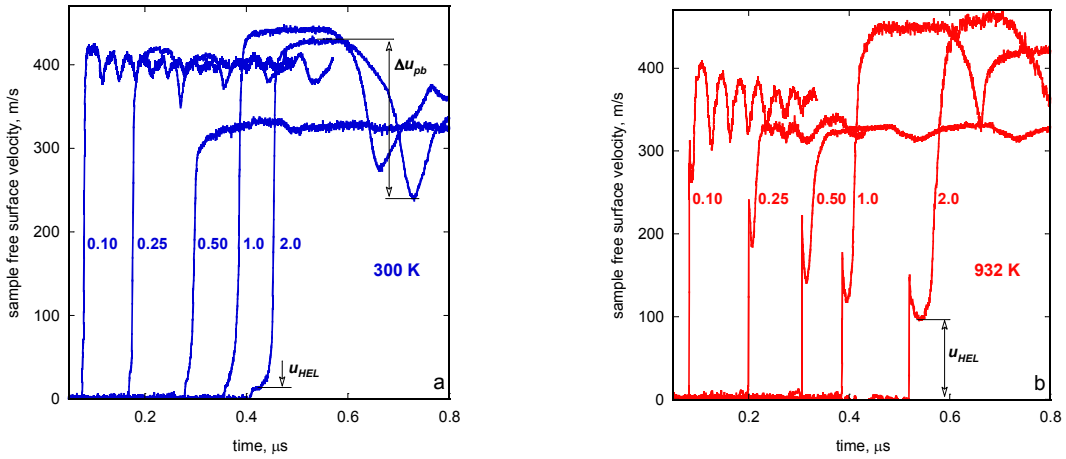

Figure 1. Velocity histories recorded at 300 K (a) and 932 K (b) after impact loading of aluminum samples of different thickness (shown, in mm, near the waveforms. The arrows show the waveform parameters u_{HEL} and Δu_{pb} used for estimating the yield and spall strengths, respectively.

Assuming that the phonon drag of moving dislocations is the only mechanism responsible of the material dynamic strength allows determination of the density of the mobile dislocations at different strain rates and temperatures. The found values of the mobile dislocations densities, Fig. 2, suggest that in order to maintain high rate of the plastic deformation just behind the elastic precursor front the intense and very fast

dislocation multiplication is required. Noteworthy that the strain rate dependence of the density of mobile dislocations in aluminum stays almost unchanged between 300 K and the aluminum melting point, Fig.3.

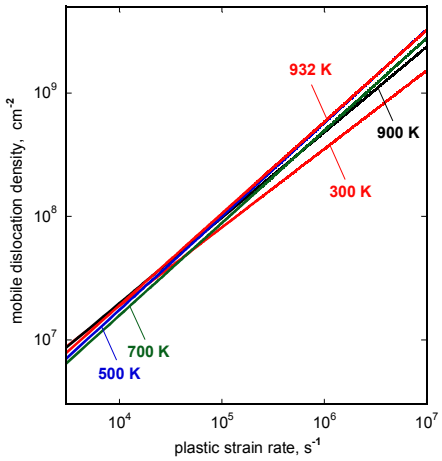

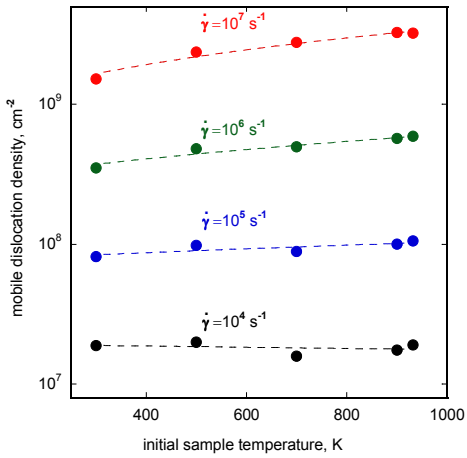

Figure 2. Density of mobile dislocations in aluminum as a function of plastic strain rate.
Figure 3. Density of mobile dislocations in aluminum as a function of temperature.

The spall strength of aluminum (determined with the samples of 1 and 2-mm thickness) is found to be constant and equal ~ 1 GPa over the 300 - 800 K temperature range. Preheating of the aluminum samples above 800 K results in the gradual decline of the spall strength although at 1 K below the melting point the dynamic tensile strength of aluminum is still substantial, of about 0.6 GPa. Such variation of the spall strength of pure metals with temperature was found previously in silver and tin and seems to be typical for pure metals.

To summarize, the presently obtained data confirm earlier observed anomalous thermal strengthening of fcc metals at high strain rates. The temperature effect on the flow stress at fixed strain rate is compatible with the strength mechanism based on dislocation deceleration by oncoming phonon flow. The performed analysis of the decay of elastic precursor wave with propagation distance allows estimating the densities of mobile dislocations at different plastic strain rates. The values of these densities imply that at the top of elastic precursor wave an intense and fast multiplication of dislocations takes place. The amount of dislocations required for maintaining a definite plastic strain rate stays virtually constant between 300 and 932 K.

Acknowledgement

Financial support from Israeli Science Foundation via research Grant No. 56/09 (85300221), from Israeli Planning and Budget Committee for High Education via research Grant No. 84647601 and from Russian Foundation for Basic Research via the Grant No 11-02-01141-a is gratefully acknowledged.

References

[1] G.I. Kanel, S.V. Razorenov, V.E. Fortov. *Shock-Wave Phenomena and the Properties of Condensed Matter*. Springer, New York, 2004.
[2] L. M. Barker, R.E. Hollenbach. Laser interferometer for measuring high velocities of any reflecting surface, *J. Appl. Phys.* **43**: 4669–4675, 1972.
[3] G.E. Duvall. Propagation of plane shock waves in a stress-relaxing medium. In: *Stress Waves in Anelastic Solids*, edited by H. Kolsky, W. Prager, 20–32, Springer-Verlag, Berlin, 1964.
[4] E.B. Zaretsky, G.I. Kanel. Plastic flow in shock-loaded silver at strain rates from 10^4 s^{-1} to 10^7 s^{-1} and temperatures from 296 K to 1233 K. *J. Appl. Phys.,* **110** (7): 073502, 2011.

LIST of REGISTERED PARTICIPANTS

Achenbach Jan D.
Department of Mechanical Engineering
McCormick School of Engineering and Applied Science
Northwestern University
Evanston
IL 60208-3020
USA
E-mail: achenbach@northwestern.edu
Page: 21

Andrianov Igor
Institute of General Mechanics
RWTH Aachen University
Aachen
Germany
E-mail: andrianov@iam.rwth-aachen.de
Page: 23

Berezovski Arkadi
Centre for Nonlinear Studies
Institute of Cybernetics at Tallinn University of Technology
Akadeemia tee 21
12618 Tallinn
Estonia
E-mail: Arkadi.Berezovski@cs.ioc.ee
Page: 29

Bramwell Jamie
The Institute for Computational Engineering and Sciences
University of Texas at Austin
Austin
Texas
USA
E-mail: jbramwell@ices.utexas.edu
Page: 31

Brasil Reyolando M. L. R. F.
Federal University of ABC
UFABC
Sto. Andre
Brazil
E-mail: reyolando.brasil@ufabc.edu.br
Page: 33

Bulant Petr
Department of Geophysics
Faculty of Mathematics and Physics
Charles University in Prague
http://sw3d.cz
Czech Republic
E-mail: bulant@seis.karlov.mff.cuni.cz
Page: 35

Červ Jan
Institute of Thermomechanics AS CR, v.v.i.
Dolejkova 1402/5
Prague
Czech Republic
E-mail: cerv@it.cas.cz
Page: 37

Červená Olga
Institute of Thermomechanics AS CR, v.v.i.
Plzeň
Czech Republic
E-mail: cervena@cdm.it.cas.cz
Page: 63

Chaillat Stéphanie
POEMS
ENSTA
Paris
France
E-mail: fstephanie.chaillat
Page: 39

Cho Soon Cho
Korea Atomic Energy Research Institute
989-111 Daedeok-daero
Yuseong-gu
Daejeon 305-353
Korea E-mail: sscho96@kaist.ac.kr
Page: 41, 103

Collet Bernard
Institut Jean le Rond d'Alembert
Universit Pierre et Marie Curie CNRS UMR 7190
Paris
France
E-mail: bernard.collet@upmc.fr
Page: 43

Dai Hui-Hui
Department of Mathematics
City University of Hong Kong
Hong Kong
China
E-mail: mahhdai@cityu.edu.hk
Page: 65

Engelbrecht Jüri
Centre for Nonlinear Studies
Institute of Cybernetics at Tallinn University of Technology
Akadeemia tee 21
12618 Tallinn
Estonia
E-mail: je@ioc.ee
Page: 29

Erofeyev Vladimir I.
A.A. Blagonravov Mechanical Engineering Institute RAS.
Nizhny Novgorod
Russia
E-mail: erf04@sinn.ru
Page: 45

Feireisl Eduard
Institute of Mathematics AS CR, v.v.i.
Prague
Czech Republic
E-mail: feireisl@math.cas.cz
Page: 47

Fink Mathias
Institut Langevin
Ecole Suprieure de Physique et de Chimie Industrielles de la Ville de Paris
10 rue Vauquelin
75005 Paris
France
E-mail: mathias.fink@espci.fr
Page: 49

Gabriel Dušan
Institute of Thermomechanics AS CR, v.v.i.
Dolejkova 1402/5
Prague
Czech Republic
E-mail: gabriel@it.cas.cz
Page: 51, 73

Georgiadis H.G.
Mechanics Division
National Technical University of Athens
Zographou
Greece
E-mail: georgiad@central.ntua.gr
Page: 53

Givoli Dan
Department of Aerospace Engineering
Technion
Haifa
Israel
E-mail: givolid@aerodyne.technion.ac.il
Page: 27

Grinfeld Michael
US Army Research Laboratory
Aberdeen Proving Ground
USA
E-mail: michael.greenfield4.civ@mail.mil
Page: 55

Grote Marcus J.
Institute of Mathematics
University of Basel
Switzerland
E-mail: marcus.grote@unibas.ch
Page: 57

Hagstrom Thomas
Department of Mathematics
Southern Methodist University
Dallas, TX
USA
E-mail: thagstrom@smu.edu
Page: 25

Herrman Benny
BGU
P.O.Box 3377
Beer-Sheva
Israel
E-mail: bpher@013.net
Page: -

Hilton Harry H.
Aerospace Engineering Department
the College of Engineering
and
Private Sector Program Division
the National Center for Supercomputing Applications
University of Illinois at Urban-Champaign
Urbana
IL 61801-2935
USA
E-mail: h-hilton@illinois.edu
Page: 59

Hirsch Eitan
Private consulter
Tachkemony St. 6
Netanya 42611
Israel
E-mail: heitanon@bezeqint.net
Page: 61

Hora Petr
Institute of Thermomechanics AS CR, v.v.i.
Plzeň
Czech Republic
E-mail: hora@cdm.it.cas.cz
Page: 63

Jansson Tomas
Sandvik Mining AB
SE-811 34 Sandviken
Sweden
E-mail: tomas.sh.jansson@sandvik.com
Page: 67

Khazaie Shahram
Laboratoire MSSMat UMR8579
École Centrale Paris
CNRS
France
E-mail: shahramkhazaee@gmail.com
Page: 69

Klimeš Luděk
Department of Geophysics
Faculty of Mathematics and Physics
Charles University in Prague
http://sw3d.cz
Czech Republic
E-mail: klimes@seis.karlov.mff.cuni.cz
Page: 71

Kolman Radek
Institute of Thermomechanics AS CR, v.v.i.
Dolejkova 1402/5
Prague
Czech Republic
E-mail: kolman@it.cas.cz
Page: 73

Kopačka Ján
Institute of Thermomechanics AS CR, v.v.i.
Dolejkova 1402/5
Prague
Czech Republic
E-mail: kopacka@it.cas.cz Page: 51, 73

Krylov Slava
School of Mechanical Engineering
Tel Aviv University
Tel Aviv
Israel
E-mail: vadis@eng.tau.ac.il
Page: 75

Landa Michal
Institute of Thermomechanics AS CR, v.v.i.
Dolejkova 1402/5
Prague
Czech Republic
E-mail: ml@it.cas.cz
Page: 119, 121

Lazar Markus
Heisenberg Research Group
Department of Physics
Darmstadt University of Technology
D-64289 Darmstadt
Germany
E-mail: lazar@fkp.tu-darmstadt.de
Page: 77

Le Guennec Yves
ONERA - The French Aerospace Lab
Châtillon
France
E-mail: yves.le_guennec@onera.fr
Page: 79

Leindl Mario
Institute of Mechanics at University of Leoben
Leoben
Austria
E-mail: mario.leindl@unileoben.ac.at
Page: 81

Lew Adrian J.
Department of Mechanical Engineering
Stanford University
USA
E-mail:lewa@stanford.edu
Page: 83

Lombardo Mariateresa
Loughborough University
School of Civil and Building Engineering
Sir Frank Gibb Building
Loughborough
Leics, LE11 3TU United Kingdom
E-mail: m.lombardo@lboro.ac.uk
Page: 85

Lundberg Bengt
The Ångström Laboratory
Uppsala University
Box 534
SE-751 21
Uppsala
Sweden
E-mail: bengt.lundberg@angstrom.uu.se
Page: 67

Lurie Konstantin A.
Worcester Polytechnic Institute
Worcester
Massachusetts
USA
E-mail: klurie@wpi.edu
Page: 75, 87

Machová Anna
Institute of Thermomechanics AS CR, v.v.i.
Dolejkova 1402/5
Prague
Czech Republic
E-mail: machova@it.cas.cz
Page: 63

Malkhanov Alexey
A.A. Blagonravov Mechanical Engineering Institute RAS
Nizhny Novgorod
Russia
E-mail: alexey.malkhanov@gmail.com
Page: 45

Maugin Gérad A.
Institut Jean le Rond d′Alembert
Universit Pierre et Marie Curie CNRS UMR 7190
Paris
France
E-mail: gerard.maugin@upmc.fr
Page: 89

Michelitsch Thomas M.
Universite Pierre et Marie Curie
Institut Jean le Rond dAlembert
CNRS UMR 7190
Paris 6
France
E-mail: michel@lmm.jussieu.fr
Page: 91

Mitsui Noa
Wigner Research Centre for Physics
Hungarian Academy of Sciences
XII. Konkoly Thege Miklós út 29-33
Budapest
Hungary
E-mail: n.mitsui@gmail.com
Page:

Morsbøl Jonas
Department of Mechanical and Manufacturing Engineering
Aalborg University
Aalborg
Denmark
E-mail: jm@m-tech.aau.dk
Page: 93

Nguyen Duc C.D.
Department of Civil and Structural Engineering
University of Sheffield
United Kingdom
E-mail: cia07dn@sheffield.ac.uk
Page: 95

Nguyen Vu-Hieu
Université Paris-Est
Laboratoire Modélisation et Simulation Multi Echelle
MSME UMR 8208 CNRS
France
E-mail: vu-hieu.nguyen@univ-paris-est.fr
Page: 97

Nielsen Rasmus B.
Department of Mechanical and Manufacturing Engineering
Aalborg University
Aalborg
Denmark
E-mail: rn@m-tech.aau.dk
Page: 99

Norris Andrew N.
Mechanical and Aerospace Engineering
Rutgers University
Piscataway
USA
E-mail: norris@rutgers.edu
Page: 101

Oberaigner Eduard R
Institute of Mechanics at University of Leoben
Leoben
Austria
E-mail: Eduard.Oberaigner@unileoben.ac.at
Page: 81

Okrouhlík Miloslav
Institute of Thermomechanics AS CR, v.v.i.
Dolejkova 1402/5
Prague
Czech Republic
E-mail: ok@it.cas.cz
Page: 73

Park K.C.
Department of Aerospace Engineering Sciences
University of Colorado at Boulder
CO 80309-0429
USA
and
Division of Ocean Systems Engineering
KAIST
Daejeon 305-701
Republic of Korea
E-mail: kcpark@colorado.edu
Page: 41, 103

Parnell William J.
School of Mathematics
Alan Turing Building
University of Manchester
Manchester
United Kingdom
E-mail: William.Parnell@manchester.ac.uk
Page: 105

Plešek Jiří
Institute of Thermomechanics AS CR, v.v.i.
Dolejkova 1402/5
Prague
Czech Republic
E-mail: plesek@it.cas.cz
Page: 51, 73

Porubov Alexey V.
Institute of Problems in Mechanical Engineering of the RAS
Saint-Petersburg
Russia
E-mail: alexey.porubov@gmail.com
Page: 107

Pšenčík Ivan
Institute of GeophysicsAS CR, v.v.i.
Prague
Czech Republic
E-mail: ip@ig.cas.cz
Page: 109

Renno Jamil M.
Institute of Sound and Vibration Research
University of Southampton
Southampton SO17 1BJ
United Kingdom
E-mail: renno@isvr.soton.ac.uk
Page: 111

Rohan Eduard
Faculty of Applied Sciences
University of West Bohemia
Pilsen
Czech Republic
E-mail: rohan@kme.zcu.cz
Page: 113

Saksala Timo
Department of Mechanics and Design
Tampere University of Technology
Tampere
Finland
E-mail: timo.saksala@tut.fi
Page: 115

Salupere Andrus
Centre for Nonlinear Studies
Institute of Cybernetics at Tallinn University of Technology
Akadeemia tee 21
12618 Tallinn
Estonia
E-mail: salupere@ioc.ee
Page: 117

Sorokin Sergey V.
Department of Mechanical and Manufacturing Engineering
Aalborg University
Aalborg
Denmark
E-mail: svs@m-tech.aau.dk
Page: 93, 99

Stoklasová Pavla
Institute of Thermomechanics AS CR, v.v.i.
Dolejkova 1402/5
Prague
Czech Republic
E-mail: pavla.stoklasova@it.cas.cz
Page: 121

Tamm Kert
Centre for Nonlinear Studies
Institute of Cybernetics at Tallinn University of Technology
Akadeemia tee 21
12618 Tallinn
Estonia
E-mail: kert@cens.ioc.ee
Page: 117

Valsamos George
Joint Research Centre
European Laboratory for Structural Assessment (IPSC/ELSA)
T.P. 480
I-21027
Ispra (VA)
Italy
E-mail: georgios.valsamos@jrc.ec.europa.eu
Page: 123

Ván Peter
Department of Theoretical Physics
Wigner Research Centre for Physics
and
Department of Energy Engineering
Budapest University of Technology and Economics
Budapest
Hungary
E-mail: van.peter@wigner.mta.hu
Page: 125

Zakharov Dmitrii D.
Department of Mathematical Analysis
Moscow State University of Railway Engineering
Moscow
Russia
E-mail: dd_zakh@mail.ru
Page: 127

Zaretsky Eugene
Department of Mechanical Engineering
Ben-Gurion University
P.O.B. 653
Beer Sheva 84105
Israel
E-mail: zheka@bgu.ac.il
Page: 129

Academy of Sciences of the Czech Republic, v.v.i.
Dolejškova 1402/5
182 00 Prague 8
Czech Republic
http://www.it.cas.cz

ISBN: 978-80-87012-41-3